SPATIO-TEMPORAL DYNAMICS OF BADLANDS IN SOUTHERN GUAM: A CASE STUDY OF SELECTED SITES

By

Maria Kottermair
Mohammad Golabi
Shahram Khosrowpanah
Yuming Wen

WERI

WATER AND ENVIRONMENTAL RESEARCH INSTITUTE
OF THE WESTERN PACIFIC
UNIVERSITY OF GUAM

SPATIO-TEMPORAL DYNAMICS OF BADLANDS IN SOUTHERN GUAM: A CASE STUDY OF SELECTED SITES

by

Maria Kottermair
Mohammad Golabi
Shahram Khosrowpanah
Yuming Wen

Water and Environmental Research Institute of the Western Pacific
University of Guam, UOG Station, Mangilao, Guam 96923

Technical Report No. 133
September 2011

ABSTRACT

Soil erosion is a major environmental problem in southern Guam affecting soil quality and water quality as well as the coral reef system. Badlands, the extreme form of soil erosion, appear throughout the savanna landscape and contribute large amounts of sediments into the waterways. This study investigated changes in badland extent over a 60-year period in three different sub-basins in southern Guam. Historical aerial photos from 1946 and 1994 and recent QuickBird satellite imagery from 2006 were analyzed in a Geographic Information System (GIS) to detect changes over time. In addition, GIS modeling was used to relate badland occurrence to slope, aspect, and elevation. Basic soil characteristics from field sampling were also investigated.

Results indicate an overall increase in badland cover in 2006 compared to 1946. Large badland patches (>500 m^2) seen today in areas with little or no human activity generally existed before 1946. In contrast, areas extensively used by humans, mainly in the form of off-roading, experienced a drastic increase of large badland patches, indicating a large impact of human activities on badland expansion. New badland patches in the form of mass wasting were found in an area with no human impact, indicating natural factors, especially tropical cyclones, as a cause. Despite the general increase in the number of badlands and patch sizes, some badland areas were also able to re-vegetate naturally at all three selected study sites. Re-vegetation occurred rarely in an entire patch but rather on parts of it, hence decreasing the size of some badland patches. It was also found that badland occurrence is strongly influenced by topography (slope, aspect, and elevation) which controls the exposure of badlands to rain, wind, and sun and determines the degree of weathering and erosion. Soil properties of badlands and adjacent vegetative sites were very similar except for the organic matter content, which was almost completely absent in badlands indicating low fertility of the soil and associated lack of vegetation.

Overall, badland dynamics are complex and the result of various human and natural factors. Since it is unrealistic to stop badland expansion altogether and re-vegetate all existing badlands, erosion from badlands and associated sedimentation will continue to impact water quality. However, managing human activities, particularly off-roading, is essential to counteract the accelerated badland expansion caused by humans. This is especially important since human activities are likely to increase significantly with the anticipated military buildup on Guam.

KEYWORDS: Southern Guam, Badlands, Spatio-temporal Change, Soil Characteristics, Geographic Information System, Spatial Analysis

ACKNOWLEDGEMENTS

TABLE OF CONTENTS

APPENDIX A. Terrain Analysis – Raw Data.

APPENDIX B. Examples of Badland Changes.

APPENDIX C. Examples of Misclassification.

APPENDIX D. Soil Samples.

APPENDIX E. Examples of Badlands at the Study Sites.

LIST OF TABLES

LIST OF FIGURES

Chapter 1 Introduction

1.1. *Background*

Soil erosion, rather common in the southern part of Guam, marks the savanna landscape in the form of erosion scars. These large, orange-red patches of bare earth are often called badlands. Soil erosion not only degrades the quality of the topsoil, but also severely impacts the water quality in the streams and ocean, ultimately impacting the health of Guam's coral reef system and marine flora and fauna. Several studies (*e.g.*, NRCS, 1996; Lewis, 1999; Scheman, 2002; Golabi *et al.* 2005a; Park, 2007) have shown that badlands are one of the major contributors of soil erosion and associated sedimentation on Guam. Anthropogenic activities such as wildfires, poorly managed construction sites, off-roading, as well as mis-managed farming can alter erosion and sedimentation rates significantly (Minton, 2006).

Guam faces a drastic population increase and associated construction boom with the anticipated military expansion by 2014. The increase in construction will result in a direct loss of natural habitats; whereas the increase in population will have an indirect impact on the natural environment—mostly through recreational use such as diving, hiking, biking, and off-roading. It is, therefore, more crucial than ever to protect natural habitats before they are irreversibly degraded or destroyed.

Managing badlands properly is fundamental in stopping or at least slowing the rate of the degradation process and restoring the natural habitat. However, to manage badlands properly, a better understanding of their behavior is essential. Besides the erosion rate, which has been studied by several researchers on Guam, the behavior of badlands (including origin, development, and characteristics) is not at all well known. To date, only one study (Khosrowpanah *et al.*, 2010) specifically addressed badland change and terrain attributes. Although this study revealed that badlands are dynamic in extent, more data (at different sites and finer time resolution) is needed to more reliably reconstruct changes in the past and predict changes in the future. In addition, we need to better understand the factors—natural (*e.g.*, climate, soils) as well as anthropogenic (land use) factors—governing these changes to recommend management strategies accordingly. Natural factors, like tropical cyclones, earthquakes, soil properties and behavior, and terrain are all factors that might influence badland formation. Human impacts by certain land use activities, especially off-roading and improper farming techniques, are believed to have a significant impact on badland evolution and soil degradation that, in turn, alter erosion rates. Unlike natural factors, which cannot be controlled, human factors can be controlled through proper management. With an increase in population, especially military personnel, and with off-roading being a popular recreational activity of people in the military, off-roading activities are likely to increase significantly in the near future. Considering the aforementioned factors, it is important that we understand badland dynamics to better manage them and prevent their expansion. Only then can erosion and associated sedimentation be decreased, resulting in a healthier watershed with better water quality and sustainability of coastal resources.

1.2. Scope and Objectives

This study involved Geographic Information System (GIS) analysis, field sampling, and soil laboratory analysis. A GIS was used to analyze the change of badland extent over time in addition to terrain attributes. Fieldwork was carried out to obtain soil samples and determine the soil characteristics of badlands and compare them with adjacent vegetative savanna. The soil samples were tested and analyzed in the Soil Laboratory of the University of Guam.

The scope of this study is to provide quantitative support for the following hypotheses:

Badland dynamics are based on:

- Change over time.
    1. Badlands grow in size and number, but also have the ability to recover and become vegetated again.
    2. Land use and natural events (*e.g.*, tropical cyclones and earthquakes) have an influence on badland development.
- Terrain attributes such as elevation, slope, and aspect ratio.
- Soil properties, which differ from adjacent vegetative areas (savanna).

The following objectives were achieved in this study:

- Georeferenced historic photographs and delineated badlands at three study sites.
- Determined and compared rate of change of badlands caused by natural factors (tropical cyclones, climate change, and earthquakes) and different land use at all three study sites.
- Analyzed and compared relationship between badlands and terrain attributes.
- Identified landscape metrics of badlands.
- Collected, analyzed, and compared soil samples in badlands and adjacent areas.
- Recommend management strategies based on the study findings.

Chapter 2   Literature Review

2.1.   *Badlands on Guam*

Badlands on Guam are described by Young (1988) as continuously eroding areas of very deep, well-drained saprolite derived from tuff and tuff breccia and supporting little if any vegetation. However, this description does not take into account areas that are also bare earth, have a very similar appearance, but rather than eroding, accumulate sediments from eroding areas. In that sense, describing badlands as pitted, sloping sites without vegetation (NRCS, 1996) includes these sedimentary areas; however, it could also include rock outcrops. In this study, the term badland refers to exposed saprolite and barren volcanic soil.

Saprolite is a soft, usually clay-rich, thoroughly decomposed rock that formed in place by chemical weathering of rock while retaining its original structure (Figure 1); in humid and tropical climates, saprolite can reach 100 meters in depth (Neuendorf *et al.*, 2005). Original rock minerals are replaced by clay minerals through leaching. Clay particles are then subject to a shrink-swell mechanism, which is especially pronounced in climates with high temperate, rainfall, and alternating wet and dry periods (Doerge and Smith, 2008) like on Guam. The shrink-swell mechanism forms soil aggregates, which are easily erodible (Gavenda, 2009). Saprolite is also strongly acidic and nutrient poor, creating a hostile environment for most plants. Badlands usually form on heavily eroded Akina and Atate soils (Young, 1988).

Slopes in badlands are generally short, irregular, and vary from relatively shallow to very steep. Undisturbed saprolite can maintain almost vertical slopes of significant height due to its general stiffness (Doerge and Smith, 2008). Permeability is moderately slow with rapid runoff and severe erosion (Young, 1988). Gullies and ravines are a common feature in most badlands created by channeled overland flow. The color is usually a shade of red but may vary from white, orange, yellow to purple.

It is unclear when the first badlands formed on Guam. However, the first written account dates back to naturalist Antonio de Pineda, who explored Guam in 1792. In his diary, he notes "an open and cleared site that was largely covered with strata of ocherous soil, whose yellow, red, and greenish colors appeared in breccia-like arrangement" east southeast of Agat (De Pineda, 1792). De Pineda (1792) also mentions the "banks of red soil that is so common in the central part of the island." Although the exact extent of badlands at that time is unknown, it is evident from De Pineda's description that badlands were already a noticeable feature of Southern Guam.

Figure 1. Picture of a badland where saprolite is exposed. Note the original structure of the bedrock that is preserved in the saprolite despite weathering.

2.2   *Factors controlling Badland Development*

Badland development is complex and includes many factors and processes, which vary between badlands and within badlands over time (Bryan and Yair, 1982). Badland occurrence is generally attributed to soil properties, climatic factors, agricultural practices, and tectonic activities (Moretti and Rodolfi, 2000; Summa *et al.*, 2007).

The genesis of badlands on Guam may fall into two categories: a rapid and a slow mechanism. The first refers to the exposure of saprolite through rapid mass wasting in the form of slumping or translational landslides. The second mechanisms may take years or decades and is initiated by the disturbance of the topsoil followed by continued wind- and water erosion. Over time, the erosion process can also expose saprolite. Both mechanisms are a result of soils with high plasticity, sloping terrain, and seasonal wet and dry periods. In addition, mass wasting is a result of higher permeable weathered rock over less permeable rock in combination with very high amounts of rainfall that saturate the upper more permeable layers (Doerge and Smith, 2008). Also, earthquakes have reportedly triggered mass wasting (*e.g.*, Tracey at al., 1964).

Removal of the toe slope and over-steepening of hillsides such as in road construction can lead to mass wasting. In contrast, the disturbance of topsoil is often caused by repeated burning, off-roading, mis-managed farming, or grazing (Gavenda, 2009). Once the topsoil is eroded, wind- and water erosion along with the inherent characteristics of saprolite (*e.g.*, low fertility) make it difficult or almost impossible for plants to re-establish, and the soil then continues to erode. The disturbance of topsoil, however, also decreases slope stability, which in turn may lead to mass wasting in combination with the aforementioned factors.

4

Both mechanisms may be the result of natural and human factors. However, mass wasting on Guam may primarily be considered natural as most mass wasting has been observed in areas with no or very little human activities (personal observation). Indirectly, it may be caused by human activities through de-forestation in the past or burning which is mainly due to arson. The removal of topsoil is largely due to human activities. In respect to badlands, the most destructive current human activities are off-roading and intentionally-set wildfires. Off-roading loosens soil particles but may at the same time compact the soil leading to increased surface strength and bulk density, reduction of soil moisture, greatly reduced infiltration rate, and reduction of organic carbon (Wilshire *et al.*, 1978). These changes in chemical and physical soil properties increase the erosion potential, decrease biological productivity, and increase sediment yields off-site (Wilshire *et al.*, 1978). Off-roading is a very popular activity on Guam and has dramatically increased in recent years according to a study at Mt. Tenjo (PCR, 2009). The total soil movement measured at Mt. Tenjo was also greater at off-roading sites versus control sites (PCR, 2009). Wildfires do not disturb the soil directly, but continued burning increases the erosion potential. The reason wildfires are considered a large contributor of erosion and associated sedimentation is their high frequency and the large areas affected by them.

Local terrain attributes may also influence badland development. Canton *et al.* (2004) studied the influence of terrain attributes on the spatial distribution of ground cover, including bare marl regolith, in the Tabernas badlands of southeastern Spain. They found that local terrain attributes (*e.g.*, slope angle, aspect, and elevation) have a greater influence on ground cover types than non-local terrain attributes (contributing area, wetness index, length slope factor). A correlation of badland occurrence and certain terrain attributes like slope, aspect, elevation, and distance to drainage divide was observed in the Ugum Watershed (Khosrowpanah *et al.*, 2010).

2.3   *Erosion and Sedimentation Rates*

Several researchers (Lewis, 1999; Scheman, 2002, and Golabi, *et al.* 2005a) conducted field studies to measure sediment yields directly.

Lewis (1999) measured sediment yield, slope retreat, and fracture movement in four individual badland basins within the Taelayag watershed in southern Guam. The study revealed erosion rates of badlands are ranging from 5.2 to 23.5 tons/ha/yr (2.1–9.5 tons/acre/yr). Although the erosion rate is lower than expected, the impact of badland erosion is still significant (Lewis, 1999).

Scheman (2002) also measured erosion rates of badlands with different slopes in the La Sa Fua Watershed. By comparing the measured results with erosion rates calculated using the Revised Universal Soil Loss Equation (RUSLE), Scheman (2002) found that RUSLE consistently overestimated the erosion rates. As expected, the highest average erosion rate occurred in badlands. The soil loss at the different test sites (badlands and grasslands) is equally connected to slope angle, but barren soil exhibits a stronger relationship with precipitation accumulation than soil in grasslands. Following a typhoon, erosion increased in the steep badland areas. Scheman (2002) concluded that various topographic and climatological factors might influence the development of badlands. By means of a time-series photograph (one year apart), the author also showed that the number of badlands increased.

Golabi *et al.* (2005a) studied the effects of different soil surface conditions on sedimentation and water quality in southern Guam. The runoff from four different plots (natural savanna vegetation, vetiver system, controlled burn, and bare soil) was tested for sediments and turbidity. The vetiver system proved to be very successful in trapping sediments but also in improving the water quality. The plot with no vegetative cover—representing badlands—showed by far the highest amounts of sediment and turbidity values. The overall projected soil loss for barren soil was seventy times (104.75 tons/ha/yr) more than that of the vetiver system

5

(1.47 tons/ha/yr); the natural condition (savanna) lost three times more soil, while the burned plot lost about ten times more than the vetiver system treatment. The researchers recommend the vetiver system with its distinctive characteristics to control soil erosion and to restore natural resources.

Several modeling studies (*e.g.*, Park, 2007; NRCS, 1996, 2001, & 2006) have been conducted to quantify sediment yields in different watershed across southern Guam.

Park (2007) developed a GIS-based soil erosion model of the Ugum watershed. The model combines the Universal Soil Loss Equation (USLE) with the capabilities of GIS to identify the maximum potential rate of soil loss within the entire Ugum watershed. The model has a 10-meter resolution. The results showed greatest erosion potential in badlands and in areas with steep slopes ($\geq 30°$). The mean sediment yield for badlands computed by Park (2007) was 460 tons/ha/yr (186 tons/acre/yr).

Studies by the Natural Resources Conservation Service (NRCS) estimated that the sediment yield of badlands was 600 tons/ha/yr (243 tons/acre/yr) in the Ugum Watershed (NRCS, 1996), 593 tons/ha/yr (240 tons/acre/yr) in the Fena Watershed (NRCS, 2001), and 321 tons/ha/yr (130 tons/acre/yr) in areas with 30–60 percent slopes in Sella Bay and Cetti Bay (NRCS, 2006).

2.4   Land Cover Change

The cause for the extensive savanna grasslands (primarily sword grass) found today in southern Guam is mainly attributed to repeated human-set fires over many years, as mentioned by various authors (Minton, 2006, Mueller-Dombois, 1998; Falanruw, 1976; Stone, 1970; and Fosberg, 1960). Natural fires on the island are generally considered rare now and in the past due to unfavorable ignition conditions (Minton, 2006). A recent paleoenvironmental study by Athens and Ward (2004) supports the idea that the forest was gradually replaced by savanna grasslands due to repeated man-made fires first evident at 4,3000 cal. B.P., suggesting initial human settlement of the island around this time. The results of this study (Athens and Ward, 2004) further indicate that the southern uplands were fully forested before the arrival of humans. A sharp decline in native forest is evident in the core data around 2,900 cal B.P. concurrent with a significant expansion of savannas; by 2,300 cal B.P. only remnant patches of native forest were left (Athens and Ward, 2004). However, Hunter-Anderson (2009) argues the human-caused savanna theory in favor of a geo-climatic-based theory.

The dynamics of fire and its effect on the evolution of savanna communities has been investigated by Minton (2006). His study suggests that the species composition changes due to burning; non-native species (mainly *Dicanthium bladhii* and *Pennisetum polystachion*) established in burned areas before the fire-intolerant native species like *Dimeria chloridiformis* could re-establish. Furthermore, the invasive grasses can increase frequency and intensity of fires, eventually superseding the native grass species (Minton, 2006). Besides the deleterious effect of fire on native savanna species, burning also significantly increases erosion rates: six times higher erosion rates compared to pre-burned conditions in the following wet season, and still twice as high after vegetation has fully grown back after 18 months of the fire (Minton, 2006).

Khosrowpanah *et al.* (2010) conducted a study about badland change in southern Guam. By comparing the extent of badlands in 1946 and 2006, the study revealed that about two thirds of today's badlands are older than 60 years, while a considerable amount has disappeared over the same time period; hence, the spatial extent of badlands is very dynamic.

A quantitative land cover change study for southern Guam was conducted by Wen *et al.* (2009). Land cover was derived from multi-date satellite Landsat imagery from 1973 (the oldest available satellite imagery for Guam) and 2001. According to Wen *et al.* (2009), the barren area in southern Guam decreased from 4.5 percent in 1973 to 3.6 percent in 2001. Grassland decreased

6

from 48.1 percent to 31.0 percent, while forest increased from 43.6 percent to 46.46 percent between 1973 and 2001, respectively. The resolution of the Landsat imageries ($\geq$ 30 m x 30 m) is suitable for a large scale land cover change analysis of southern Guam, but not for fine-scale changes focused on badlands like in this analysis.

2.5   *Management Practices*

Re-vegetation is costly and time-consuming, but attempts on a small scale have been made by several agencies on Guam. The Navy has successfully restored some badland areas in the Naval Ordinance around Fena Lake as shown in Figure 2 (Grimm, 2009). The National Park Service planted vetiver grass and sun hemp on test plots in the Asan Park a few years ago to evaluate their suitability for re-vegetation (Coffmann, 2010). Before the plants were fully established, the plots were vandalized, and the project then stopped. The Guam Department of Agriculture has planted many Acacia trees in badland areas in the Ugum Watershed in 1998 and in the Cotal Reserve in the Tarzan area to reduce erosion. The non-native Acacia trees have established but will be replaced by native trees such as *Calophyllum inophyllum, Cerbera dilatata*, and *Pandanus tectorius* in the near future (Crago, 2005). The Natural Resources Conservation Service (NRCS) successfully planted bahia grass and vetiver grass on bare saprolite (Doerge and Smith, 2008). All successful re-vegetation efforts required soil amendments (*e.g.*, increasing organic matter) because of the extremely poor soil quality of the badlands in southern Guam.

Figure 2. Restoration of badlands at the Naval Ordinance. Photos show badland with newly planted vetiver grass (left) and restored badland (right). *Photos courtesy of Dr. Anne Brooke, U.S. Navy.*

Chapter 3　Overview of Study Sites

3.1.　*Location*

Guam is the largest and southern-most island of the Mariana Archipelago in the Western North Pacific (Figure 3). The elongated island is about 48 kilometers (30 miles) long and 7 to 15 kilometers (4 to 9 miles) wide with a total area of 549 square kilometers (212 square miles). It is bordered by the Pacific Ocean on the east and the Philippine Sea on the west. The Mariana Trench lies about 400 kilometers (250 miles) southwest of Guam. Three study sites were selected in the central part of southern Guam (Figure 4). Views of badlands at each study site are shown in Figure 3. The selection of the study sites is described in Methods Chapter 4.1.
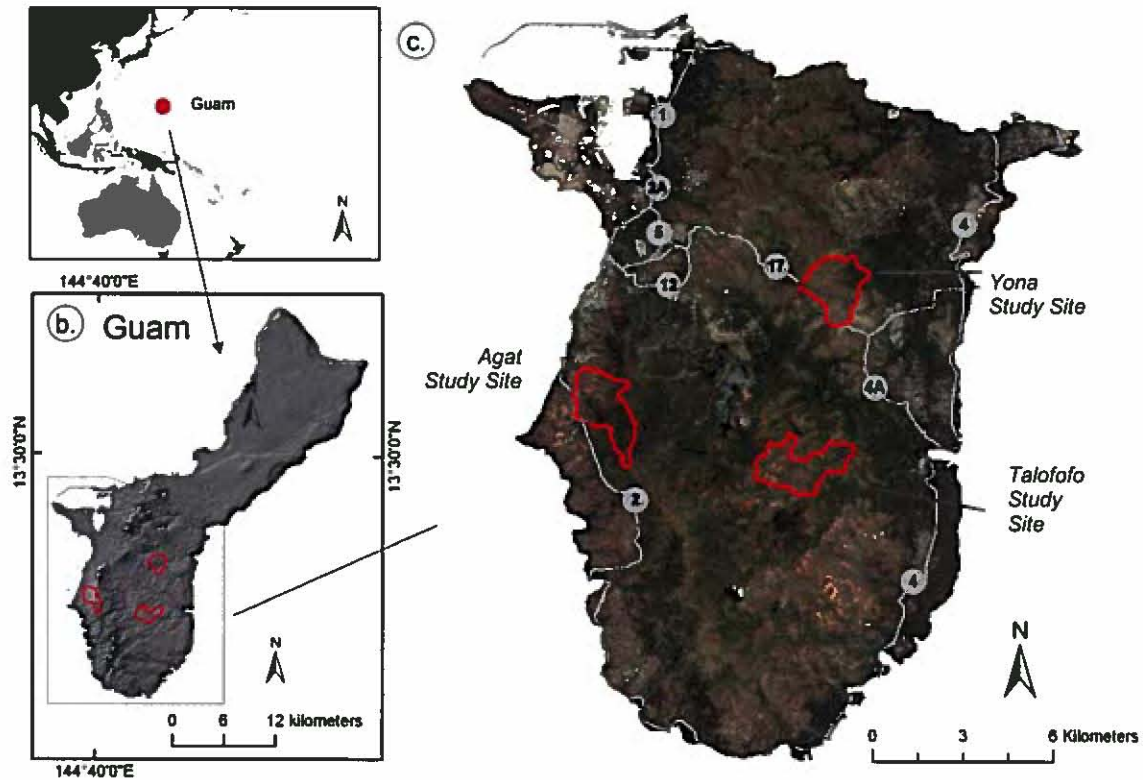
Figure 3. Maps of the study area; (a) regional map of the Western Pacific; (b) overview map of Guam with outline of study sites in red; (c) southern Guam with route network and outline of study sites in red.
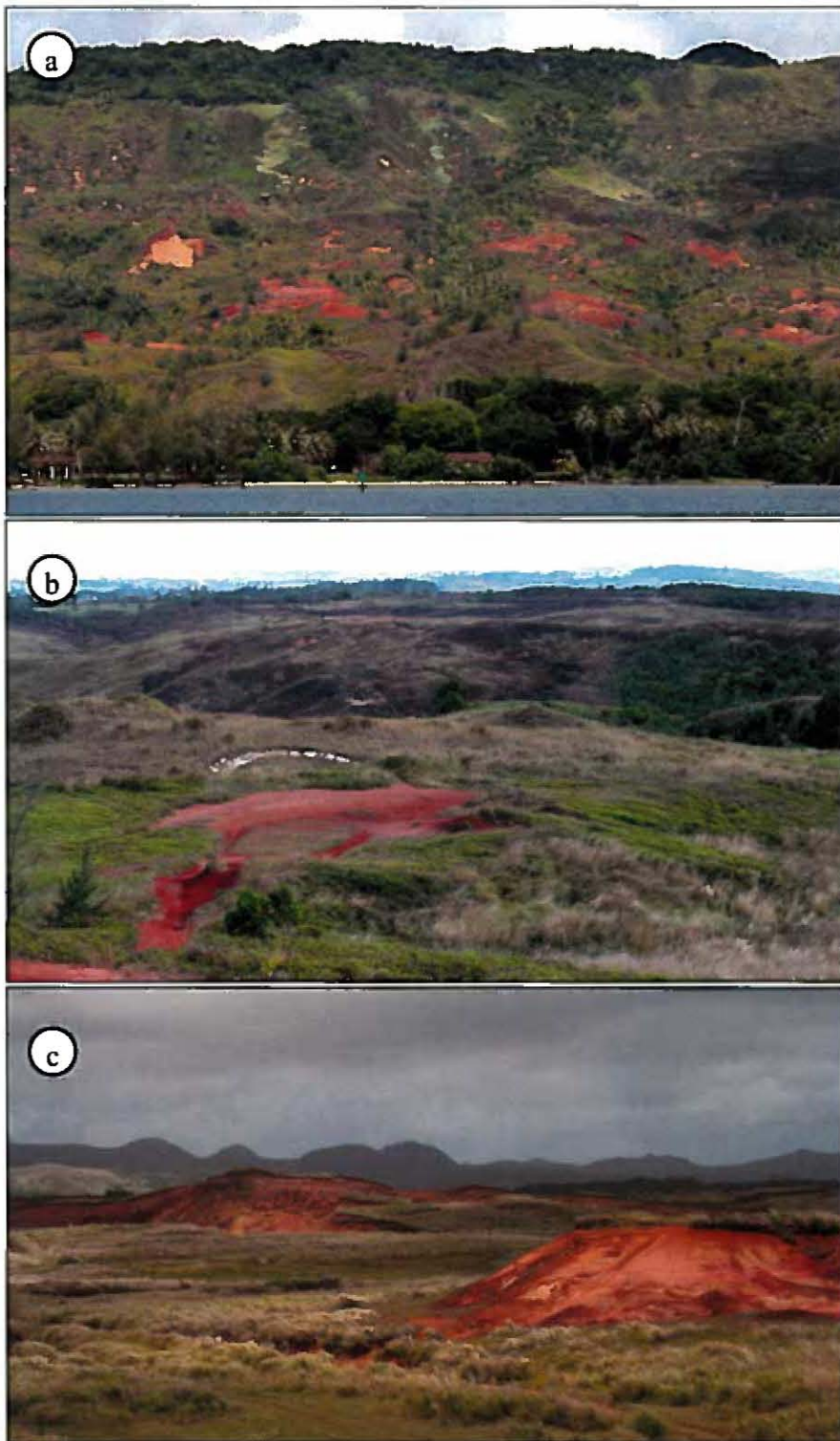
Figure 4. View of badlands of a. Agat study site; b. Yona study site; and c. Talofofo study site.

Agat Study Site

The Agat study site (13° 21' N, 144° 39' E) comprises the Ascola Silo Creek basin, a sub-basin of the Taclayag watershed. It is located in the village of Agat inland of Route 4 on the western side of the mountain ridge that stretches in north-south direction along southwestern Guam. This study site encompasses an area of 352 hectares (870 acres). The Ascola Silo Creek basin has four streams with a southwestern trend (Figure 5).

The Ascola Silo Creek is the longest stream in this basin and merges into the Taleyfac River outside the sub-basin which drains into the Philippine Sea. The Pagachao Creek and two unnamed streams are tributaries of the Ascola Silo Creek. The elevation ranges from 5 (16 ft) to 403 meters (1322 ft) with an overall relief of 398 meters (1306 ft).
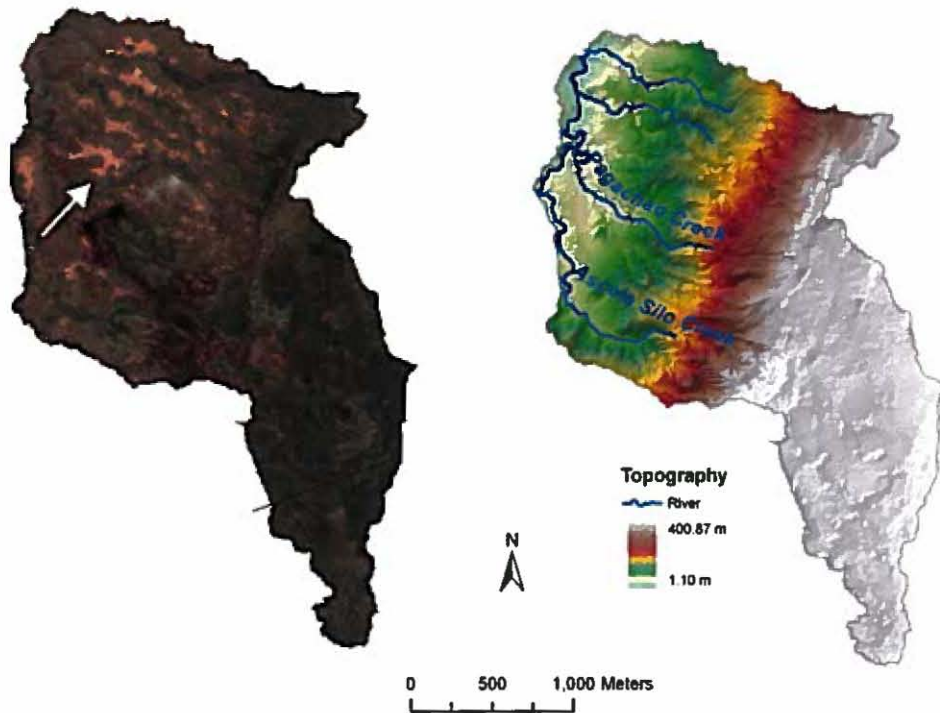
Figure 5. Satellite imagery with arrow pointing to a badland area (left) and topography with rivers (right) of the Agat study site.

Yona Study Site

The Yona study site (13° 23' N, 144° 44' E) comprises two adjacent smaller sub-basins which are both part of the Ylig watershed and border the Talofofo watershed to the south. This study site is located along Route 17 (Cross Island Road) on the east side of the mountain ridge and adjacent to the Tarzan sub-basin to the west. It is part of Yona Village.

Two streams flow into the Ylig River, which cuts through the study site on the northeastern part (Figure 6). The Ylig River, one of the major rivers on Guam, drains into the Pacific Ocean at Ylig Bay. This study site encompasses an area of 347 hectares (857 acres). The elevation ranges from about 9 (30 ft) to 267 meters (30 ft) with a relief of 258 meters (876 ft).

10
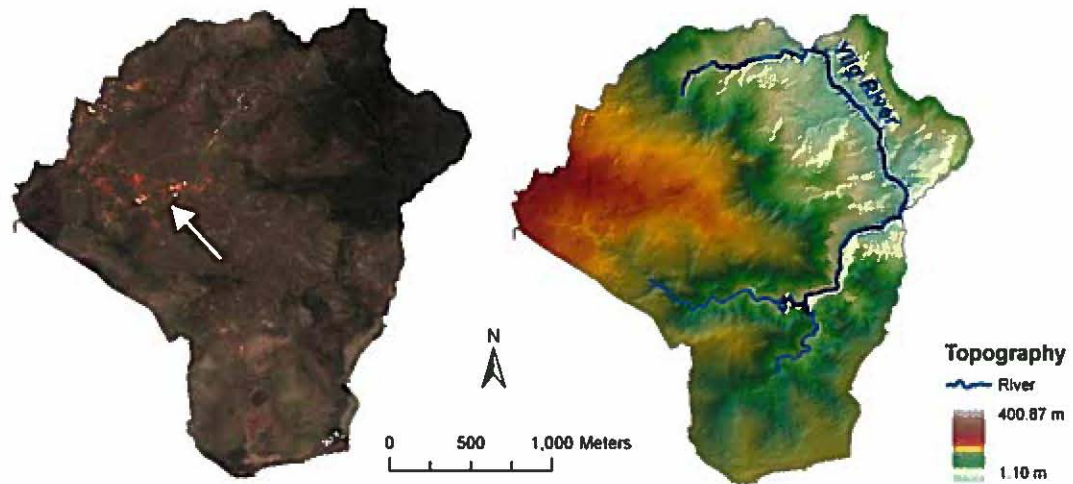
Figure 6. Satellite imagery with arrow pointing to a badland area (left) and topography with rivers (right) of the Yona study site.

Talofofo Study Site

The Talofofo study site (13° 20' N, 144° 43' E) also comprises two adjacent sub-basins. Both sub-basins are part of the Talofofo watershed, the largest drainage system on the island. This site is located inland about two kilometers (1.5 miles) southwest of Talofofo Village, on the east side of the mountain ridge. It can be reached through the Babulao Road.

The Malaja Stream merges into the Sarasa River, which converges with the Talofofo River on the northeast border of the sub-basin (Figure 7). The smaller sub-basin of the study site has a small stream flowing into the Sagge River, which also drains into the Talofofo River. The rivers have a northeasterly trend.

This study site encompasses an area of 307 hectares (759 acres). The elevation ranges from about 9 meters (30 ft) to 142 meters (466 ft) with an overall relief of 133 meters (436 ft).
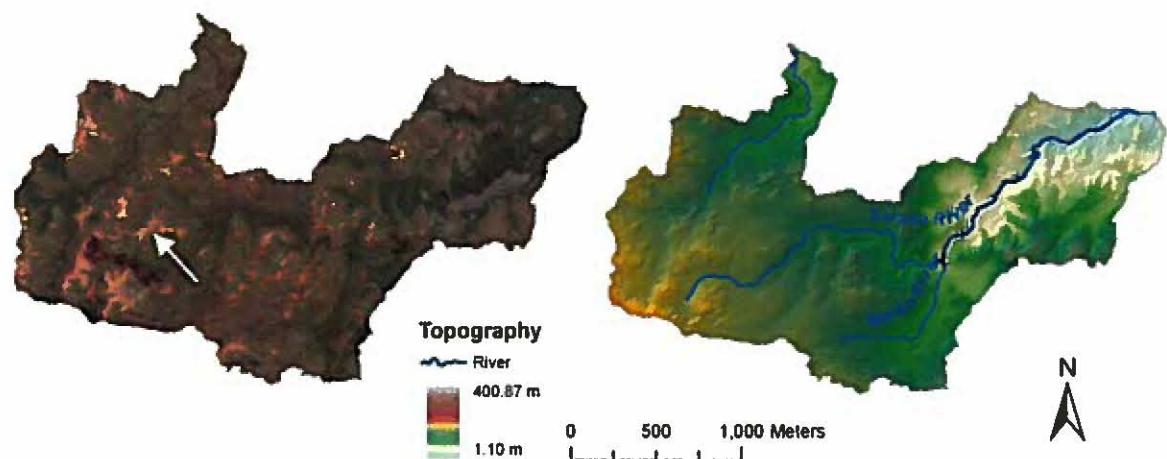
Figure 7. Satellite imagery with arrow pointing to a badland area (top) and topography with rivers (bottom) of the Talofofo study site.

11

3.2. Climate

The mean annual temperature is 27° Celsius (81° Fahrenheit), with little seasonal variation. Guam has two distinct seasons, a dry (January–June) and a wet season (July–December). The mean annual rainfall on the island ranges from 2160 mm to over 2920 mm (85 in. to over 115 in.), depending on the topography. About 70 percent of rain falls during the wet season (Lander and Guard, 2003). The inter-annual variability of Guam's rainfall is strongly related to the irregular recurrence of episodes of El Nino Southern Oscillation (Lander 1994). The year following El Nino is usually very dry (Lander and Guard, 2003). The annual rainfall distribution map for southern Guam (Figure 8) shows the strongest rainfall gradients along the western and southern mountains (Lander and Guard, 2003), where the study sites are located. The Agat and Talofofo study sites have an average annual rainfall of over 2800 mm (110 in.), while the Yona study site gets between 2400 mm and 2550 mm (95–100 in.) rain annually (Figure 8).
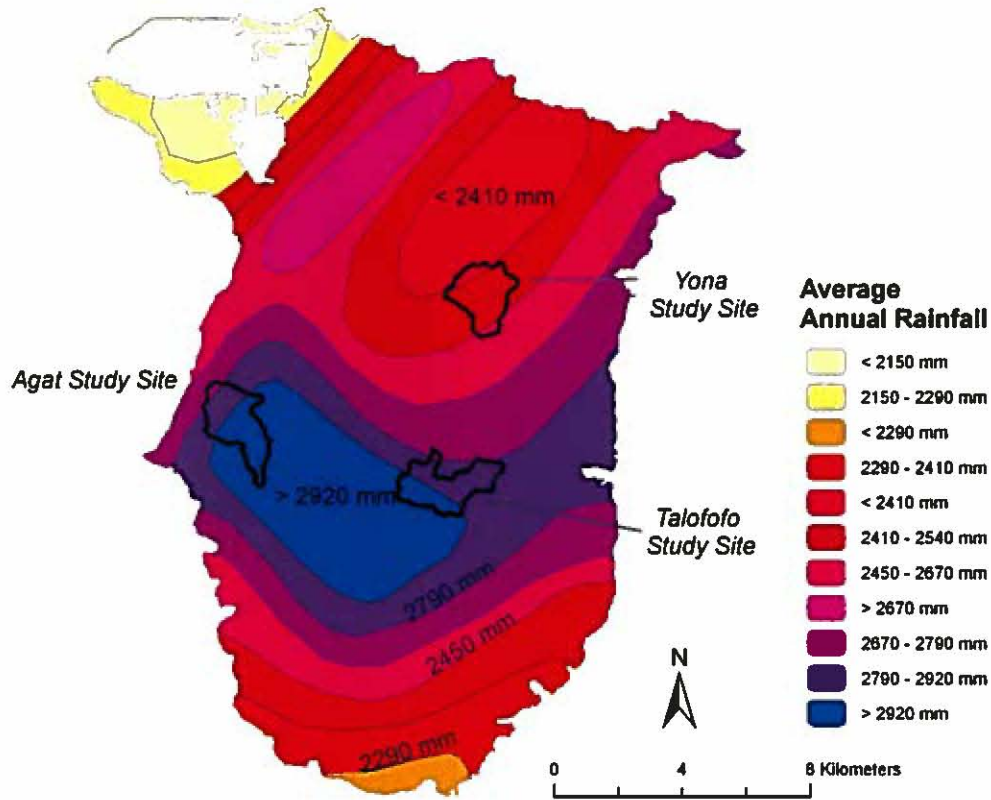
Figure 8. Average annual rainfall distribution in southern Guam. Study sites are outlined in black. *Data Source: www.hydroguam.net.*

During the wet season, the wind generally has a southeasterly direction (or southwest direction during occasional monsoons), whereas during the dry season trade winds, predominantly from east-northeast, are prevailing (Lander 2009). Guam is also frequently subjected to tropical cyclones because of its location in the world's most active ocean basin (Lander, 1994). During the period 1945–2007, 183 tropical cyclones (maximum sustained winds ≥34 knots) passed within 180 nautical miles (nm), 75 of them reached typhoon intensity (Kottermair and Olsen, unpubl.). Although only passing by shortly, tropical cyclones contribute about 12 percent to Guam's average annual rainfall (Lander, 1994). During a direct eye passage of a typhoon, the island experiences extremely high short-term rainfall rates that can exceed 18 centimeters (7 in.) an hour as encountered during Typhoon Pongsona in 2002 (Lander and

Guard, 2003). A list of the major typhoons between 1991 and 2007 is presented in Table 1. Climate change has affected Guam in temperature rise of about 0.23° Celsius (0.42° F) per decade since the 1950s (Lander, unpub.).

Table 1. List of typhoons (max. sustained wind speed [VMax] ≥64 knots) from 1991–2007 passing Guam within 180 nautical miles.

Year	Month	Day	VMax[1]	Distance	Name
1991	5	10	110	180	Walt
1991	9	20	85	180	Mirelle
1991	11	4	130	180	Seth
1991	11	27	150	60	Yuri
1992	8	29	120	180	Omar
1992	10	21	65	60	Brian
1992	11	3	100	120	Elsie
1992	11	22	105	180	Gay
1992	11	18	75	120	Hunt
1994	10	25	115	180	Wilda
1994	11	3	95	180	Zelda
1996	9	25	125	180	Yates
1996	11	7	90	180	Dale
1997	4	17	110	180	Isa
1997	10	17	140	180	Ivan
1997	11	2	155	180	Keith
1997	12	17	145	180	Paka
2002	7	5	105	180	Chataan
2002	7	10	95	120	Halong
2002	12	8	130	60	Pongsona
2003	4	15	125	180	Kujira
2004	6	28	65	180	Tingting
2004	8	23	155	120	Chaba
2004	10	20	95	180	Nock-ten
2005	8	31	90	180	Nabi
2007	4	3	75	180	Kong-rey

3.3. Geology

Guam is divided into two distinct geologic zones, which are separated by a major fault zone stretching from Adelup Point to Pago Bay in central Guam. The northern half of the island is comprised of an elevated limestone plateau with steep cliffs and underlain by volcanic rock that protrudes to the surface at Mount Santa Rosa and Mataguac Hill. The high permeability of the limestone allows water to percolate quickly into the ground before runoff is generated. For this reason, no rivers form in the north. In contrast, the southern half is primarily of volcanic origin with some peaks and ridges capped with limestone and characterized by dissected volcanic uplands and an extensive stream network.

The three volcanic formations that build the base of the island are the Facpi, Alutom, and Umatac Formation (Figure 9). Facpi, the oldest formation, dates back to the Eocene (Reagan and Meijer, 1984) and underlies the Umatac Formation over most of the southern part of southern Guam; it only protrudes at the very southwestern part around Facpi point, after which the formation is named. The Facpi Formation is characterized by mafic lava flows, pillow basalt, dikes, and in the upper layers tuffaceous shale and sandstone (Tracey *et al.*, 1964). Dikes are more resistant to erosion than the surrounding rock and are easily recognized when exposed. Most of the Umatac formation belongs to the Bolanos Pyroclastic Member with small patches of the Dandan Flow Member, remnants of the last volcanic eruption during the Miocene age. The Bolanos Pyroclastic Member consists of thick-bedded to massive tuff breccia, thin-bedded tuffaceous sandstone, and lenses of volcanic conglomerate. The tuff breccia is a conglomerate of basaltic and andesitic rock, tuffaceous shale, and Maemong Limestone fragments in a sandy

13

tuffaceous matrix (Tracey *et al.*, 1964). Tuffaceous sandstone is prevalent in the dissected uplands between Ugum and Inarajan River and exposed in badlands (Tracey *et al.*, 1964). The Alutom Formation consists primarily of well-bedded fine-grained water-laid tuffaceous shale, which usually weathers to small (≤2.5 cm in diameter), rounded polygons when exposed; also common are tuffaceous sandstone, conglomerate, and breccia. Lava flows with pillow structures occur within the reworked pyroclastic deposits and are highly weathered in most outcrops (Tracey *et al.*, 1964).

Guam's proximity to the Marianas Trench, the deepest subduction zone in the world, makes it seismically very active. The island has experienced several very strong earthquakes in the past (Table 2), but also many earthquakes of lesser magnitude occur frequently.

Table 2. List of large earthquakes from 1940–2007 listed by date, location, and magnitude. *Source: NGDC, 2010.*

Year	Month	Day	Latitude	Longitude	Magnitude
1975	11	1	13.843	144.754	6.1
1990	4	6	15.125	147.596	7.5
1993	8	8	12.982	144.801	7.8
1997	4	24	13.986	144.901	6.5
2001	10	13	12.686	144.980	7.0
2002	4	27	13.088	144.619	7.1
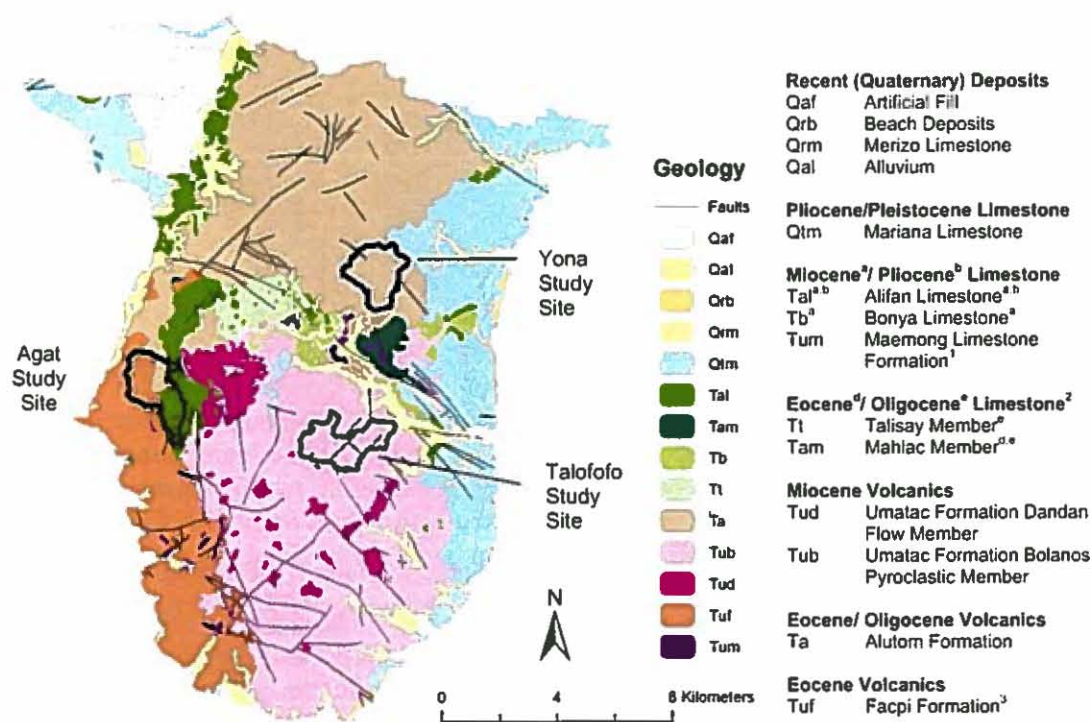
Data Source: Tracey et al. (1964) - outlines of geologic units and faults downloaded from (epochs) revised after Siegrist and Reagan (2008); Any other revisions by Siegrist and Reagan (2008) not included here.
    [1] in Tracey et al. (1964) mapped as Umatac Formation Maemong Limestone Member
    [2] in Tracey et al. (1964) mapped as Miocene/ Pliocene Limestone
    in Tracey et al. (1964) mapped as part of Umatac, revised by Siegrist and Reagan (2007)

Figure 9. Geologic map with faults of southern Guam. Study sites are outlined in black.

Agat Study Site

Most of this study site (45.7%) on the lower western part is classified as the Facpi Formation (Tuf), while a smaller area (14.8%) on the steeper mountain side is classified as the Alutom formation (Ta) (Table 3). The mountain ridge and upper plateau is capped by Alifan Limestone (Tal). A very small area of 0.1 ha within the study site is Maemong Limestone (Tum).

Table 3. List of geologic units and respective area (ha and %) at the Agat study site.

Geology	Area	
	ha	%
Ta	52.1	14.8
Tal	139.0	39.5
Tuf	160.7	45.7
Tum	0.1	<0.1
Total	351.9	100.0

Yona Study Site

Almost the entire study site (97.1%) belongs to the Alutom Formation (Ta) (Table 4). A small part on the very northeast of the study site is classified as the Mariana Limestone (Qtm).

Table 4. List of geologic units and respective area (ha and %) at the Yona study site.

Geology	Area	
	ha	%
Ta	297.8	97.1
Qtm	8.8	2.9
Total	306.64	100.0

Talofofo Study Site

Almost the entire study site (98.5%) belongs to the Umatac Formation and is classified as the Bolanos Pyroclastic Member (Tub) with two small patches of the Dandan Flow Member (Tud) on the western border (Table 5). A very small part (1.5%) on the northeastern border is classified as Alluvium (Qal).

Table 5. List of geologic units and respective area (ha and %) at the Talofofo study site.

Geology	Area	
	ha	%
Qal	3.1	0.9
Tub	338.9	97.7
Tud	4.7	1.4
Total	346.7	100.0

3.4. *Soils*

Soils generally follow the bedrock type (volcanic soils in southern Guam and limestone soils in northern Guam) but not the specific rock units (Young, 1988). In the soil survey of Guam, Young (1988) delineated eight general map units and 55 detailed soil map units for Guam. The map units are named after one or more major kinds of soil within the unit; most detailed map units are further differentiated by topographic characteristics. More than half of the detailed soil map units occur within the study sites. The most common soil series within the study sites are Akina, Agfayan, and Togcha (Figure 10).

The soil of the Akina series commonly found on volcanic uplands is very deep, well drained, and moderately slowly permeable with slopes up to 45 degrees (Young, 1988). It formed from tuff and tuff breccia. The soil of the Togcha series has similar properties to that of the Akina series, but it formed in slope alluvium and is less steep. The soil of the Agfayan series is very shallow and shallow to strongly weathered tuff. It is more fertile than the Akina series.

Badlands are not considered a separate soil series as they are very patchy and difficult to map. However, they are usually associated with the Akina series. Young (1988) mapped them as either Akina-Badland association or Akina-Badland complex.
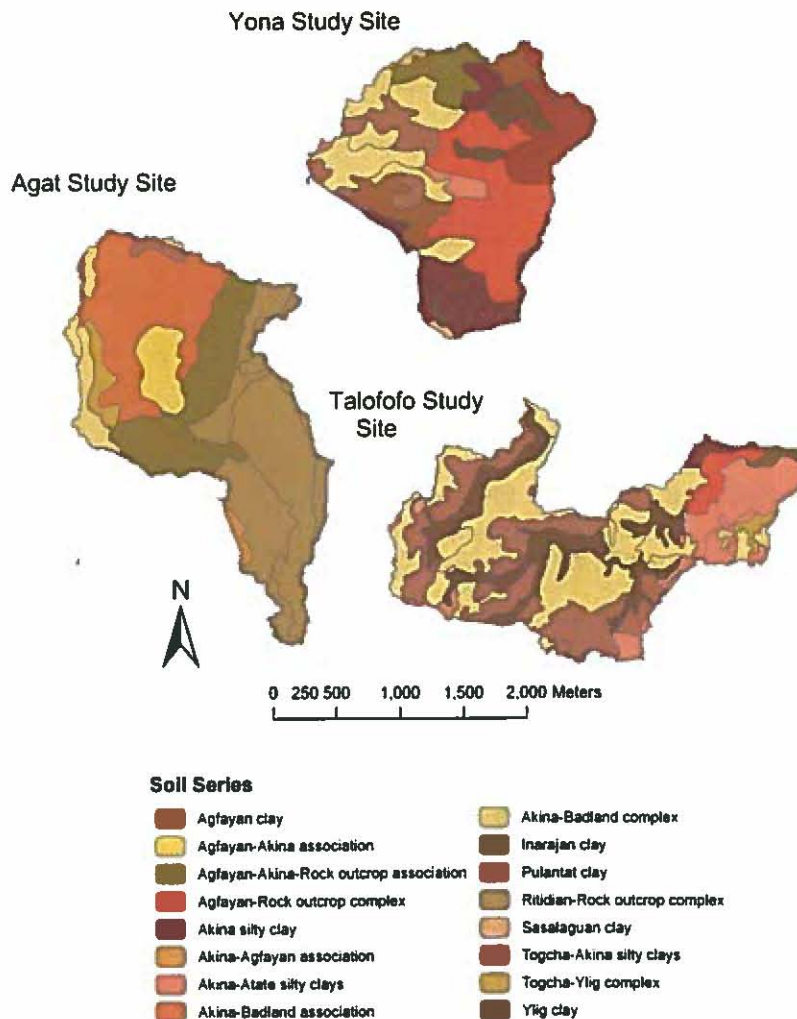
Figure 10. Map of soil map units of study sites.

16

Agat Study Site

The soils on the limestone cap on the ridge line belong to the Ritidian-Rock outcrop complex, which covers almost 40 percent of the study site (Table 6). The second most prevalent soil map unit is the Akina-Badland association (24.8%), followed by the Agfayan-Akina-Rock outcrop association (18.9%). Only a small part of this study site is associated with Togcha.

Table 6. List of soil map units and respective area (ha and %) at the Agat study site.

Soil Mapping Unit	Area	
	ha	%
Agfayan-Akina-Rock outcrop association	66.4	18.9
Akina-Agfayan association	3.8	1.1
Akina-Badland association	87.4	24.8
Akina-Badland complex	19.7	5.6
Ritidian-Rock outcrop complex	139.4	39.6
Togcha-Akina silty clays	5.5	1.6
Togcha-Ylig complex	10.0	2.8
Total	351.9	100.0

Yona Study Site

The majority of the soils in this study site are classified as the Agfayan-Rock outcrop complex with 24.5 percent followed by the Akina-Badland complex with 18.0 percent (Table 7). More than half the soil map units in this study site belong to various clay soils; *e.g.*, Akina silty clay or Pulantat clay.

Table 7. List of soil map units and respective area (ha and %) at the Yona study site.

Soil Mapping Unit	Area	
	ha	%
Agfayan clay	26.0	8.5
Agfayan-Akina-Rock outcrop association	18.9	6.2
Agfayan-Rock outcrop complex	75.0	24.5
Akina silty clay	45.0	14.7
Akina-Atate silty clays	7.5	2.4
Akina-Badland complex	55.1	18.0
Pulantat clay	34.4	11.2
Sasalaguan clay	3.3	1.1
Togcha-Akina silty clays	25.0	8.2
Ylig clay	16.6	5.4
Total	306.6	100.0

Talofofo Study Site

By far the most common soil map unit in this study site is the Akina-Badland complex with more than 35 percent. The Togcha-Akina silty clays comprise more than one fourth of the site (Table 8). About 16 percent Ylig clays and about 15 percent Akina-Atate clays are found in this area.

Table 8. List of soil map units and respective area (ha and %) at the Talofofo study site.

Soil Mapping Unit	Area	
	ha	%
Agfayan-Rock outcrop complex	11.4	3.3
Akina silty clay	5.1	1.5
Akina-Atate silty clays	53.3	15.4
Akina-Badland complex	123.7	35.7
Inarajan clay	3.9	1.1
Togcha-Akina silty clays	88.8	25.6
Togcha-Ylig complex	3.9	1.1
Ylig clay	56.7	16.3
Total	346.7	100.0

3.5. Land Use

Agat Study Site

Most of the Agat study site is zoned agricultural. A small area on the very eastern boundary is federal property (Ordnance Annex). About 40 percent of the study site in the northern and northwestern part is privately owned, the remaining is publicly owned. Besides a few houses along the western boundary of the study site, the area is not developed and only accessible by foot. Satellite imagery and field observation indicate that this area is not used for off-roading. Highly eroded steel remnants, maybe relics from WWII or from off-roaders, in some of the badlands observed during field visits, however, indicate some kind of human activity in the past.

Yona Study Site

The Yona study site is privately owned and zoned agricultural. About two percent of the study site is part of the larger Cotal Conservation Reserve, which is located on the very western side of the study site and extends northward of Route 17. The conservation area is managed by the Guam Division of Aquatic and Wildlife Resources (GDAWR), Department of Agriculture. GDAWR has planted many Acacia trees as part of their reforestation program.

A small section is zoned hotel, which belongs to the Windward Hills Country Club (before 1995 called the Takayama Golf Club), the oldest golf course on the island, which opened in 1951. The golf course extends beyond the study site to the southeast. Another golf course was planned at the study site in the early 1990s. A gravel road was already built when the project was stopped due to the economic downturn in Japan. This road is about two kilometers long and stretches from Route 17 across the study site to Ylig River. Most of the now dirt road is still visible on current satellite imagery. The western part of this study site is a popular recreational area for hikers and off-roaders (Figure 11). The trail to the Tarzan Falls starts on the study site but

then veers off to the west into the Tarzan sub-basin. Off-roading is very popular in this area likely because of its easy access. A large network of tracks on the western half of the study site connects major badland areas. Most of these badlands are highly eroded with deep gullies. Most gullies observed in this area are likely the result of frequent off-road vehicle (ORV)-use.

Figure 11. Off-roaders at the Yona study site.

Talofofo Study Site

The Talofofo study site is zoned agricultural. The majority of land (91%) belongs to private land owners. Only about 9 percent on the northern and southeastern part belongs to the Government of Guam. Six separate areas were at some point farmed. According to satellite imagery and field observations none of these fields are cultivated at present; in fact, all of the farm fields were overgrown during field visits in 2010.

3.6. Land Cover

The land cover of Guam is approximately 48 percent forest, one third grass and shrub lands, 18 percent urban areas, and one percent barren lands (Donnegan *et al.*, 2004). The forested area consists of about 70 percent limestone and thirty percent volcanic, ravine forest. Guam's present vegetation is a result of several factors, including tropical cyclones, arson, erosion, invasion of introduced weeds and feral ungulates, past military actions, and logging (Donnegan *et al.*, 2004).

The vegetation of the southern, volcanic part of Guam is characterized by a mix of grassland (savanna) and patches of forest (Figure 12 and 13). The savanna comprises a mosaic of Miscanthus grasslands (Miscanthus floridulus, sword grass), badlands, Dimeria and mixed grass lands (primarily Dimeria chloridiformis, an endemic tuft grass found in more level areas), Phragmites wetlands (Phragmites karka, found in water-logged area), and savanna shrub lands (Bell *et al.*, 2002).

19

Land Cover

- Bare Land
- Cultivated Crops
- Developed, High Intensity
- Developed, Open Space
- Estuarine Emergent Wetland
- Estuarine Forested Wetland
- Estuarine Scrub/Shrub Wetland
- Evergreen Forest
- Grassland/Herbaceous
- Open Water
- Palustrian Aquatic Bed
- Palustrine Emergent Wetland
- Palustrine Forested Wetland
- Palustrine Scrub/Shrub Wetland
- Pasture/Hay
- Scrub/Shrub
- Unconsolidated Shore

Agat Study Site

Yona Study Site

Talofofo Study Site

N

0   4   8 Kilometers

Figure 12. Map of land cover of southern Guam. Land cover classification is based on the 2006 QuickBird satellite imagery (NOAA, 2009).
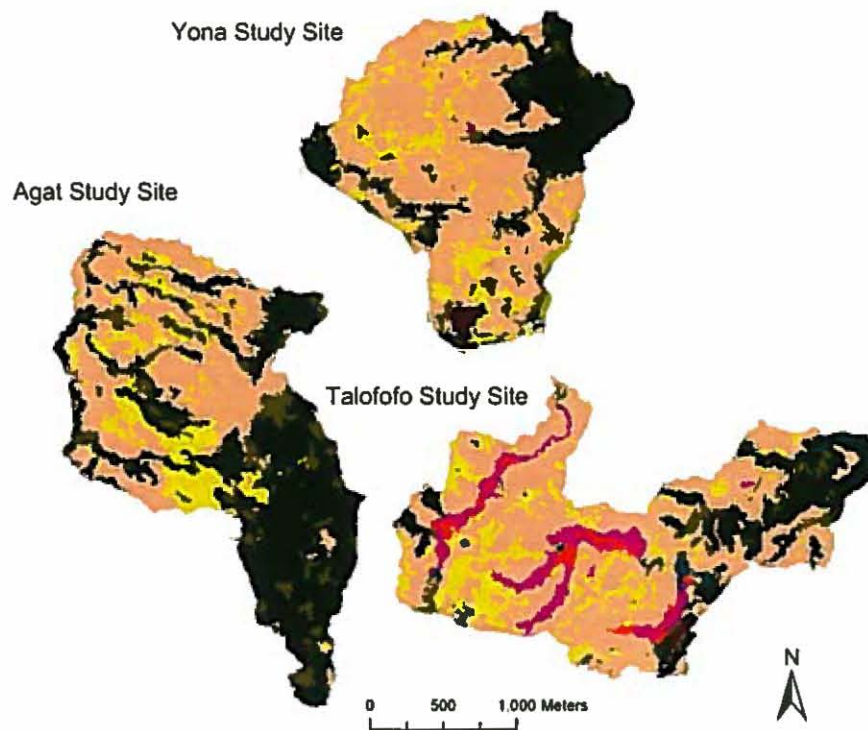
Figure 13. Map of land cover of the study sites. Land cover classification is based on the 2006 QuickBird satellite imagery (NOAA, 2009).

Agat Study Site

The lower elevation of this study site is mostly savanna (grassland) with ravine forest and shrubs along the stream valleys, while the limestone ridge is a mix of shrub and limestone forest (Table 9). About 0.3 percent is considered developed. Burned areas and badlands, both classified as bare lands, comprise more than 10 percent of this study site.

Table 9. List of land cover classes and respective area (ha and %) at the Agat study site.

Land Cover	Area	
	ha	%
Bare Land	36.5	10.4
Developed, High Intensity	0.4	0.1
Developed, Open Space	0.6	0.2
Scrub/Shrub	45.4	12.9
Grassland/Herbaceous	138.6	39.4
Evergreen Forest	130.4	37.0
Total	351.9	100.0

Yona Study Site

The majority of the land cover in this study site is classified as savanna with 59.3 percent, followed by forest with 21.0 percent and scrub with 7.5 percent (Table 10). More than 9 percent is considered bare lands. Less than 2 percent is developed and less than 1 percent is cultivated. A negligible area (less than 0.2%) is classified as open water and palustrine emergent wetland.

Table 10. List of land cover classes and respective area (ha and %) at the Yona study site.

Land Cover	Area	
	ha	%
Scrub/Shrub	22.9	7.5
Grassland/Herbaceous	181.8	59.3
Bare Land	28.0	9.1
Evergreen Forest	64.8	21.2
Open Water	0.4	0.1
Palustrine Emergent Wetland	0.1	<0.1
Developed, Open Space	4.4	1.4
Developed, High Intensity	1.2	0.4
Cultivated Crops	3.0	1.0
Total	306.6	100.0

Talofofo Study Site

The majority of land cover, as in the other two study sites, consists of savanna (59.5%), followed by forest (13.5%) (Table 11). Bare land constitutes the third most common land cover type with almost 12 percent. More than 10 percent of this study site is classified as palustrine (non-tidal) wetland (emergent 5.8%, scrub/shrub 3.2%, and forested 1.2%).

Table 11. List of land cover classes and respective area (ha and %) at the Talofofo study site.

Land Cover	Area	
	ha	%
Bare Land	41.5	12.0
Evergreen Forest	46.7	13.5
Scrub/Shrub	14.3	4.1
Palustrine Emergent Wetland	20.1	5.8
Grassland/Herbaceous	206.5	59.5
Open Water	0.1	<0.1
Palustrine Forested Wetland	4.2	1.2
Palustrine Scrub/Shrub Wetland	11.2	3.2
Developed, High Intensity	0.1	<0.1
Cultivated Crops	2.0	0.6
Total	346.7	100.0

Chapter 4   Methods

The study addresses badland dynamics in terms of spatio-temporal change, terrain attributes, landscape metrics, and soil characteristics. The first three analyses were performed using a GIS, and the latter was performed using field sample analysis and soil laboratory methods. Results from the spatio-temporal change analysis were evaluated with respect to natural and human impact on badland dynamics.

Spatio-temporal change of badlands was investigated at three study sites in southern Guam. Badland change over time was based on aerial photographs from 1946 and 1994 and satellite imagery from 2006. Landscape metrics (total area, number of patches and mean patch size) were determined using a free GIS-program called V-LATE (LARG, 2005). The relationship of badlands and terrain attributes (elevation, slope, aspect, geology, and soil) was examined by overlaying the change detection results with the different terrain layers, which were derived from recent LiDAR data (except geology and soils). A flow chart of the GIS analysis is presented in Figure 14.

Basic physical and chemical soil properties were determined using field samples collected during the 2010 dry season. The soil sample analysis was performed in the Soil Laboratory of the University of Guam.
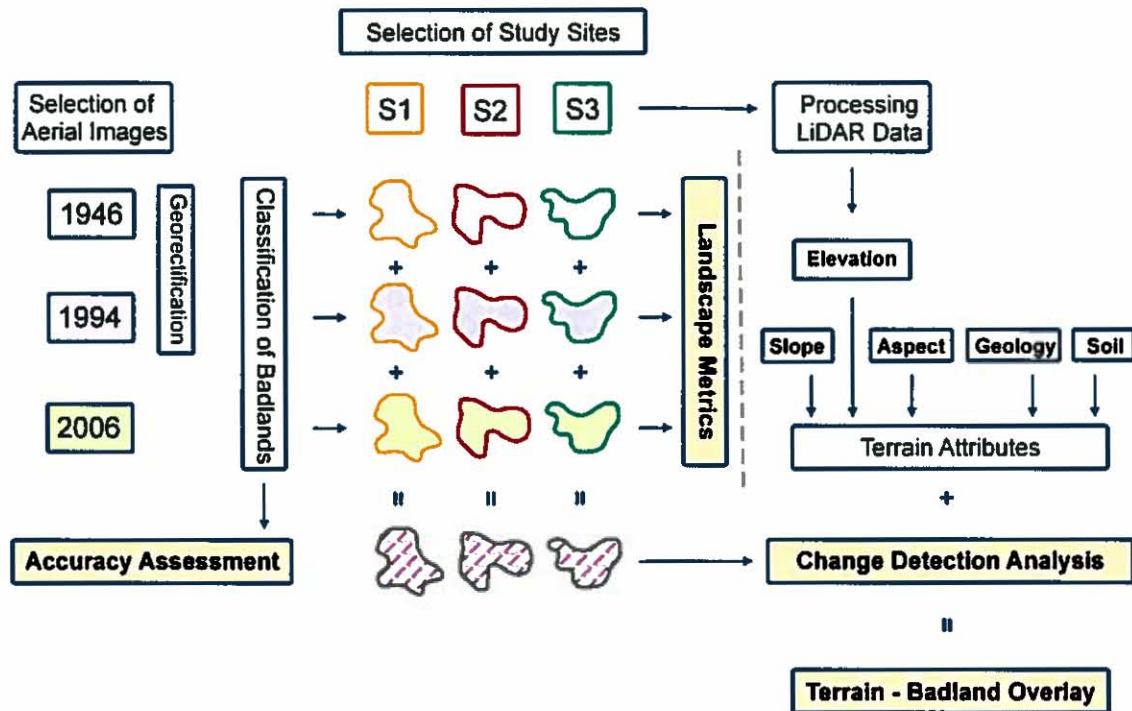
Figure 14. Workflow of the GIS analysis.

4.1.   Selection and Delineation of Study Sites

Three separate study sites were chosen to compare factors impacting badlands in southern Guam. Most badlands in southern Guam occur in the undeveloped, dissected inland. Although largely undeveloped, humans use these inland areas for farming and recreational purposes like hunting, off-roading, and hiking.

The largest human impact on soil erosion in general and badlands in particular is attributed to off-roading and mis-managed farming practices. Study sites were chosen that are representative of the land uses impacting badlands the most; one study site was chosen with no (or little) human impact for comparison. Soil erosion from construction without proper erosion prevention measurements is also a big problem on the island, but—since this issue is not directly related to badland development—it is not further considered here.

In addition to land use, the selection criteria for the study sites were (in order of priority) a relative high occurrence of badlands; availability and quality of historical aerial photographs; accessibility for field work; and comparable size of sub-basins.

Study site boundaries were based on sub-basin (or sub-watershed) boundaries. Sub-basins were delineated based on a five-meter–resolution Digital Elevation Model (DEM) using the ArcGIS ArcHydro Extension. The DEM was derived from 2007 LiDAR data.

4.2.   Data Sources and Image Processing

The archives of the Micronesian Area Research Center and the Bureau of Statistics and Plans, Government of Guam, were searched for available historical aerial photographs. A list (Table 12) was compiled to compare all available aerial photographs and to select the most suitable ones for this analysis. Special attention was given to the scale and resolution of the images and the quality of information they yield: easily identifiable badlands, coverage of study area, and clear (cloud-free) image. The selected historical aerial photographs were from 1946 and 1994. The selected, most recent imagery was from 2006.

Table 12. List and description of all available aerial imagery covering Guam.

Type	Year	Date Collected	Color/ Bands	Resolution	Comment
QuickBird Satellite	2006	May 05–Mar 06	Multi-spectral	2.4 m	
	2005	Nov 03–Feb 05	pan-sharpened	0.6 m	
IKONOS Satellite	2004	Nov 02–Jan 04	Multi-spectral	4 m	
	2001		Multi-spectral	4 m	
			panchromatic	1m	
Landsat TM Satellite	2001	15 Mar 2001	Multi-spectral	30 m	
Color Vertical Aerial Photograph	1994	Nov 1994	Color hardcopy	1200 dpi	
Panchromatic Orthophotos	1993	~ April 1992–May 1993	Scanned b/w hardcopy	0.6 m	Scale: 1: 4,800
Vertical Aerial Photograph	1986	1985–1986	Scanned b/w hardcopy		
Ortho-rectified	1975		Scanned b/w hardcopy	23cm x 23 cm	
Landsat MSS Satellite Image	1973	14 Nov 1973	multispectral	80 m	
Vertical Aerial Photograph	1970		Scanned b/w hardcopy		
	1964		Scanned b/w hardcopy		
	1953	26, 28 Jan 1953	Scanned b/w hardcopy	600 dpi (TIFF)	Mission No. VU-5-139 by U.S. Navy Scale: 1: 24,000
	1946	1 Feb 1946	Scanned b/w hardcopy	600 dpi (JPEG)	#__-3RS-M-30ENG-1FEB46-MI" Sheet numbers: 63–120

2006 Satellite Imagery

The QuickBird satellite imagery (QB06), acquired between 21 May 2005 and 31 March 2006 by DigitalGlobe®, provided the most current satellite image of Guam. The panchromatic (black-and-white) imagery has a 0.6-meter resolution and the multispectral imagery (blue, green, red, near-IR), collected at the same time, a 2.4-meter resolution. A fusion of the panchromatic and the multi-spectral imagery, known as pan-sharpened imagery, was used for this analysis. The pan-sharpened imagery has the advantage of having a high resolution (from the panchromatic imagery) and color-information (from the multi-spectral imagery).

1994 Color Aerial Photographs

The 1993 panchromatic orthophoto project also included color vertical aerial photographs, acquired in November 1994. These were, however, not ortho-rectified. At first, the orthophotos were selected as part of the three-date analysis and classified, but the 'salt-and-pepper'—appearance of the orthophotos affected the badland classification and many pixels were misclassified. For this reason and that badlands are easier to depict in color photographs, the color aerial photo series was chosen for this study. In addition, the average scale of approximately 1: 4,800 is comparable to that of the orthophotos. Many areas are covered in more than one sheet. The sheets with the least cloud cover and with the study site closest to the center were selected; thus, sheets *3590*, *3580*, and *3342* were selected for Agat, Yona, and Talofofo, respectively. Because only hard copies (10 inch x 10 inch sheets) of these photographs were produced by the contractor, these sheets were scanned at 1200 dots per inch using an EPSON 10000XL flatbed scanner and saved them in TIFF format.

1946 Panchromatic Aerial Photographs

The panchromatic vertical aerial images were taken by the U.S. military on 1 February 1946 and provide the oldest aerial photographs available. The average scale is about 1: 32,000. Each image is inscribed with "GC12B.#__-3RS-M-30ENG-1FEB46-MI". The photos are numbered 63 through 120. Most areas are covered in more than one sheet. The sheets covering the study sites the best were *111*, *85*, and *83* for the Agat, Yona, and Talofofo study site, respectively. The hardcover images (25.5 cm x 21.47 cm) were scanned and saved as JPEG files at 600 dots per inch by the Micronesian Area Research Institute at the University of Guam. The images were enhanced in PHOTOSHOP to adjust contrast and gradient differences across photographs.

Georeferencing

Georeferencing describes the process of assigning a spatial location (coordinates) to a data set, *e.g.* an aerial photograph. A georeferenced data set can then be directly compared to other geographical data in a GIS.

For this study, a total of six aerial photographs from the 1946 and 1994 series (Figure 15) were georeferenced to the QB06 imagery, a so-called image-to-image registration, using ArcGIS 9.3 (Figure 16). Normally, prominent features like road intersections or corner of buildings found in both sets of images are used as ground control points (GCP). The study sites, however, are largely undeveloped and lack permanent structures (*e.g.*, impervious surfaces) that can be identified in both sets of images as GCPs. Therefore, few ideal GCPs were selected close to each study site and additional GCPs inside each study site, which were based on distinct features. The most distinct features were found in sharp edges of some badlands that apparently have not changed over the study period and could easily be depicted in both sets of images.
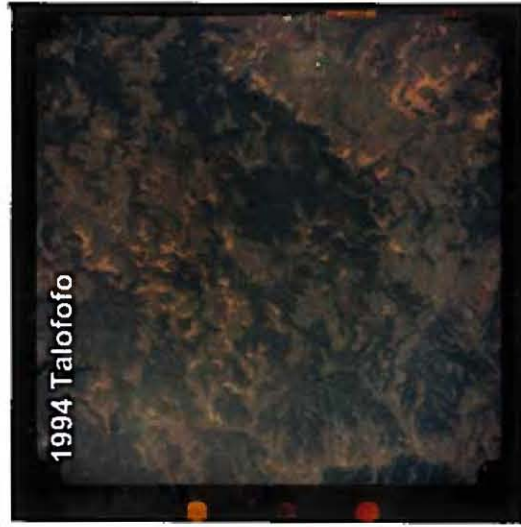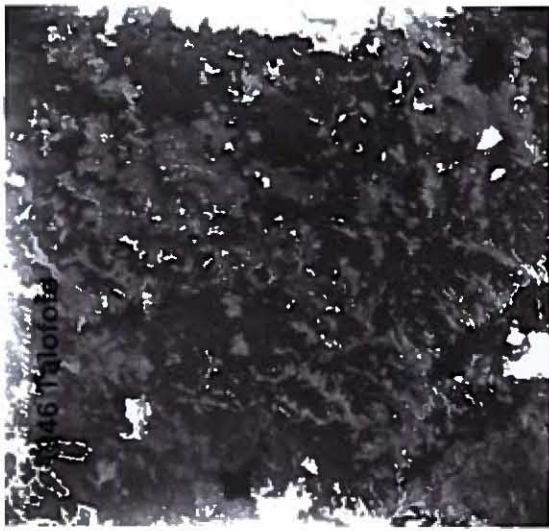
Figure 15. Original sheets of the 1946 and 1994 historical aerial photo series chosen for this study.

Erroneously linked GCPs may produce a high total root mean square error (RMSE). To reduce the overall error, GCPs with a high residual RSME were removed in the link table (part of the georeferencing tool) and new ones were added. This process was repeated until enough (minimum of 11) well distributed GCPs were established and the total RSME was acceptable.
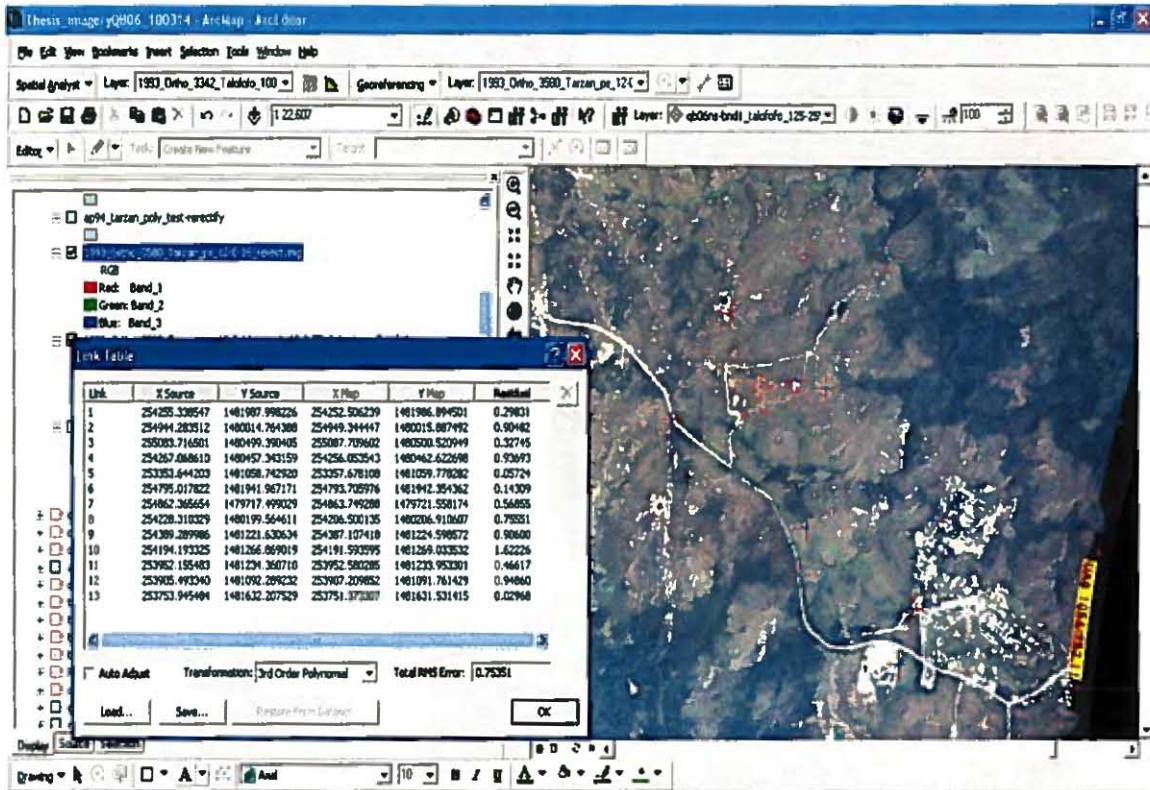
Figure 16. Screen shot of the georeferencing process. The link table displays the map and source location of the control points with the individual residual error and also the total root mean square error. A third-order polynomial transformation was used here.

A third-order polynomial transformation with a bilinear interpolation algorithm was used to rectify and resample each image to a cell size of one meter by one meter. The coordinate system of the rectified images is the Universal Transverse Mercator (UTM) coordinate system Zone 55 North, same as the QB06.

4.3. Badland Classification - Tonal Analysis

Land cover information from remotely sensed data can be classified using a variety of techniques. Depending on the information captured by the image sensor (*e.g.*, spectral bands) and the detail of classification required (*e.g.*, major versus detailed land cover classes) certain techniques prove more useful than others. In this study, only the badland cover at different times was of interest. The method to classify (delineate) badlands was based on tonal segmentation. This approach was chosen for several reasons: a) it could be applied to the panchromatic and color historical aerial photographs as well as the satellite imagery, b) badlands could easily be identified, and c) it is semi-automated; hence, it provides a faster and more standardized classification method with only some user's input versus time-consuming, manual on-screen delineation.

Tonal segmentation, also called density slicing, classifies an image based on user-defined grayscale (brightness) values (0–255) of a panchromatic photograph or a single band of a color image. Mast *et al.* (1997) and Hudak and Wessmand (1998) applied density slicing in historical aerial photographs to determine tree cover and woody plants, respectively. This approach also seemed appropriate to discriminate badlands from the surrounding areas because badlands generally have a higher reflectance value in the visible light spectrum than other land cover types, mainly vegetation such as grassland and forest, found at the study sites. The high brightness values are especially pronounced in the red spectral band of the color images (1994 and 2006). The 1946 panchromatic photographs also show badlands in a higher gray value than surrounding land cover. Impervious surfaces (*e.g.*, roofs) and clouds also have a high reflectance value and could be considered as badlands by mistake using this approach. However, the study sites only included very few such surfaces and very few light cloud cover on few images, which were manually removed after the density slicing was applied.

Badlands (very light areas) were classified by determining the grayscale range (total tonal range: 0–255) based on visual interpretation (Figure 17). The upper boundary was set at 255. The lower boundary was determined individually for each image by highlighting different tonal ranges and subjectively determining the best fit while paying attention to not over- or under-classifying the badlands. The image (Band 1) was then reclassified into badland versus non-badland areas and saved in a new IMAGE raster file clipped to the respective study site. The resolution of the reclassified raster layers was set to one meter by one meter.

Each reclassified raster layer was converted to a polygon shapefile. Each shapefile was then visually compared to the respective original image for classification accuracy. Obviously misclassified polygons were then edited. The most misclassified areas were due to light cloud cover (no image had dense cloud cover), paved road (Agat and Yona study site), and some highly reflective parts of wetlands. Few badlands with a rather dark-brown appearance (often new mass wasting sites) were not classified as badlands but were manually added. All polygon shapefiles were then converted back to raster images. The last step in the badland classification was to assign unique values to the 1946, 1994, and 2006 raster images: *1* for badland and *2* for non-badland for the 1946 image; *10* and *20* for 1994, respectively; and *100* and *200* for 2006, respectively. The unique values build the basis for the change detection analysis described in Section 4.5.

29

True Color QuickBird Imagery 2006   Band 1 (red) of QuickBird Imagery 2006   Band 1 (red) of QuickBird Imagery 2006
with Values 130-255 highlighted

0   100   200 Meters
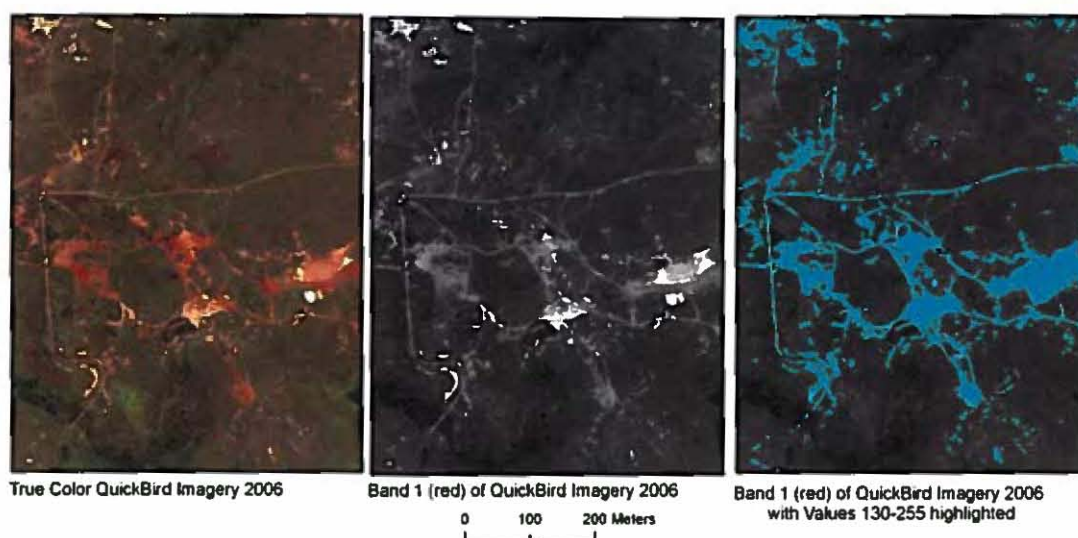
Figure 17. Example of the tonal segmentation process used to delineate the badlands. The example here shows the QuickBird satellite imagery of the ORV-area at the Yona study site.

4.4. Classification Accuracy Assessment

Accuracy assessment is an essential part of land cover classification as it identifies classification errors and quantifies the reliability of the classification (Congalton *et al.*, 1998). It is usually assessed using random sampling points. However, simple random sampling may often under-sample small but significant areas (Congalton, 1991) like badlands. Using stratified random sampling, where random sampling points are placed in each land cover class (referred to as stratum), solves this problem (Congalton, 1991).

Here, a modified stratified random sampling method was used. The two strata in this classification are badlands and non-badlands. All areas which were classified as badland at some point in the three-date analysis (all classes except *222*, compare Chapter 4.5) were included in the badland stratum; the non-badland stratum was restricted to a 20-meter buffer extending from the badland stratum. A 20-meter buffer instead of all non-badland areas was chosen for more accurate classification assessment because most badlands are assumed to have been classified correctly or are in the vicinity of classified badlands and, therefore, should fall within the two strata.

The general rule of at least 50 sampling points per land cover category (Lillesand *et al.*, 2008; Congalton, 1991) was applied and 50 random points were generated for each stratum at each study site, using the *Create Random Points* tool in ArcEditor 9.3. For all study sites combined, the accuracy assessment incorporated 300 sampling points (a total of 150 points per stratum). Depending on the year, between 71 (for 1946) and 99 (for 2006) sampling points were classified as badlands.

The accuracy assessment was based on image interpretation of the original imageries used for the classification. This approach could be argued as biased but seemed to be the best considering large registration errors (how well the images overlap); differences in spatial and spectral resolution; and land cover changes between the source and reference image. As a result, the assessment is free of registration errors between the source and reference image. However, registration errors between the classified images still exist and may exaggerate or mask change (Foody, 2002).

The land cover information (badland or non-badland) was extracted at all sampling points from the classified image and the respective reference image for all three dates (1946, 1994, and 2006). The reference images for the 1994 and 2006 images were the original color images. The reference images for the 1946 images were the original panchromatic aerial images, but aerial photographs from 1953 served as secondary reference. Other reference imagery was considered but dismissed because of registration errors, low resolution, and land cover changes between the source and reference image.

The accuracy data was then summarized in an error matrix including producer's and user's accuracy (Congalton, 1991), see Table 13. The producer's accuracy indicates the probability of a pixel in the reference data to be classified correctly in the classification, while the user's accuracy indicates the probability of a pixel in the classification to be truly from a certain class.

Table 13. Error matrix logic from classifying randomly sampled points (pixels). An error matrix was generated for each time period and study site.

	Reference Data		
	Badland	Not Badland	Row Total
Classification Data			
Badland	X_{11}	X_{12}	$X_{11}+X_{12}$
Not Badland	X_{21}	X_{22}	$X_{21}+X_{22}$
Column Total	$X_{11}+X_{21}$	$X_{12}+X_{22}$	$X_{11}+X_{21}+X_{12}+X_{22}$

Producer's Accuracy

$BL = X_{11}/(X_{11}+X_{21})$ [1]

$NBL = X_{22}/(X_{12}+X_{22})$

User's Accuracy

$BL = X_{11}/(X_{11}+X_{12})$ [2]

$NBL = X_{22}/(X_{21}+X_{22})$

Overall Accuracy $= (X_{11}+X_{22})/(X_{11}+X_{21}+X_{12}+X_{22})$

[1] Percentage of all badlands correctly identified as badlands.
[2] Percentage of badlands classified as badlands correctly identified.

4.5. *Badland Change Detection Analysis*

The total area covered by badlands at each study site was calculated for 1946, 1994, and 2006. Since each pixel has an area of one meter by one meter, the number of pixels classified as badland equals the area in square meters. For example, if 1200 pixels are classified as badland, the area covered by badlands is 1200 square meters. Next, the relative and absolute change in badland cover was determined between these years. This method determines the overall badland cover in each year and the net change between these years. However, it does not give any information on *how* the badland areas changed; *e.g.*, the overall badland cover might have increased from 1946 to 1994, but, for example, some badlands might have converted to non-badlands, or new badlands developed, or existing ones expanded.

To get more information on the nature of the change, a change detection (overlay) analysis was performed. This analysis was based on raster cell values. In Spatial Analyst, an ArcGIS extension, mathematical calculations (*e.g.*, addition, multiplications, *etc.*) can be performed on multiple raster input layers. Each cell in the new layer has a value based on the respective cell(s) of the input layer(s) and the mathematical calculation performed upon them.

31

Here, all three raster layers (1946, 1994, and 2006) were added and summarized in a new raster layer. By adding these three layers, each pixel in the resulting layer has a three-digit number indicating the change each area (pixel) experienced. The change detection logic is shown in Figure 18. For example, an area non-badland in 1946 (value of *2*) but badland in 1994 (*10*) and 2006 (*100*) resulted in a value of *112* (*2 + 10 + 100*); an area that was non-badland in any one year would have a value of *222* (*2 + 20 + 200*) and so forth. The total number of possible results for each pixel value by adding all three layers, each containing a binary value (badland or non-badland), is 2 x 2 x 2 or eight. The total area of each category (in m^2) was again calculated by counting the number of pixels, as explained in the beginning of this section.
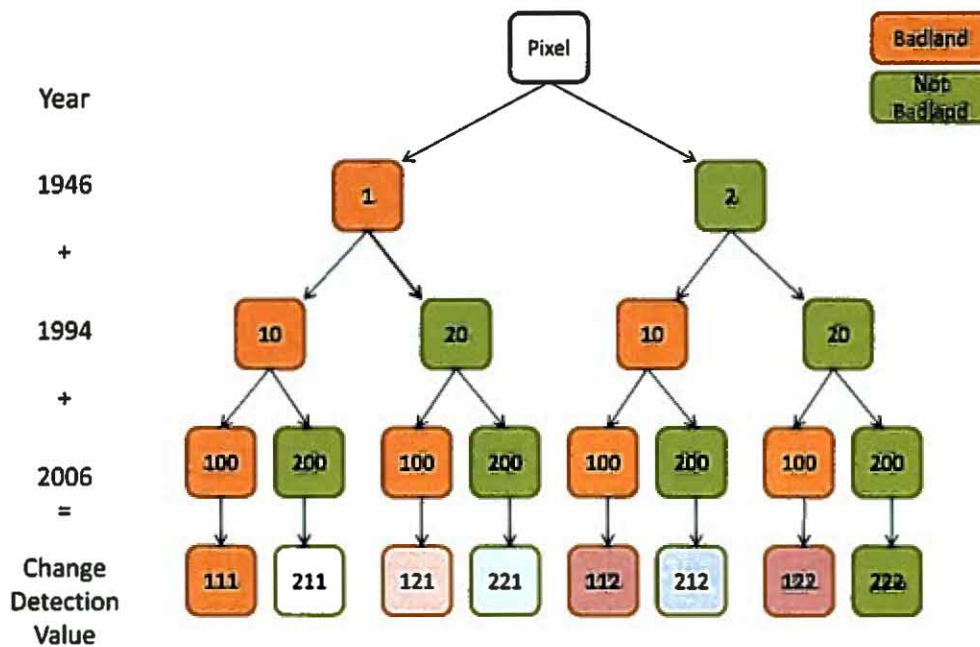
Figure 18. Change detection logic tree. Each pixel is classified as either badland (1, 10, and 100) or non-badland (2, 20, and 200) in 1946, 1994, and 2006, respectively. By adding all three layers, each pixel of the resulting layer has a three digit number indicating the change that area (pixel) experienced.

4.6.   Terrain Attribute Analysis

The distribution of the badlands was compared to their terrain attributes. Terrain attributes may play an important role in badland formation. Here, badland occurrence was examined in terms of elevation, slope, aspect, geology, and soils.

Elevation is defined as the height of a surface above mean sea level. Slope is the angle of the ground surface. In a GIS, slope is defined as the maximum rate of change between each cell and its eight neighboring cells (ESRI, 2010). The algorithm used in GIS to calculate slope in degrees is based on the rate of change of the surface in the horizontal (dz/dx) and vertical (dz/dy) direction from the center cell (Equation 1):

$$\text{Slope(degrees)} = \text{ATAN}(\sqrt{([dz/dx]^2 + [dz/dy]2)}) * 57.29578$$

$$\text{where rise/run} = \sqrt{([dz/dx]^2 + [dz/dy]2)}$$

Equation 1

A high slope value means steep terrain, a low or zero slope value means flat terrain. Aspect is the direction (compass bearing) a slope is facing, looking downslope. In GIS, it is defined by the steepest downslope direction from each cell to its neighboring cells. Aspect is measured clockwise in degrees, where zero and 360 is due north, 90 due east, 180 due south, and 270 due west (Figure 19). A flat area (cell) which does not face any direction has the value -1.
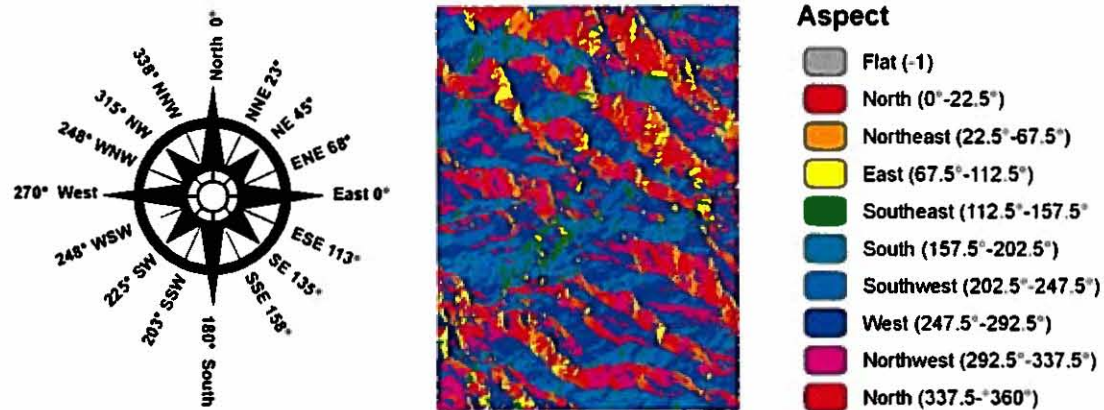
Figure 19. Description of aspect with map sample and legend.

The 2007 LiDAR data by the Bureau of Statistics and Plans provided the basis for the elevation, slope, and aspect layer. These layers were created with the *Surface* Spatial Analysis Tool in ArcGIS 9.3. The resolution of each raster layer was set to one meter by one meter. First, an elevation raster was created using LiDAR bare earth multipoint data. Next, slope and aspect raster layers were derived from the elevation raster. Elevation, slope, and aspect layers have a continuous scale. For further analysis, each layer had to be reclassified into several categories. For example, slope information was summarized (reclassified) into six categories, each representing an interval of 10 degrees (*e.g.*, 0–10°, 10–20°, *etc.*). Geology and soil layers were obtained from the digital Natural Resources Atlas of Southern Guam (*www.hydroguam.net*) and the Natural Resources Conservation Service Office (NRCS), respectively.

To examine the correlation of badlands and terrain attributes the proportional abundance (PA) of badlands per terrain category was determined. Each reclassified terrain layer was added to the change detection layer separately using the Raster Calculator. The results were then displayed in a contingency table. This table shows the number of cells which fall into each category with the columns representing the terrain (*e.g.*, slope) categories and the rows representing the change detection classes (*e.g.*, *111*, *112*). The PA of badlands per terrain category was then calculated by dividing each number in the original contingency table by the sum of the respective column. In addition, change detection classes (*111*, *121*, *221*, *and 211*) were combined to show the PA of badlands in 1946, where human influence was minimal and, therefore, the potential relationship of terrain attributes unmasked. Example below (Equation 2) shows the calculation of the PA of the badlands in 1946 on slopes from 0–10°:

$$\text{PA of BL in 1946 on slopes } 0\text{-}10° = \frac{\#cells\,111, 121, 221, \text{and } 211 \text{ on slope } 0\text{-}10°}{\sum(\#cells \text{ on slope } 0\text{-}10°)} \quad \text{Equation 2}$$

The relative PA was also calculated to make comparison between the study sites easier. Each PA was divided by the sum of the PA of each study site.

The elevation, slope, and aspect layer at the Agat study site were clipped to exclude the large area covered by Alifan Limestone (over 40 percent of the study site), where no badlands occur due to the bedrock. Including this area would have likely obscured the results since the PA takes the overall area of each category into account.

4.7.   Landscape Metrics

Changes in the landscape metrics or geometry of badland patches may reveal how they have evolved. By comparing the landscape metrics, especially patch size, at different times, information can be gained about the composition of badland patches. Number of Patches, Mean Patch Size, Total Area, and Mean Area were analyzed with the Vector-based Analysis Tool Extension V-LATE developed by the Landscape and Resource Management Research Group (LARG, 2005). In addition, the area of each patch was calculated with the *Field Calculator*. The number of patches was then summarized into different size classes.

4.8.   Soil Analysis

Field Methods

Soil properties including texture, moisture content, organic matter, pH, nutrients, and color were examined at each study site. These properties were analyzed to compare differences between badlands and adjacent vegetative sites and also differences between study sites.

A minimum of three composite samples (CS) from two badlands and one adjacent savanna were collected with a soil probe from each study site (Figure 20). The samples were taken from 0–15 cm (0–6 inches) and 15–30 cm (6–12 inches), respectively. The location of each sample was recorded with a Garmin Global Positioning System (Figure 21). Each CS comprises five individual soil samples that were taken from the same patch (approximately 5–10 m apart). Each CS was divided into two Ziploc bags with respect to the depth sampled. The bags were then sealed and taken to the University of Guam soil lab for analysis. A total of 22 samples were collected.
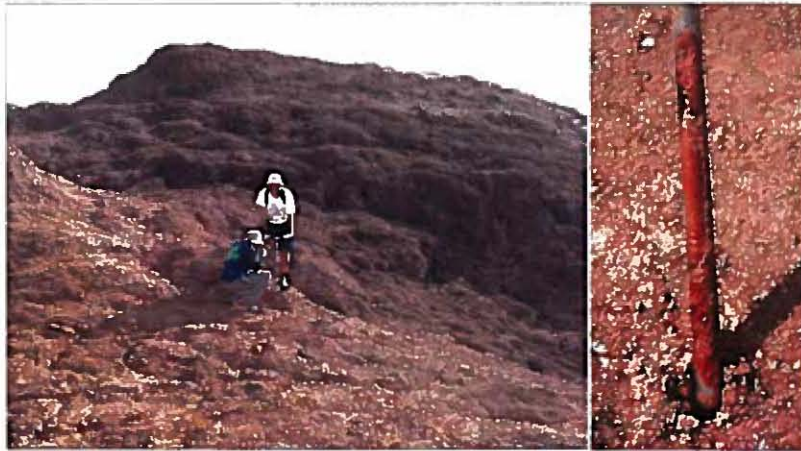
Figure 20. Researchers collecting soil samples with a soil probe in the field.
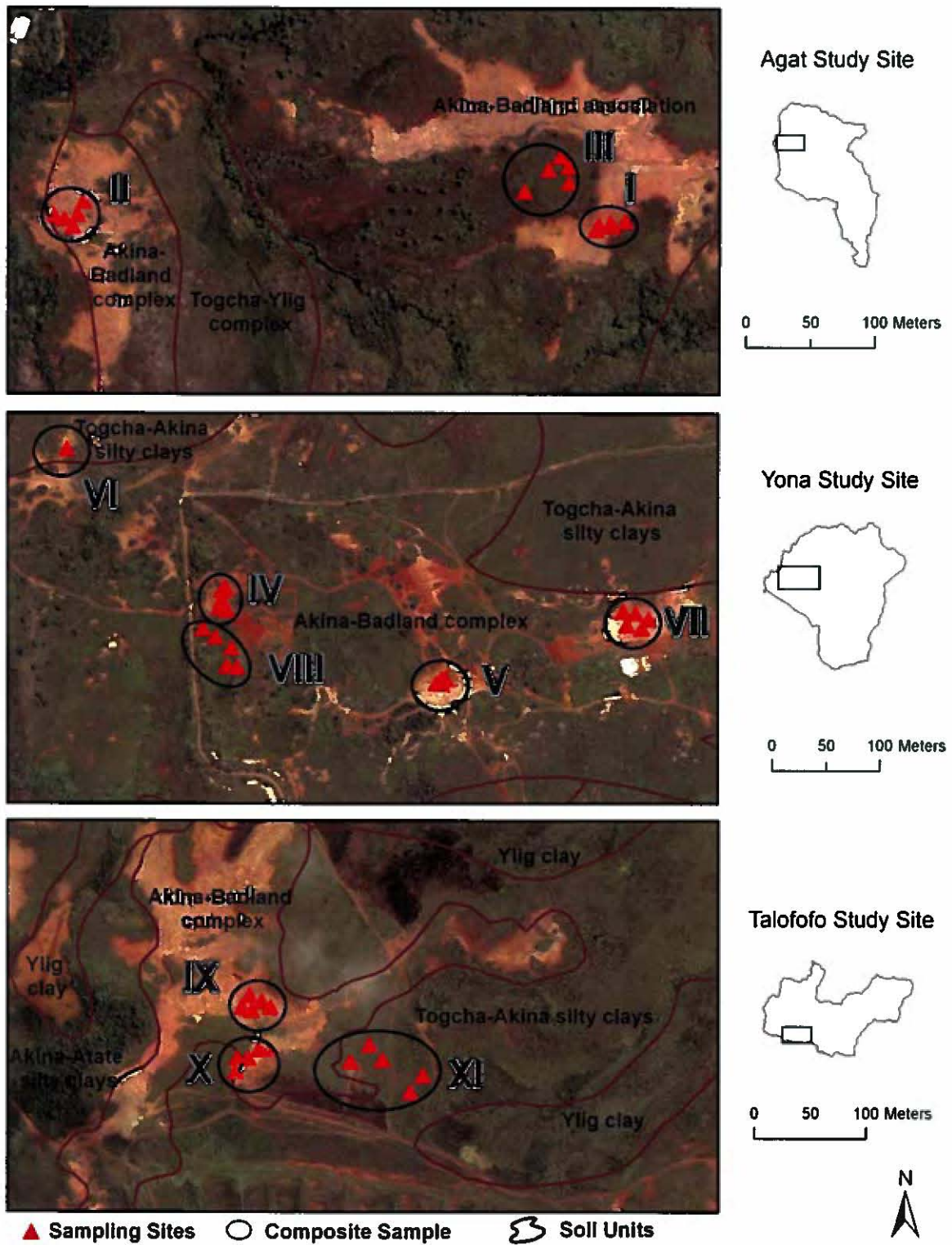
Figure 21. Location of soil sampling sites at each study site.

The soil samples were analyzed at the University of Guam Soil Laboratory. The wet and dry weight of each sample was determined before and after air-drying the samples for a minimum of 48 hours. The color of the dried samples was determined with the Munsell® Soil Color Charts (1975). The color code has three components describing the hue, value, and chroma. The entire sample was then ground with a mechanical grinder and sieved through a 2-mm–mesh for further analysis. The pH was determined using the Oakton pH Meter. Soil texture was determined using the hydrometer method with a first reading taken after 40 seconds and a second reading taken after two hours (Figure 22). The results were then plotted on a textural triangle in Excel (Gerakis and Bear, 2000). Organic matter content was also determined, using the Walkley and Black (1934) method. Available phosphorus was analyzed with a Spectronic Visible Spectrometer, using the Olsen-P method (Olsen *et al.*, 1954). Soil samples were also analyzed for routine nutrient   (K, Mg, Ca) determination.

Figure 22. Soil samples are being analyzed for texture determination.

Chapter 5   Results & Discussion

5.1.   *Changes in Badland Cover*

Change Detection

Image processing of aerial photographs and satellite imagery quantified areas covered by badlands at three study sites in 1946, 1994, and 2006 (Table 14). The overall badland extent increased at all three study sites over the 60-year study period. However, the rates of change vary between study sites and time period. The Yona and Talofofo sites show a similar increase in badland hectarage from 1946 to 1994 (5.3 ha and 5.6 ha, respectively). However, the relative increase, based on the existing badland area in 1946, in Yona is four times higher (+80.3%) than in Talofofo (19.9%). The hectarage in Agat, on the other hand, increased by only 2.3 ha, but the relative increase (20.9%) is comparable to Talofofo. From 1994 to 2006, change rates are completely different. Agat has the highest absolute (3.0 ha) and relative (22.6%) net increase in badland area while Yona only increased by 0.6 ha (5.0%). In contrast, Talofofo's overall badland area decreased by 2.1 ha (-6.2%). The causes for these different rates are linked to both natural and human factors.

Table 14. Total badland area in 1946, 1994, and 2006 at all three study sites and changes between the dates. Results are presented in ha and % per study site.

	Total Badland Area							Change of Badland Cover					
	1946		1994		2006		Total Area	1946–1994		1994–2006		1946–2006	
	ha	%[1]	ha	%[1]	ha	%[1]	(ha)	ha	%[2]	ha	%[2]	ha	%[2]
Agat	11.0	3.1	13.3	3.8	16.3	4.6	351.9	2.3	20.9	3.0	22.6	5.3	48.2
Yona	6.6	2.2	11.9	3.9	12.5	4.1	306.6	5.3	80.3	0.6	5.0	5.9	86.4
Talofofo	28.2	8.1	33.8	9.7	31.7	9.1	346.7	5.6	19.9	-2.1	-6.2	3.5	12.4
Total	45.7	4.5	59.0	5.9	60.5	6.0	1005.3	13.3	29.1	1.5	2.5	14.8	33.4

[1] percent of study site
[2] percent change

More detailed information about the kind of changes is presented in Table 15, which breaks down the badland area by change detection class. In Agat, 7.0 ha (2.0% of the study site) classified as badland experienced no change during the entire study period, while 3.5 ha (1.0%) converted to badland between 1946 and 1994 and 5.0 ha (1.4%) converted to badland between 1994 and 2006. A total area of 3.5 ha (1.0%) classified as badland in 1946 was vegetated in 2006. In Yona, 1.4 ha (0.5%) classified as badland experienced no change during the entire study period. About 10.7 ha (84.9%) of the badland area in 2006 developed since 1946. A total area of 6.0 ha (2.0%) was only badland in 1994 but not in 1946 or 2006 and 6.8 ha (2.2%) converted to badland since 1994. About 4.1 ha (1.3%) of badland in 1946 was vegetated in 1994. In Talofofo, more than half of all badlands in 2006 or 17.7 ha existed throughout the study period; about 7.4 ha developed between 1946 and 1994 and 5.1 ha developed since 1994.

Areas that converted from badland to non-badland between 1994 and 2006 (Code: *212* and *211*), hence re-vegetated, were mostly "recent" badland areas which developed after 1946 (*212*) in contrast to "persistent" ones which developed before 1946 (*211*). In Agat, Yona, and Talofofo, 79.5 percent, 90.3 percent, and 71.6 percent, respectively, of the areas that re-vegetated between 1994 and 2006 were non-badland in 1946.

Table 15. Results of the change detection analysis in ha and % per study site.

Code	Land Cover 2006-1994-1946	Agat		Yona		Talofofo	
		ha	%	ha	%	ha	%
111	BL-BL-BL	7.0	2.0	1.4	0.5	17.7	5.1
112	BL-BL-NBL	3.5	1.0	3.9	1.3	7.4	2.1
121	BL-NBL-BL	0.8	0.2	0.5	0.2	1.5	0.4
122	BL-NBL-NBL	5.0	1.4	6.8	2.2	5.1	1.5
211	NBL-BL-BL	0.6	0.2	0.6	0.2	2.5	0.7
212	NBL-BL-NBL	2.2	0.6	6.0	2.0	6.2	1.8
221	NBL-NBL- BL	2.6	0.7	4.1	1.3	6.5	1.9
222	NBL-NBL-NBL	330.2	93.8	283.3	92.4	299.9	86.5
Total		351.9	99.9*	306.6	100.1*	346.7	100.0

* Numbers do not add up to 100 because of rounding errors.
Note: BL = Badland; NBL = Not Badland

Figures 23–25 show the spatial distribution of change detection results at the different study sites. All larger badland patches in Agat are located in the northwestern part of the study site along the drainage divides and existed in their general outline before 1946. While most of these very large patches expanded since 1946, some also contracted; however, the changes did not occur homogenously around the edges of the patches. Numerous patches on the hillside of the main ridge are generally smaller in extent and clustered. Many of these small patches seem to have disappeared since 1946, while many others developed. Since 1994, a number of "isolated" patches with a rather even perimeter developed on the slopes of the river valleys in the northwest part of the study site; these patches stand out in the map (Figure 23) since they have a uniform color (consist of only one change detection class) and are not directly connected to other badlands.

In Yona, unlike Agat or Talofofo, all larger badlands seen today developed since 1946 and are located in the central western part of the study site where off-roading is very popular (Figure 24). This area is characterized by an extensive ORV-track network that connects major badland patches, which mostly developed after 1946. Important to note is the vast areal badland expansion between 1994 and 2006 that occurred around existing tracks. At the same time, however, one larger patch and several tracks within the ORV-area that developed between 1946 and 1994 were able to re-vegetate. Because of the large area that re-vegetated (6.6. ha), the overall net increase of badland area is only 0.6 ha. In addition, the largest patch and some smaller patches in 1946 (at the very western corner of the study site) had disappeared almost entirely by 1994.

In Talofofo, similar to Agat, all large badland patches existed in their general outline before 1946 and are located in the western part of the study site (Figure 25). While some of the largest patches have slightly expanded in some places, it appears that an equal or greater area has grown back. Succession of badland recovery can be seen in several badland patches on the northwestern part of the study site. In two separate but nearby patches the badland area retreated noticeably from 1946 to 1994, but tracks were still heavily eroded. However, between 1994 and 2006, these tracks also re-vegetated. The trend seen here is exactly the reverse of that seen in the active ORV-area at the Yona study site where the badland area expanded around the tracks. The central eastern area of this study site is highly eroded and consists of a network of smaller badlands. The western side of this area experienced both contraction and expansion of badlands between 1946 and 1994. The eastern side experienced hardly any contraction but instead substantial development of new badlands in the same time period. The area of new badlands coincides with farm fields that were cultivated after 1946 but before 1994. One conglomerate of abandoned farm fields was heavily eroded and classified as badland (central eastern part).

38

Another one had vegetation cover but appeared fallow, and only one (on the southeastern border) was cultivated in 1994. The farming practices as well as the reason for the cessation of farming is unknown.
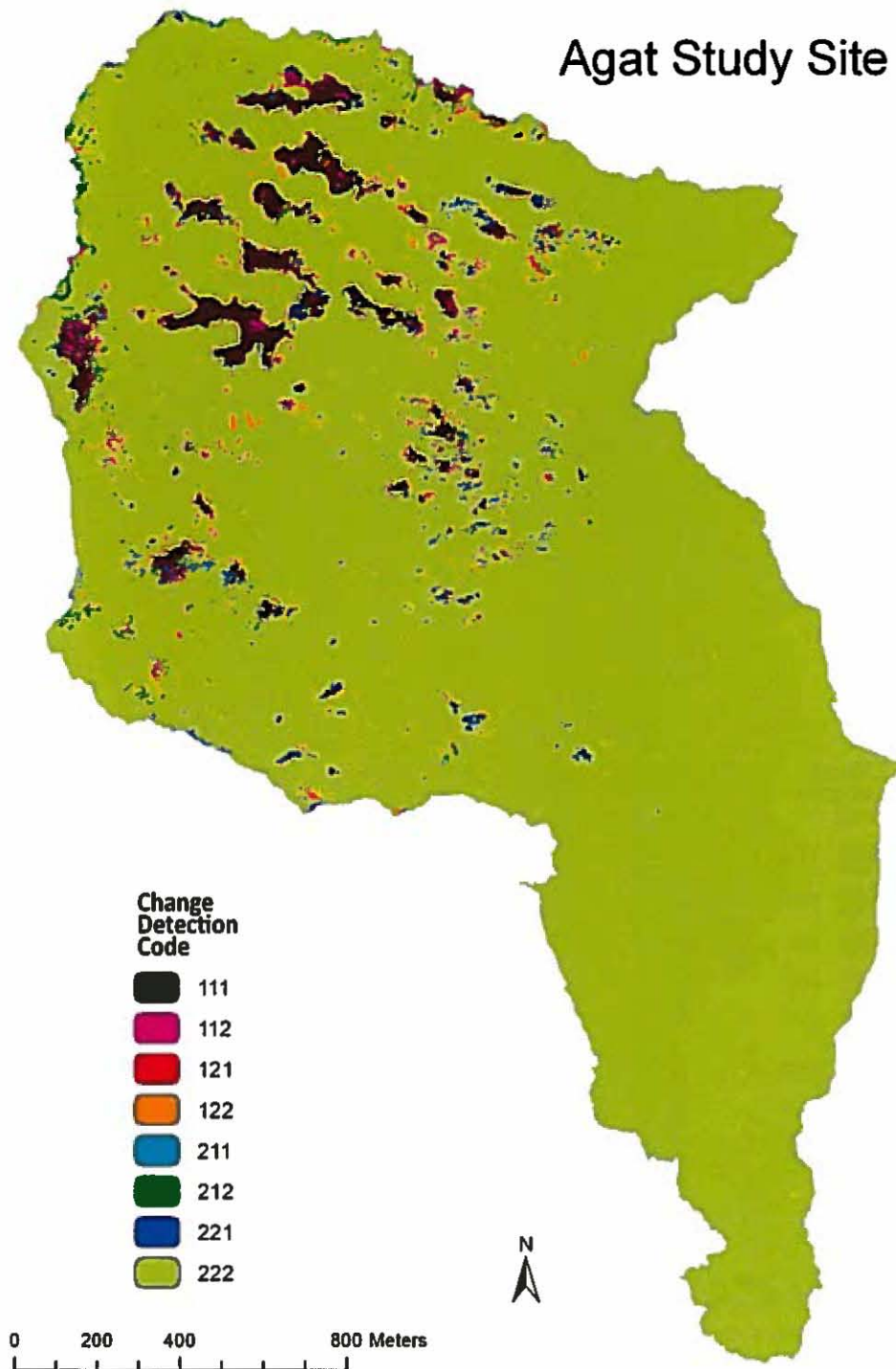
Figure 23. Map of the change detection result for the Agat study site. 111 and 222 indicate no change; all other areas experienced change: 112 and 122 converted to badlands, while 211 and 221 converted to non-badland between 1946 and 2006; 121 changed from BL to NBL and back to BL during the three dates, while 212 changed from NBL to BL and back to NBL, respectively, between 1946, 1994, and 2006.

Yona Study Site
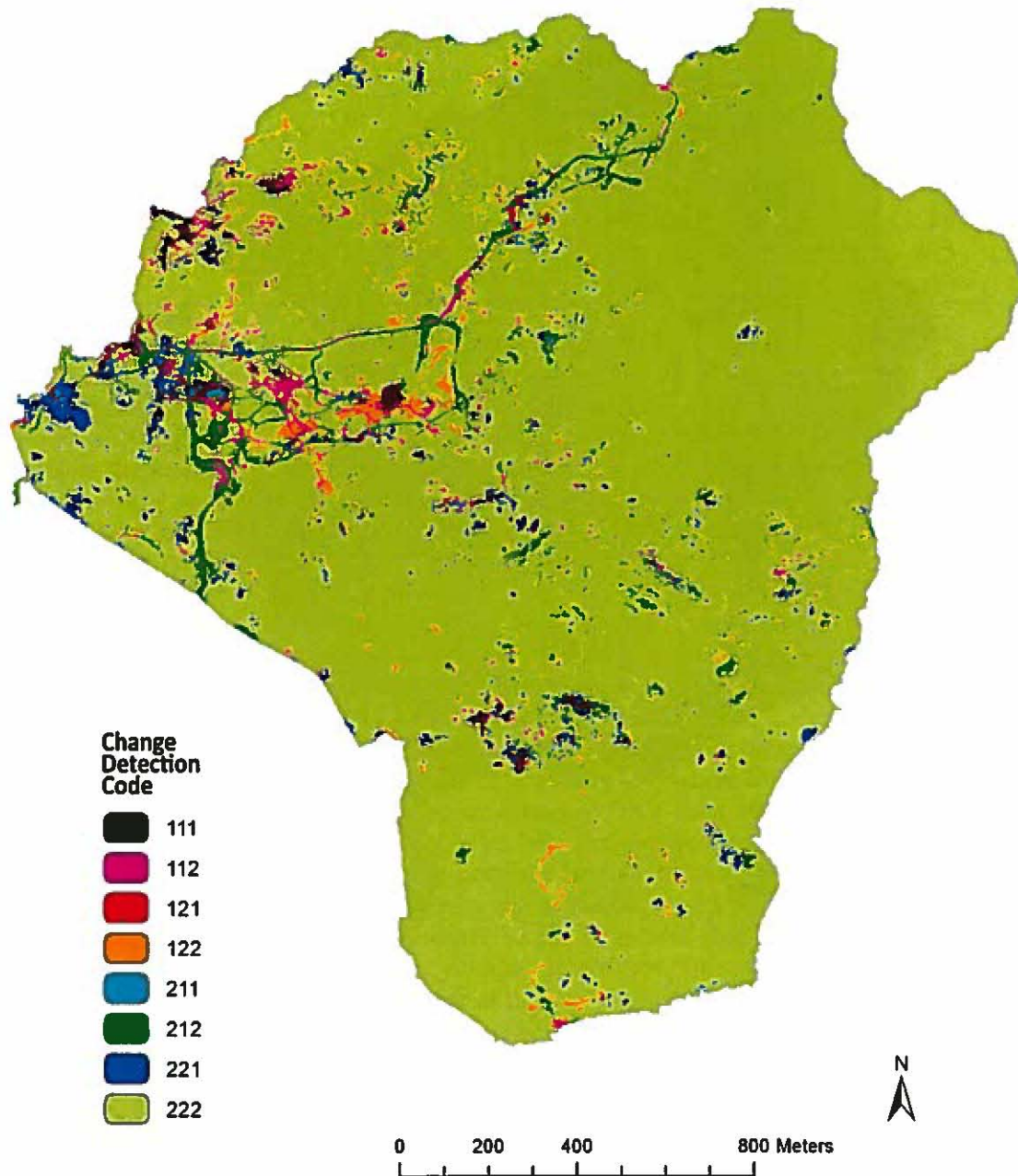
Figure 24. Map of the change detection result for the Yona study site. 111 and 222 indicate no change; all other areas experienced change: 112 and 122 converted to badlands, while 211 and 221 converted to non-badland between 1946 and 2006; 121 changed from BL to NBL and back to BL during the three dates, while 212 changed from NBL to BL and back to NBL, respectively, between 1946, 1994, and 2006.
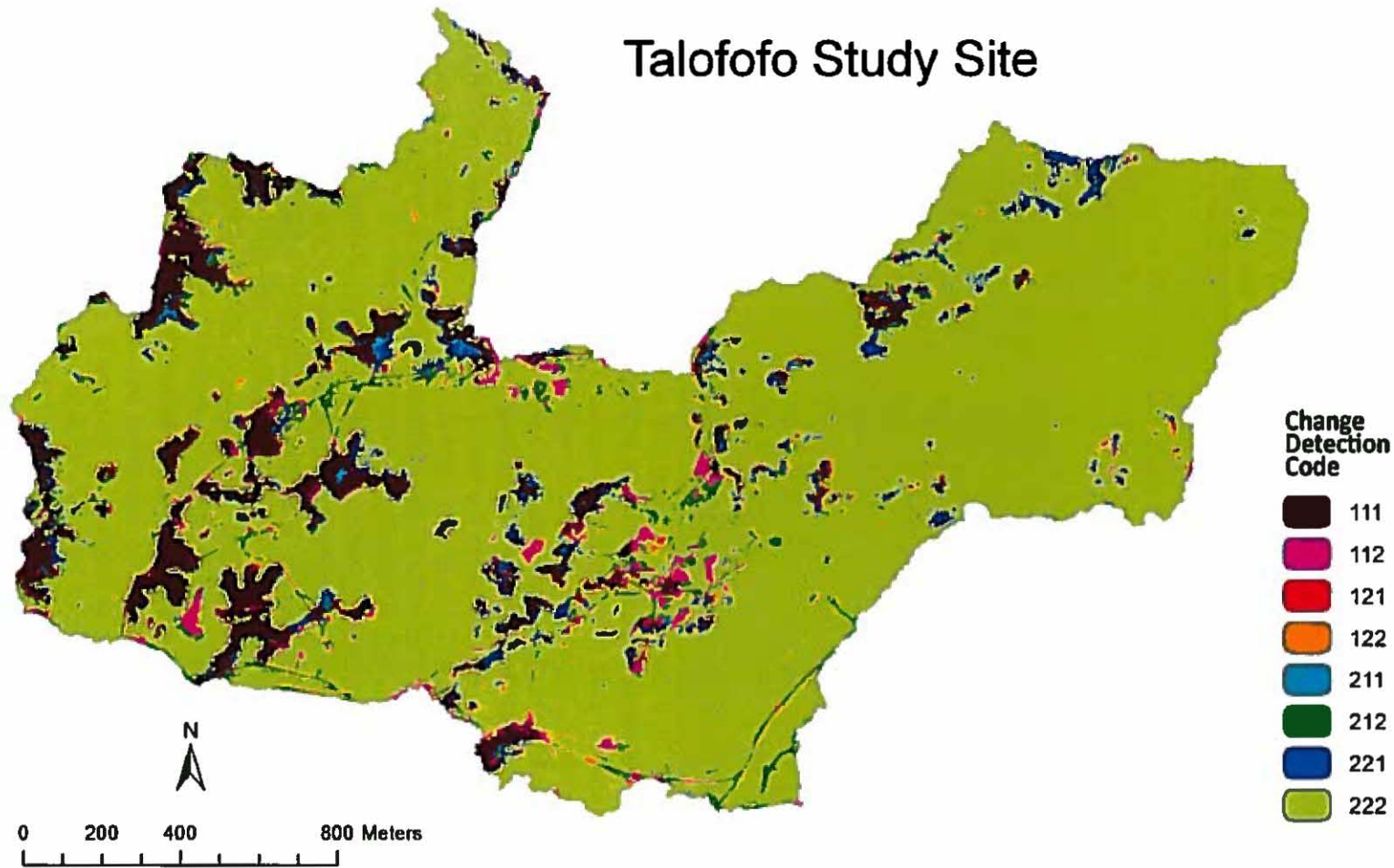
Figure 25. Map of the change detection result for the Talofofo study site. 111 and 222 indicate no change; all other areas experienced change: 112 and 122 converted to badlands while 211 and 221 converted to non-badland between 1946 and 2006; 121 changed from BL to NBL and back to BL during the three dates while 212 changed from NBL to BL and back to NBL, respectively, between 1946, 1994, and 2006.

Human versus Natural Influence

In 1946, human activities at all study sites were considered nominal in terms of land cover alteration and potential badland creation (like off-roading, construction, burning, or mismanaged farming) since no evidence was found in any of the 1946 aerial imagery. By 1994, humans had visibly altered the landscape at the Yona and Talofofo sites by creating extensive ORV-track networks and, in Talofofo, also by farming. In contrast, no human disturbance was visible in Agat in 1994. The fact that the badland expansions in Yona and Talofofo are highly concentrated in areas where humans altered the landscape and that the expansion in hectarage between 1946 and 1994 is much less in Agat strongly suggests that human activities exacerbate badland expansion.

Off-roading activities at the Yona site continued after 1994 as new tracks are evident in the 2006 imagery. In addition, numerous fresh tire marks and ORVs traversing the area were observed during field investigations in 2010 indicating continued ORV-use in this area. Despite formation of new tracks and continued use of some old tracks, many unused tracks, especially portions of the dirt road for the golf course, have overgrown since 1994. The many overgrown tracks as seen in the classification largely explain the overall area of 6.6 ha that re-vegetated since 1994. Overall, the number of tracks seems higher in 1994, which may lead one to assume that ORV activity has decreased. It is important to note though that a vast areal expansion between 1994 and 2006 occurred around existing tracks, contributing largely to the 6.8 ha of new badland area.

Human activity at the Talofofo site appears to have significantly decreased since 1994. First, most tracks clearly seen in the 1994 imagery were partially overgrown in 2006, while only very few new tracks and badland patches connected to tracks were formed, indicating an overall decrease in ORV-traffic. Secondly, only one conglomerate of farm fields was cultivated in 2006, while other fields at the border of the study site and directly adjacent (altogether of much larger area than the cultivated fields) were abandoned either before or after 1994. Also, field observations in spring 2010 showed that farming activities ceased entirely within the study site but also directly adjacent to it. With a cessation in farming, associated traffic also ceased. It was also observed that the dirt road (Bubulao Road) leading to the study site was heavily eroded in 2010, making it seemingly impassable for ORV-trucks. On occasion, golf carts and all-terrain-vehicles entering the Bubulao road were seen. Although 5.1 ha of new badland area appeared between 1994 and 2006, 8.7 ha re-vegetated, resulting in the overall net decrease of 2.1 ha. It appears that the rate of recovery can exceed the rate of formation when human activity decreases significantly. The net decrease in Talofofo after 1994 along with the decrease in human activity in addition to the net increase in Yona with continued human activity further adds to the argument that human activities influence badland dynamics.

Contrary to Yona and Talofofo, badland expansion in Agat is considered solely "natural" since no landscape-altering human activities are evident in the 2006 imagery. "Natural" here does, of course, not take into account occasional foot traffic, especially by hunters, and intentional fires set by hunters, which are frequent in this area but also at the other study sites. From field observations, it appears that most new patches, especially the bigger "isolated" ones, are chiefly the result of mass wasting. The high occurrence of mass wasting, especially in the central western part of the study site, may be linked to the decline in forest cover (as is evident when comparing the 1946, 1994, and 2006 imageries) and associated decrease of slope stability coupled with extreme events such as earthquakes or tropical cyclones. At the Agat study site, three deep-seated slumps (total area of 1000 m^2), located next to each other along the Pagachao Creek (Figure 26), occurred between the time the first IKONOS satellite imageries were taken (during 2001) and the second set (mostly in 2003); Typhoon Chata'an in July 2002 or Pongsona in December 2002 likely triggered these slumps. The area of these slumps, as well as most other slumps, converted from ravine forest to savanna between 1946 and 1994 as image comparison

shows. After forest is converted to savanna, the soil and underlying saprolite is more susceptible to mass wasting since most savanna grasses have a shallower root system than trees and also take up less water; hence, soil becomes more saturated. In addition, the soil saturation of water reaches greater depth, which accelerates the weathering processes. These soil processes, especially weathering, may take a few years or decades to reach a critical point of slope failure, which would explain the higher rate of badland expansion between 1994 and 2006 compared to 1946 to 1994.
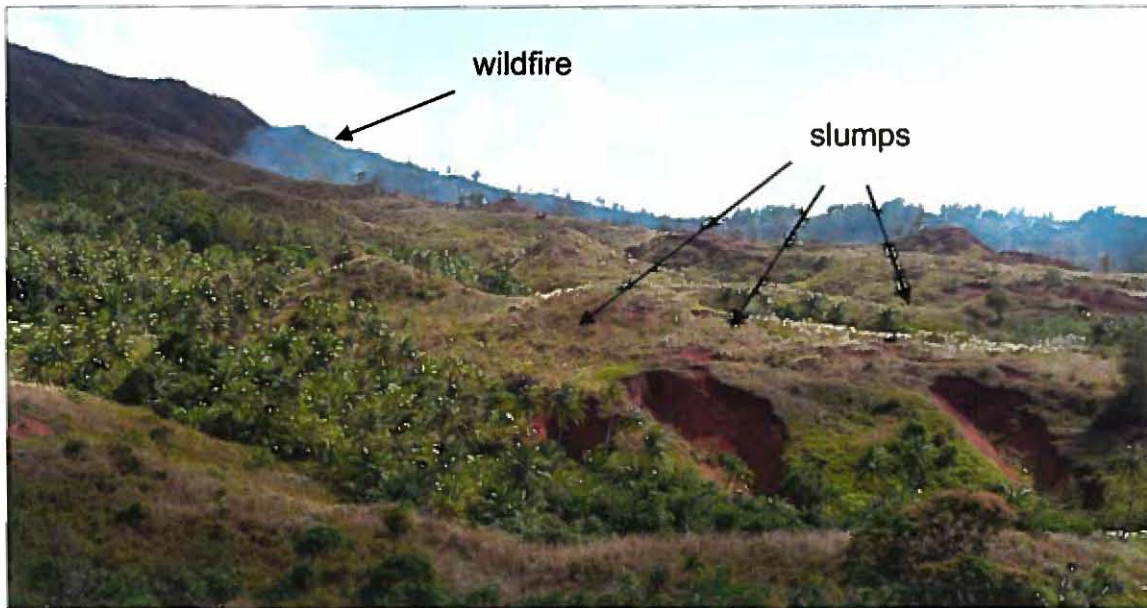
Figure 26. Slumps at the Agat site with wildfire in the background.

Re-vegetation

Despite common belief to the contrary, the results of this study show that some badland areas have the ability to re-vegetate naturally if not disturbed by human activity. Although few patches disappeared entirely, most re-vegetation only occurred in parts of a patch, while other parts of the same patch may have expanded. Furthermore, the study revealed that "newer", more recent badland areas were more likely to recover than older badland areas. This is probably due to different degree of degradation: newer badlands may still contain a subsoil layer, where certain plants like the aluminum-tolerant *Dicranopteris linearis* can establish; whereas older badlands may be eroded down to dense saprolite, which provides a physical barrier for roots. For this reason, re-vegetation efforts should be focused on recently developed badland areas as resources permit.

43

5.2.   Terrain Attributes

Slope

The relationship of badland cover in 1946 and slope is demonstrated in Figure 27. Badlands at the Talofofo site show a very strong positive correlation with slope. For example, badlands are six times more likely to occur on very steep slopes (>50°) than on very gentle slopes (<10°). This trend was expected since steeper slopes are less stable and more prone to erosion due to the increased gravitational force and increased velocity of surface runoff. Contrary to expectations, badlands at the Agat and Yona sites exhibit a general negative correlation with slope. The proportional abundance of badlands in Yona continually decreases with increasing slope from 2.9 percent on slopes smaller than 10 degrees to 0.8 percent on slopes greater than 50 degrees. The negative correlation of slope and proportional abundance of badlands is even more pronounced in Agat than in Yona, with 8.3 percent on very gentle slopes (<10°) to 2.1 percent on slopes between 40 degrees and 50 degrees. However, the badland cover on slopes greater than 50 degrees (6.5%) is almost as high as on very gentle slopes. Several factors may be responsible for the negative trend in Agat and Yona. For example, exposure and forest cover may mask the relationship of slope and badland occurrence and could largely explain the observed negative trends. The volcanic area in Agat is highly dissected with thin strips of ravine forest along streams. Although not as dissected as Agat, the Yona study site has deep river valleys on the eastern part, surrounded by a large continuous forest. Steep slopes often coincide with narrow river valleys, which are more protected from the elements; in addition, they are largely covered by ravine forest, which is much less prone to erosion than savanna vegetation. For this reason, it is possible that the proportional abundance of badlands at steeper slopes is indeed higher when forested areas are not taken into account in the analysis. Also in Agat, the very large badland areas are located on the rounded ridges between the river valleys and have generally slopes below 30 degrees. Similarly in Yona, all larger badland areas are located on a plateau, where slopes are gentle. Therefore, exposure to wind and water seems to have a bigger impact than slope. In Talofofo, the very strong positive relationship of slope and badland occurrence is likely caused by the cumulative effect of slope and exposure (most badlands are on the elevated plateau).

The results of the slope analysis, when broken down by change detection classes, are presented in Figure 28. For comparison, the results in Figure 27 were based only on the badland extent in 1946 (Code: *111*, *112*, *121*, and *122*). The proportional abundance of the change detection classes at each study site generally corresponds to the trends presented in Figure 27. Change detection classes show a continuous decrease in proportional abundance with increasing slopes up to 50 degrees and a slight increase in abundance on slopes greater than 50 degrees. In Talofofo, all classes increase almost linearly in abundance on slopes between 10 and 50 degrees. Similarly, in Yona, the relationship of slope and the different change detection classes is generally negative but the trend is not as consistent as in Agat.
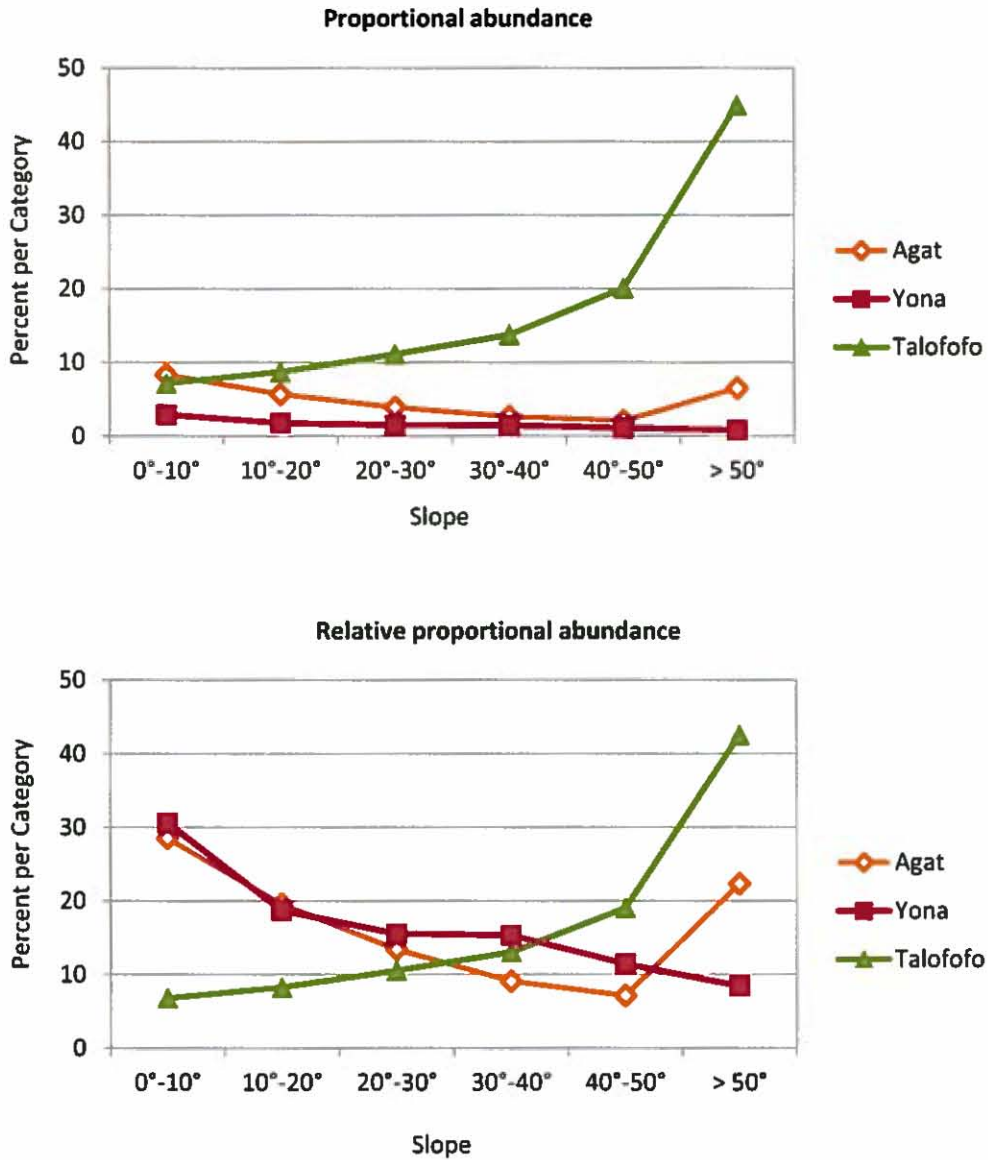
Figure 27. Proportional abundance and relative proportional abundance of badlands in 1946 at each study site broken down into six slope categories (0–10°, 10–20°, 20–30°, 30–40°, 40–50°, >50°). The relative proportional abundance normalizes the proportional abundance to allow better comparison of the study sites.
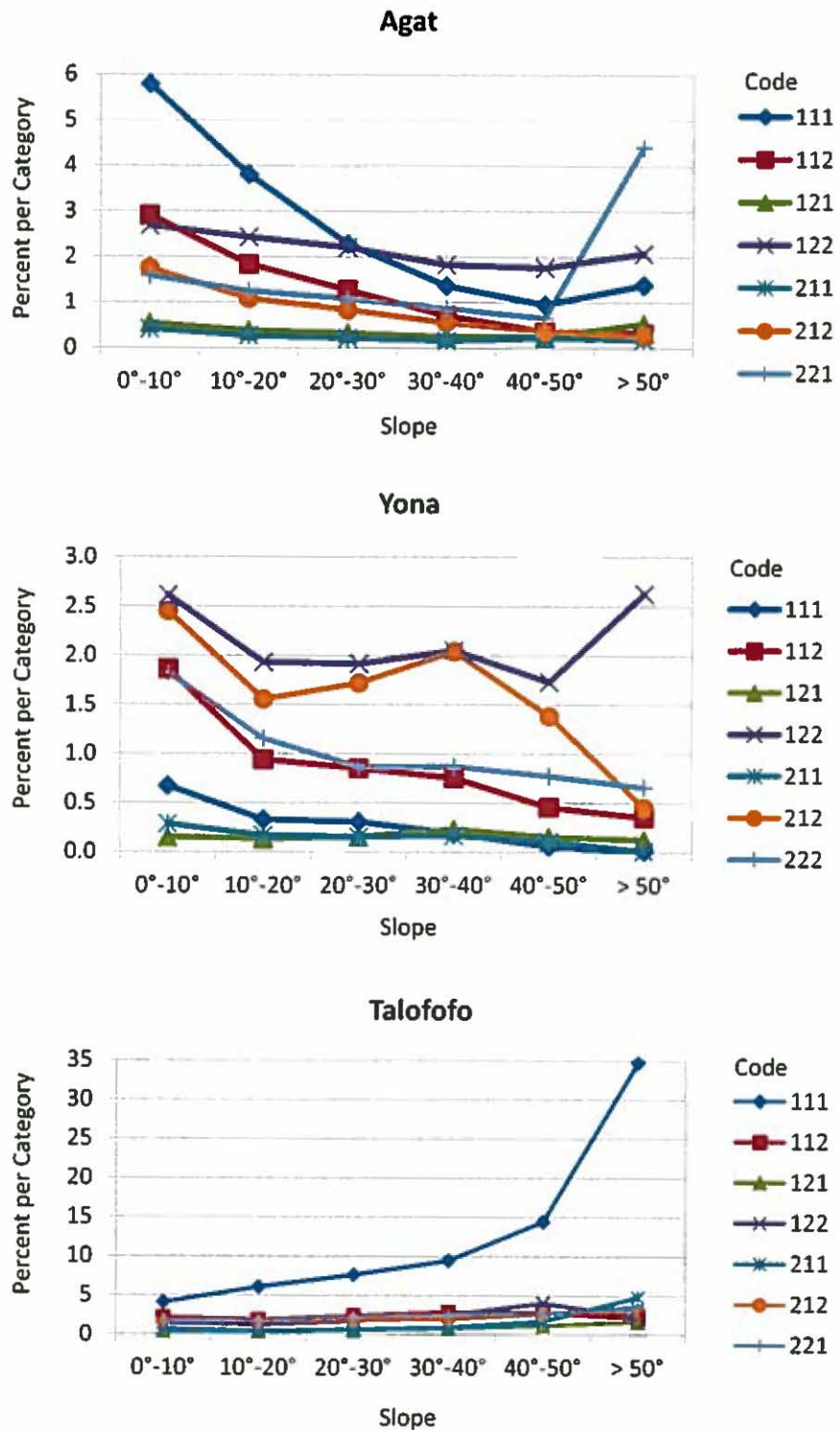
Figure 28. Proportional abundance of badland change classes per slope category for Agat, Yona, and Talofofo. Areas that were never badland (Code: *222*) are not included here.

In Yona, part of the trend in recent years is also a result of human activity. The slope analysis provided an important insight into badland dynamics related to off-road activities. The high proportional abundance of badlands in 2006 (especially those that developed after 1946, Code: *112* and *122*) on flat terrain is strongly linked to off-roading activities (Figure 29). First, these areas are chiefly located in areas heavily frequented by off-roaders. Second, the most extensive badland expansion since 1994 took place around tracks that were already established by 1994. Third, the expansion of 1994 badlands occurred downhill and is characterized by an accumulation of very loose sediments on the top layer as observed in the field. ORVs may be directly responsible for this, by driving off-track and disturbing vegetative cover, but also indirectly, by loosening soil on existing badlands. The loosened soil is then transported by surface runoff to adjacent flat areas or sinks that act as temporary sediment traps. Over time, existing, usually sparse, vegetation will eventually be covered by sediments. Because the expansion occurs chiefly downhill, one could hypothesize that the indirect impact of ORVs plays a bigger role in initiating badland expansion than the direct disturbance.
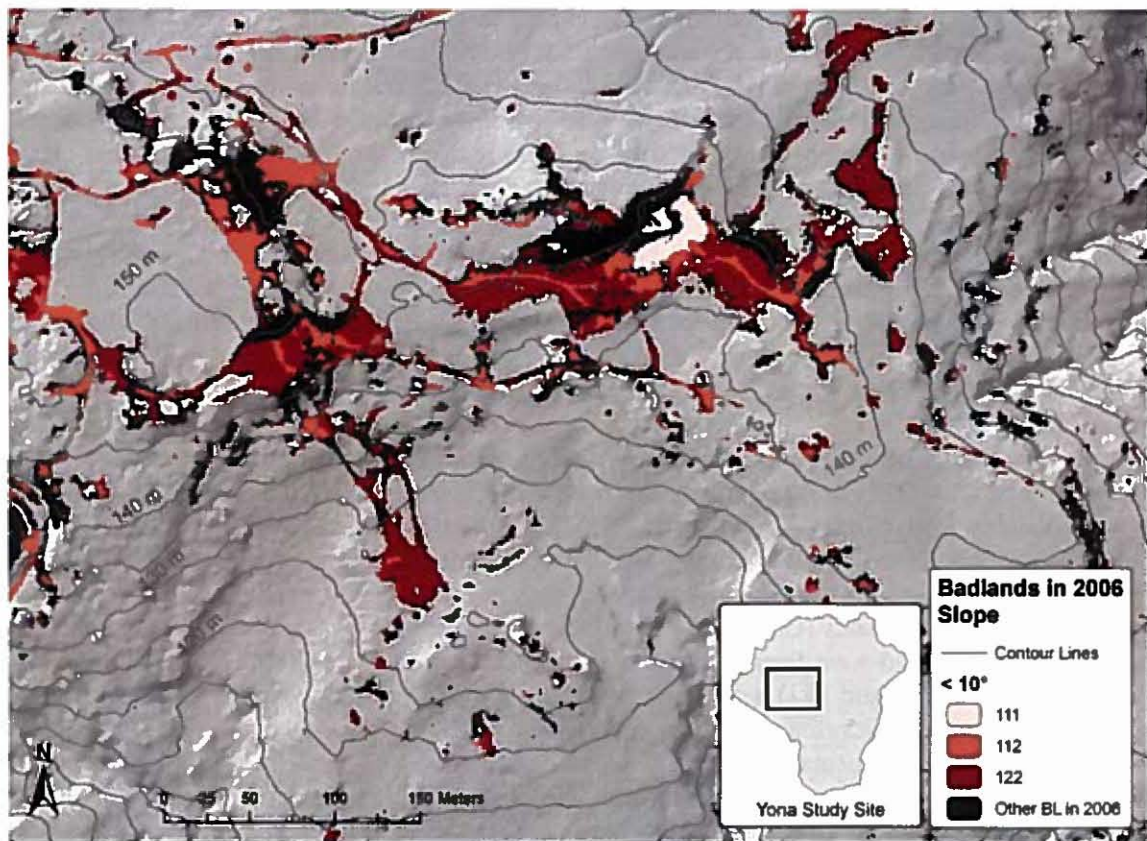
Figure 29. Topographic map of the off-roading area at the Yona site with slope information of the 2006 badland areas. Note that the majority of badlands, especially the ones that developed after 1994 (Code: *122*), is on slopes less than 10 degrees and downhill from badlands that developed before 1994 (Code: *112*).

47

Aspect

The relationship of badland cover in 1946 and aspect is shown in Figure 30. Aspect categories were divided into eight categories. Note that the proportional abundance reflects the proportion of a category that is badland.

The proportional abundance of badlands is consistently highest on southeast-facing slopes and lowest on north-, northwest-, or west-facing slopes in Agat, Talofofo, and Yona, respectively. In Agat, badlands occupy 9.7 percent of southeast-facing slopes and only 3.2 percent of north-facing slopes. Although the decrease in abundance from southeast-facing to north-facing slopes is continuous in both directions, the proportional abundance decreases sharply from southeast- to northeast-facing slopes and slowly from southeast- to north-facing slopes. In Yona, badlands occupy 3.8 percent of southeast-facing slopes and only 1.2 percent of west-facing slopes. In Talofofo, badlands occupy 11.0 percent of southeast-facing slopes and only 4.9 percent of northwest-facing slopes. While all three study sites show a very similar distribution of proportional abundances with two to three times more badland cover on southeast-facing slopes than north- or northwest-facing slopes, the distribution in Talofofo is less pronounced.

The observed trends can be largely attributed to the differential exposure to wind, rain, and sun. The highest proportional abundance of badlands in southeast-facing slopes corresponds to the general wind direction during the wet season, where about 70 percent of the annual rain occurs. Wind direction during the dry season is predominantly east-northeast, where the proportional abundance of badlands is still high although not as high as on southeast-facing slopes. One could hypothesize that water erosion has a bigger impact on badland development than wind erosion. Also, southeast- to southwest-facing slopes get more sun exposure than other slopes, although the differential effect is not as strong as in low latitudes like Guam. However, higher sun exposure enhances the weathering process and facilitates wind and water erosion. The degree of exposure to the elements also explains the large shift in proportional abundance between southeast-facing (7.0%) and east-facing (3.9%) slopes at the Agat study site because the mountain ridge to the east acts as a buffer on east-facing slopes.

The results of the aspect analysis when broken down by change detection classes are presented in Figure 31. For comparison, the results in Figure 30 were based only on areas that were badland in 1946 (Code: *111, 112, 121,* and *122*). The proportional abundance of the change detection classes at each study site generally corresponds to the results presented above (Figure 30). However, some variances occur at each study site. For example, the proportional abundance of new badlands (Code: *122*) is highest on northeast-facing slopes in Agat and Yona and on southwest- and west-facing slopes in Talofofo. Also, other badland classes in Talofofo (Code: *112, 121, 212,* and *221*) peak at south- or southwest-facing slopes. The slightly different trends of badlands that developed in Yona and Talofofo after 1946 could be attributed to land use, which may mask the influence of aspect on badland occurrence. In Agat, the almost reverse trend may be due to the direction of tropical storm Tingting, which passed northeast of Guam and caused many landslides. Clear trends of other badland categories, *e.g.,* badland areas that re-vegetated, could not be detected. In general, despite some variances, the fairly uniform increase and decrease of proportional abundances of badlands with changing aspect strongly suggest that aspect has an impact on badland development.
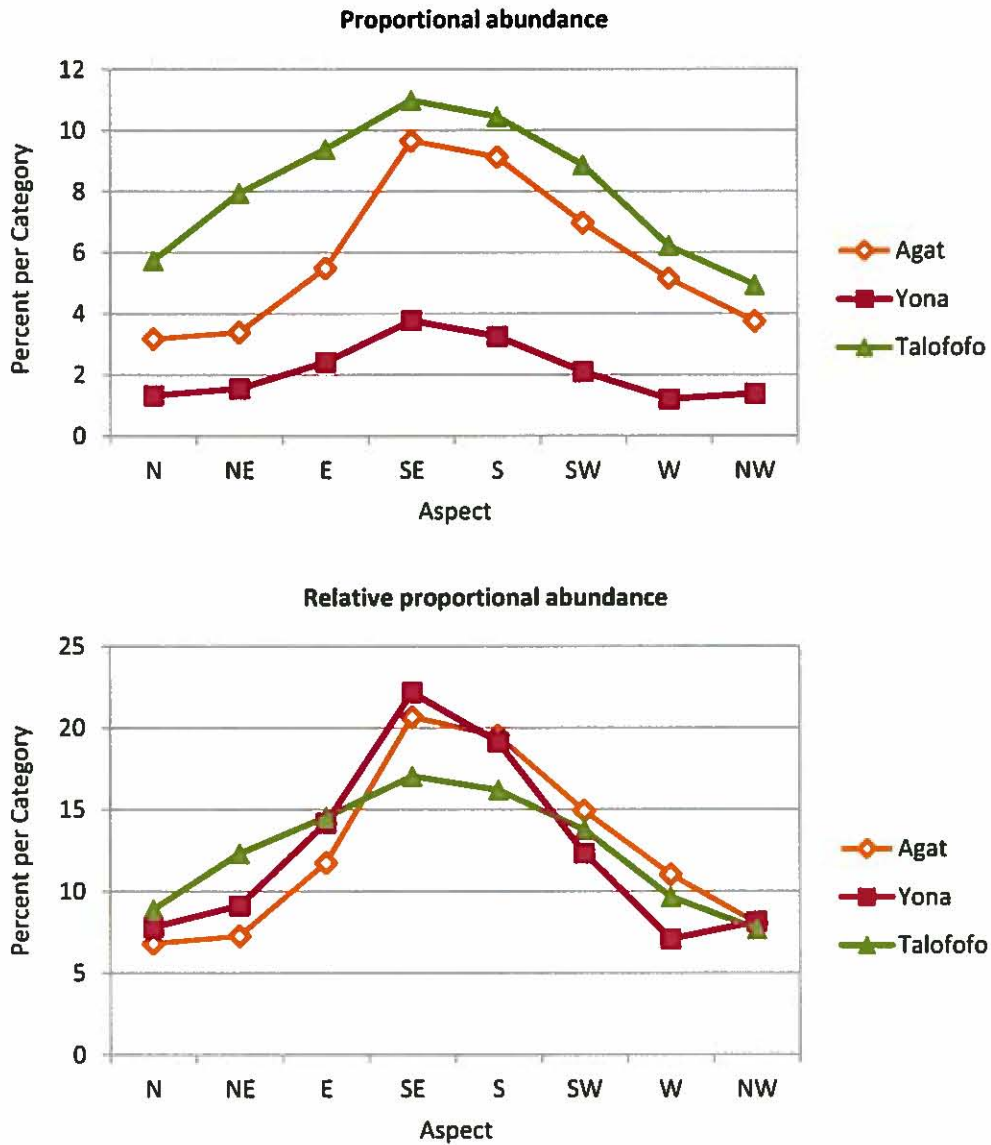
Figure 30. Proportional abundance and relative proportional abundance of badlands in 1946 at each study site broken down into eight aspect categories (north, northeast, east, southeast, south, southwest, west, and northwest). The relative proportional abundance normalizes the proportional abundance to allow better comparison of the study sites.
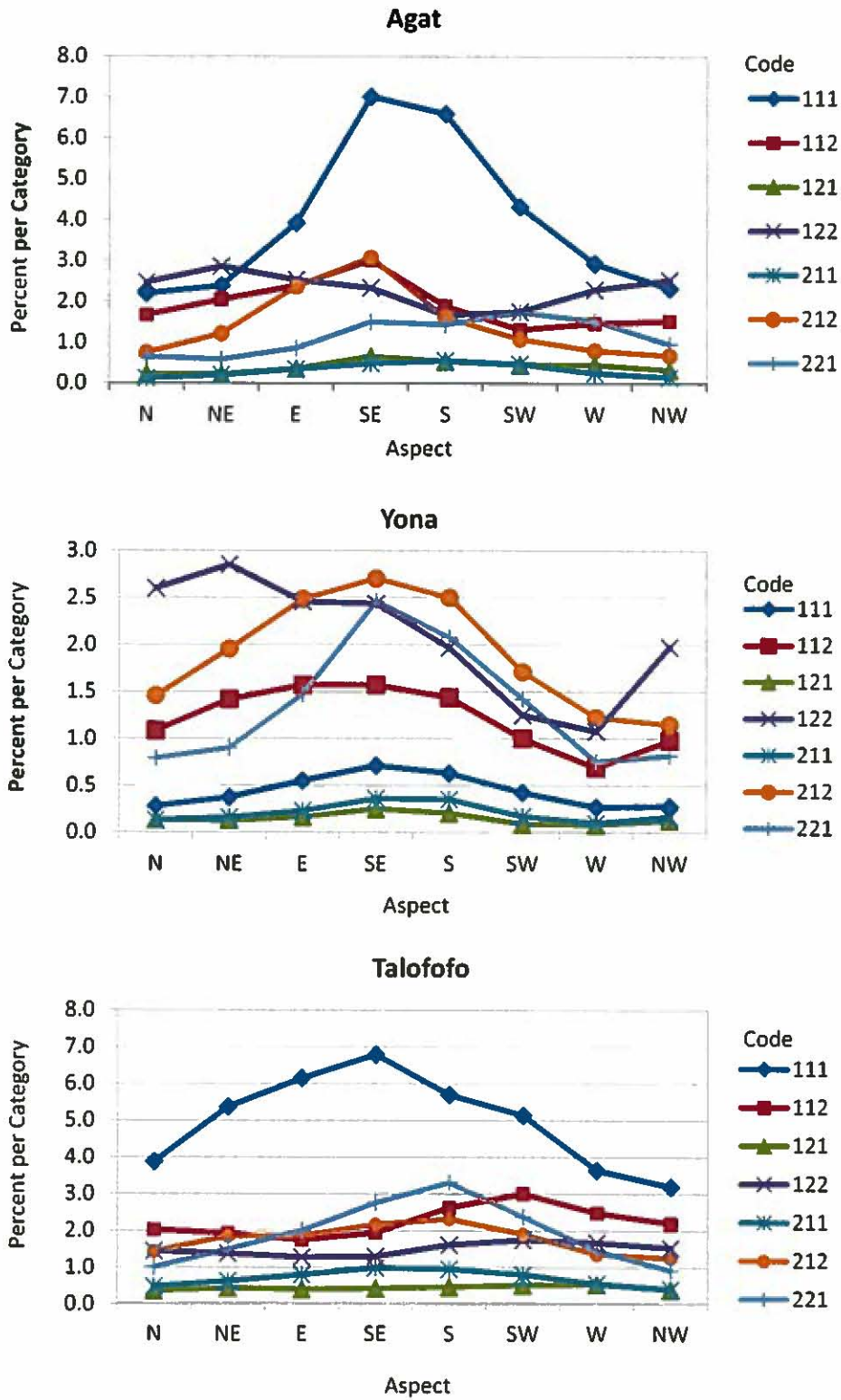
Figure 31. Proportional abundance of badland change classes per aspect category for Agat, Yona, and Talofofo. Areas that were never badland (Code: *222*) are not included here.

Elevation

The relationship of badland cover in 1946 and elevation is demonstrated in Figure 32. The badlands at the Talofofo and Yona sites show a strong positive relationship with elevation. For example, badlands in Talofofo occur seven times more likely at higher elevation of the study site (>100 m) than at lower elevation (<50 m). In Yona, badlands occur about 20 times more likely at the higher elevation of the study site (>150 m) than at lower elevation (<50 m). In contrast, badlands in Agat have the highest proportional abundance at an elevation of 50 to 100 meters with steeply decreasing proportional abundance at lower and higher elevation.

The observed trends are attributed to the location of the study sites relative to the surrounding landscape. Both study sites, Yona and Talofofo study sites, are located on the windward side of the mountain ridge and consist of a rather flat area at high elevations, which exposes these areas to the elements. On the other hand, the Agat study site, located on the leeward side of the mountain ridge, has proportionally more badlands in mid-elevations (50–100 m), which are further from the mountain ridge and, hence, more exposed to the elements than the protected higher elevations at this site. For these reasons, it seems that badland abundance is related to elevation but only in exposed windward areas.

The results of the elevation analysis when broken down by change detection classes are presented in Figure 33. For comparison, the results in Figure 32 were based on only areas that were badland in 1946 (Code: *111*, *112*, *121*, and *122*). The proportional abundance of the change detection classes at each study site generally corresponds to the results presented above (Figure 32); however, in Agat, the proportional abundance in the different elevation categories varies widely at elevations below 200 meters.

Proportional abundance

Relative proportional abundance
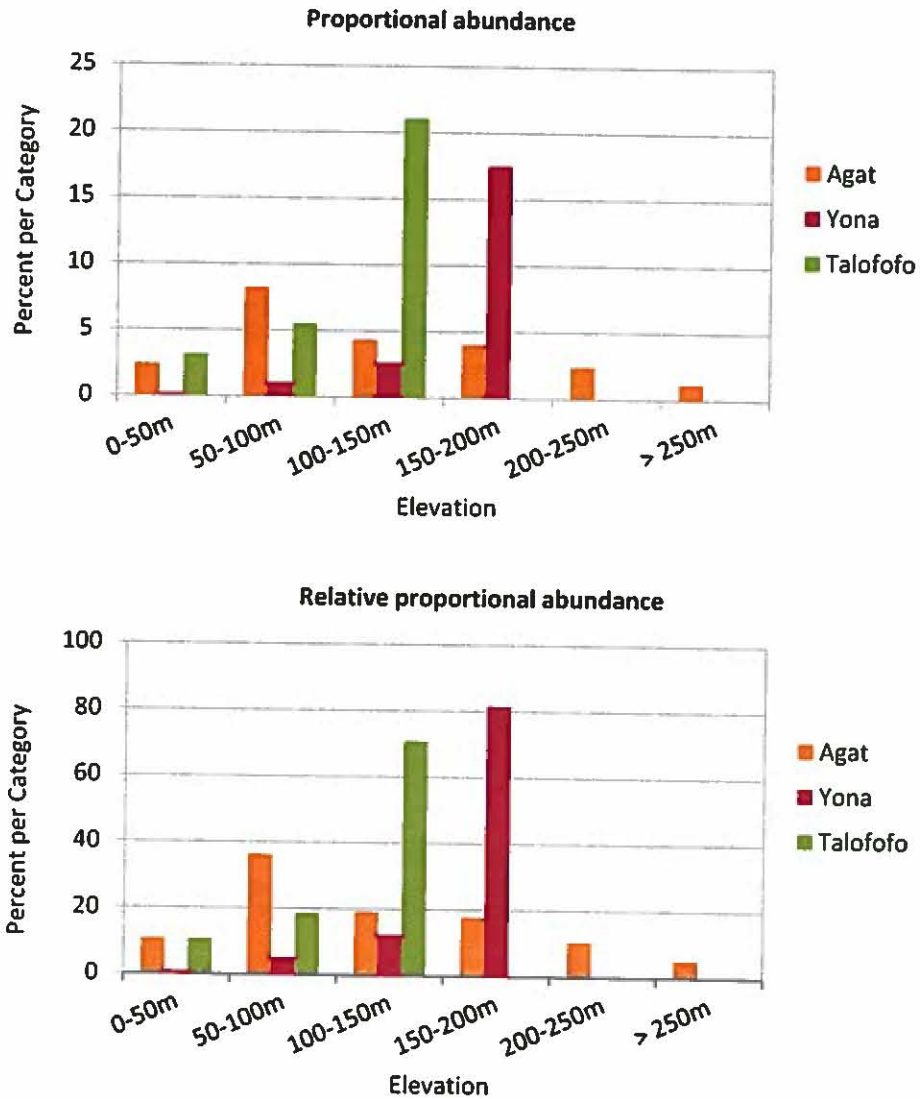
Figure 32. Proportional abundance and relative proportional abundance of badlands in 1946 at each study site broken down into seven elevation categories. The relative proportional abundance normalizes the proportional abundance to allow better comparison of the study sites.
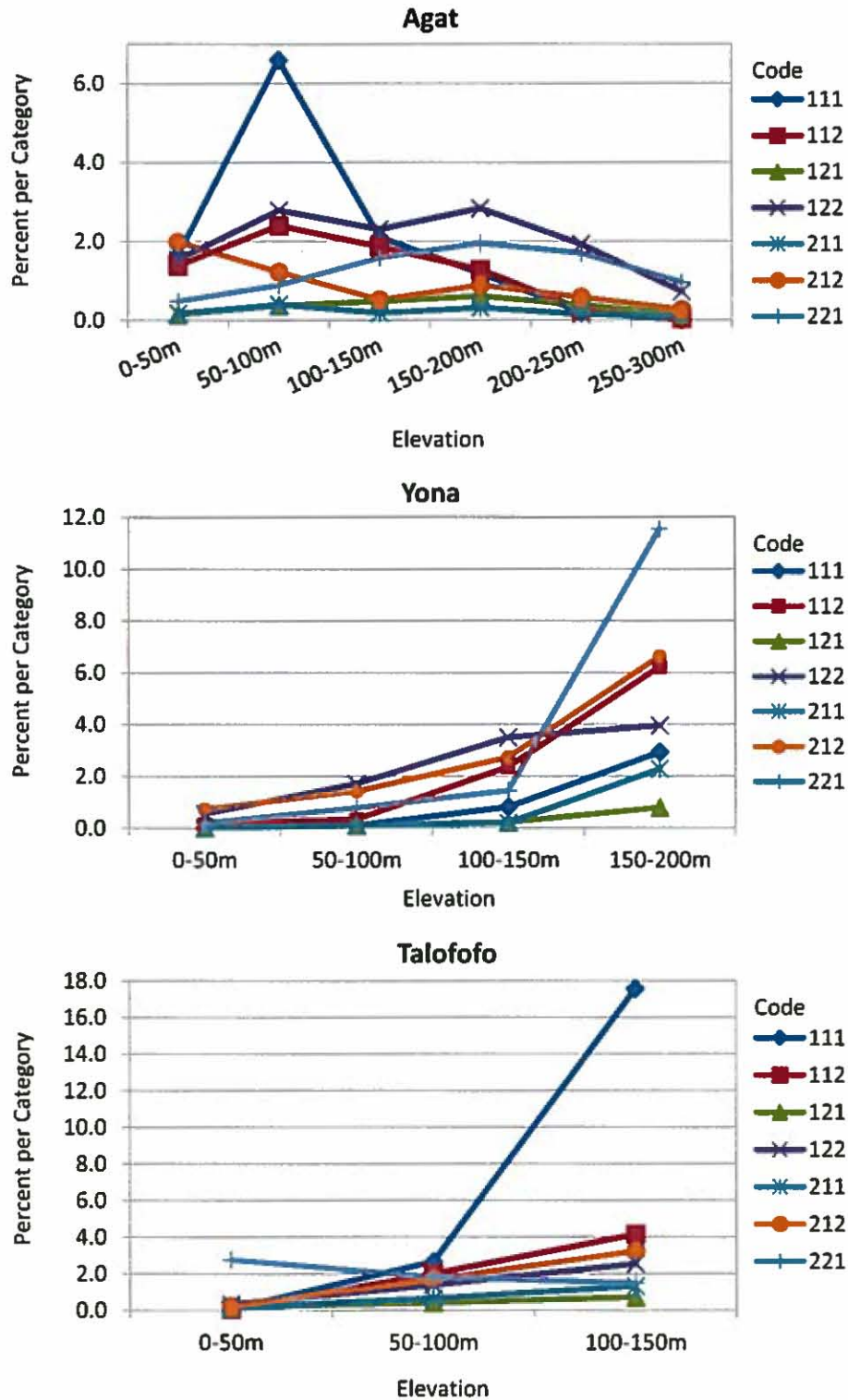
Figure 33. Proportional abundance of badland change classes per elevation category for Agat, Yona, and Talofofo. Areas that were never badland (Code: *222*) are not included here.

Geology

The relationship of badland cover in 1946 and geology is demonstrated in Table 16. The geology of the study sites is primarily volcanic except Agat, where almost 40 percent is limestone. Badlands on Guam develop in weathered volcanic rock and occur in all volcanic formations. All three volcanic formations on Guam (Facpi, Alutom, and Umatac Formation) are found at the study sites. Only negligible amounts of badland areas were detected in limestone formations, but these were likely misclassified badlands.

In Agat, the proportional abundance of badlands in the Facpi Formation (Tuf) with 5.4 percent is slightly higher than in the Alutom Formation (Ta) with 4.2 percent. The proportional abundance of badlands in the Maemong Limestone Formation (Tum) is relatively high (2.3%); however, the badland area covers only 28 square meters. Although the actual area classified as badlands in the Alifan Limestone is higher (917 m^2), the proportional abundance is only 0.1 percent. The badland cover found in both limestone formations is likely due to a mapping error of geologic units or due to misclassification since badlands sometimes have a similar appearance as rock outcrops.

More than 97 percent of the Yona study site belongs to the Alutom Formation, which has a badland cover of 2.2 percent, almost half than that of the Alutom Formation in Agat. No areas were classified as badland in the Mariana Limestone (Qtm).

Over 99 percent at the Talofofo site is classified as the Umatac Formation (Tub and Tud). The remaining one percent of the study site is Alluvium, located in the river valley where no badlands were detected. The majority of all badlands in Talofofo (92.2%) are found in the Bolanos Pyroclastic Member of the Umatac Formation (Tub). However, the proportional abundance of badlands in the Dandan Flow Member of the Umatac Formation (Tud) is similar to that of the Bolanos Pyroclastic Member with 6.7 percent and 7.7 percent, respectively.

The Agat study site had a slightly higher badland cover in the Facpi Formation (5.4%) than the Alutom Formation (4.2%). The difference may be due to the location and not necessarily the geologic formation; *i.e.*, the Alutom Formation is closer to the mountain ridge and more protected from the elements than the Facpi Formation. The Alutom Formation at the Yona study site had proportionally much less badland cover (2.2%) than at the Agat study site (4.2%); however, since the three volcanic formations are not represented at each study site, a direct comparison of the proportional abundances is problematic.

Table 16. Statistical breakdown (in ha and % of total) of the geologic units of each study site and the distribution of badland cover in 1946.

Study Site	Geologic Unit	Study Site		Badlands in 2006		Proportional Abundance per category (%)
		ha	% of total	ha	% of total	
Agat	Ta	52.1	14.8	2.2	20.0	4.2
	Tal	139.0	39.5	0.1	0.8	0.1
	Tuf	160.7	45.7	8.7	79.1	5.4
	Tum	0.1	< 0.1	<<0.1	<0.1	2.3
	Total	351.9	100.0*	11.0	100.0*	3.1
Yona	Ta	297.8	97.1	6.6	100.0	2.2
	Qtma	8.8	2.9	0.0	0.0	0.0
	Total	306.6	100.0	6.6	100.0	2.2
Talofofo	Qal	3.1	0.9	0.0	0.0	0.0
	Tub	338.9	97.7	25.9	92.2	7.7
	Tud	4.7	1.4	2.2	7.9	6.7
	Total	346.7	100.0*	28.1	100.0*	8.1

* Actual numbers may not add up to 100.0 due to rounding errors.

Soil Series

The relationship of badland cover in 2006 and soil map units is demonstrated in Figure 34. The soil map unit delineation, which Reed Sims (2008) modified based on mapping by Young (1988), were used in this study. The soil map units are named after the major soil series or miscellaneous areas but also contain "included" areas that belong to other series. In the case of the Akina-Badland Complex, the unit is about 65 percent Akina silty clay, 30 percent Badland, and 5 percent "included" soils; similarly, the Akina-Badland Association is about 60 percent Akina silty clay, 25 percent Badland, and 15 percent "included" soils. In other soil map units, Badland may be present but only as part of the "included" areas, which are often less than 10 percent of the soil map unit. Akina and Atate soils are highly prone to erosion and can lead to badlands, but also the Togcha, Agfayan, and Sasalaguan soils include actively eroding areas (Young, 1988).

Badlands occur mostly in areas mapped as Akina-Badland Complex and also, in the case of Agat, Akina-Badland Association. Specifically, badlands occupy 14.1 percent and 23.6 percent of the Akina-Badland Complex in Yona and Talofofo, respectively, whereas all other soil map units include less than 3.5 percent badland cover. Agat shows a similar pattern, but the highest proportional abundance per soil map unit occurs in the Akina-Badland Association with 13.5 percent badland cover followed by the Akina-Badland Complex with 8.6 percent. No areas in Yona and Talofofo were mapped as the Akina-Badland Association. All other soil map units present at the study sites had a very low abundance (<5%) of badlands and could be counted as "included" areas. However, a generally higher proportional abundance of badlands at all three study sites can be observed in other soil map units that include the Akina series, which has very low fertility and, hence, low re-vegetation potential.

Badland cover was either absent or negligible (<1%) in the Akina-Agfayan Association and Ritidian-Rock Outcrop Complex in Agat, and the Pulantat Clay, Ylig Clay, Inarajan Clay, or Togcha-Ylig Complex in Yona and Talofofo. The lack of badlands within these soil series can be explained by landscape characteristics and soil properties that are not favorable for badland formation.

Taking the description of the soil map units into account, the results from the badland-soil-mapping analysis were expected. Badlands are consistently most abundant in the Akina-Badland Association at all three study sites (13.5–23.6%). Although the percentage of badlands within the Akina-Badland Complex and Akina-Badland Association is relatively high compared to other soil map units, it is below the 30 percent and 25 percent badland cover, respectively, indicated by Young (1988). Overall, the trends observed here agree well with those from the Ugum study (Khosrowpanah *et al.*, 2010).
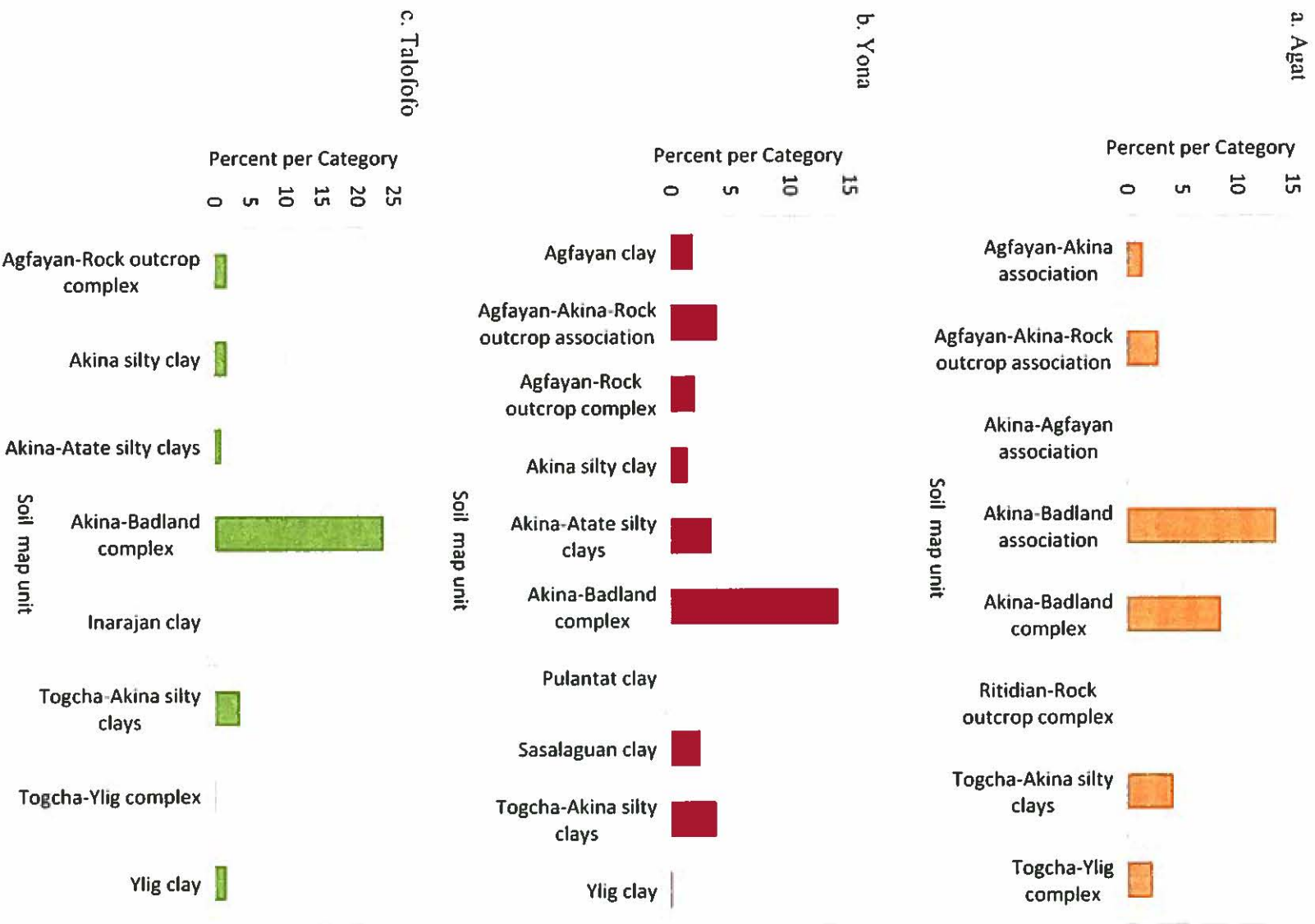
Figure 34. Proportional abundance of badlands in 2006 per soil category at a. Agat, b. Yona, and c. Talofofo study site. Only categories that are represented at each site are included here.

56

5.3. Landscape Metrics

The size distribution of badlands in 1946, 1994, and 2006 is summarized in Table 17 and Figure 35. The overall number of patches increased at all three study sites between 1946 and 2006. The total number of patches increased only slightly from 1946 to 1994 but considerably from 1994 to 2006. The high increase in the total number of patches between 1994 and 2006 is mainly due to the high increase in the number of patches smaller or equal to five square meters during this time period. This high number is likely a result of the classification process. Although a certain increase in newly developed badlands was expected and seems real, the drastic increase is mostly attributed to the badland classification process. First, many smaller badland areas that existed in 1994 and 2006 have been captured just in the 2006 due to different image sensors. Secondly, many tiny patches in 2006 were often mis-classified as badland despite editing efforts to eliminate them. In addition, the 2006 satellite image was taken in the dry season with many burned areas and may show areas that are only seasonally void of vegetation. However, patches larger than 50 square meters also increased in number. Because of their larger size, mis-classification of patches is much less likely, making this increase "real".

The total number of all larger badland patches (larger than 50 m^2) also increased at all three study sites over the 60-year study period mostly due to expansion of "older" badlands and "newer" mass-wasting–derived badlands. The highest increase of larger patches occurred in Agat with an additional 94 patches in 2006 versus 1994 (increase of 49%). Although some patches increased in size, most larger patches seem to be new patches as a result of mass wasting that occurred after 1994.

Even though the larger badland patch size classes (larger than 50 m^2) experienced an overall increase, some patch size classes decreased in number of patches. For example, patches between 500 and 5,000 square meters actually decreased in Talofofo from 63 patches in 1994 to 52 patches in 2006 while the number of patches greater than 5,000 square meters stayed stagnant at 16 in both years. The number of patches between 500 and 5,000 square meters was the same in 1946 and 2006 in Agat and Yona (28 and 18, respectively) but slightly lower in 1994 (26 and 14, respectively). Since the number of large patches ($\geq$500 m^2) did not considerably increase in the 60-year study period and since badlands on Guam were reported as early as 1792 (De Pineda), it seems very reasonable to assume that most of these patches have existed for centuries. Overall, Talofofo has by far the highest concentration of these large patches followed by Agat and then Yona.

While the number of very large patches (>5,000 m^2) in Yona increased from one patch in 1994 to two patches in 2006, the largest patch decreased considerably in size from 5.7 ha to 3.3 ha. It is important to note that the largest patch as well as some other patches consists of many smaller badland patches connected by eroded ORV-trails. As a result, the large decrease in size is mostly attributed to fewer (or partly overgrown) trails connecting the actual badland patches and not necessarily a net decrease in actual patch sizes. However, some patches within this network have decreased but most have drastically increased. Compared to Yona, the number of very large patches is significantly higher in Talofofo and Agat with 16 and 7 patches, respectively. Also, the size of the largest patch in Yona in 1946 was only 0.7 ha in 1946, 5.6 ha in 1994, and 3.3 ha in 2006; for comparison, the largest patch size in Agat was 1.6 ha in 1946, 1.8 ha in 1994, and 1.9 ha in 2006; and in Talofofo 2.9 ha in 1946, 3.3 ha in 1994, and 3.0 ha in 2006, respectively.

Overall, there seems to be a relationship between badland patch geometry and geology: very large "natural" (versus ORV-related) patches are only located in the Umatac Formation and the Facpi Formation but not in the Alutom Formation (neither in Agat nor in Yona). In addition, most badlands in the Alutom Formation tend to be small (estimated average size of 50 m^2) but organized in complex clusters and ubiquitous. This relationship was also observed outside the study sites when overlaying the geology layer with the 2006 satellite imagery in GIS.

Table 17. Results for the landscape metric analysis for all three study sites for 1946, 1994, and 2006. The columns show the number of patches broken down into seven size classes, the total number of patches, the total badland area, and the size of the largest badland patch.

	Number of Patches per Patch Size Class (m^2)								Size of largest Patch (m^2)	Total Area (m^2)
	≤ 1	(1,5]	(5,10]	(10,50]	(50,500]	(500,5000]	>5000	Total		
Agat										
1946	141	160	111	259	138	28	5	842	16114	109520
1994	92	105	108	354	161	26	6	852	18126	132963
2006	1214	1038	389	619	252	28	7	3547	19112	162961
Yona										
1946	166	194	160	312	206	18	1	1057	7409	66140
1994	197	299	192	475	236	14	1	1414	55693	119485
Talofofo										
1946	212	211	112	232	157	61	13	998	29265	281518
1994	278	315	111	280	195	63	16	1258	32761	337522
2006	758	543	192	305	236	52	16	2102	29739	316875

a.

b.

c.
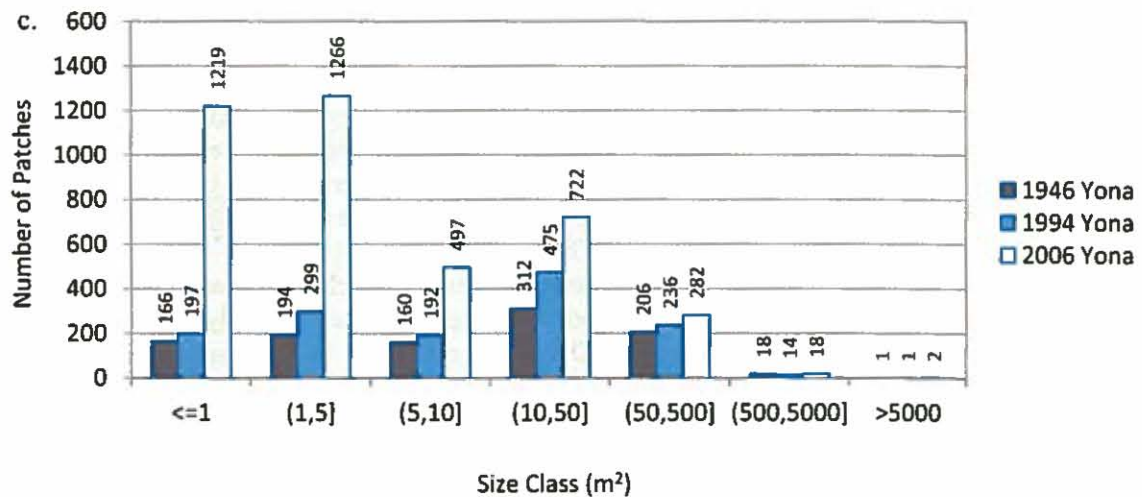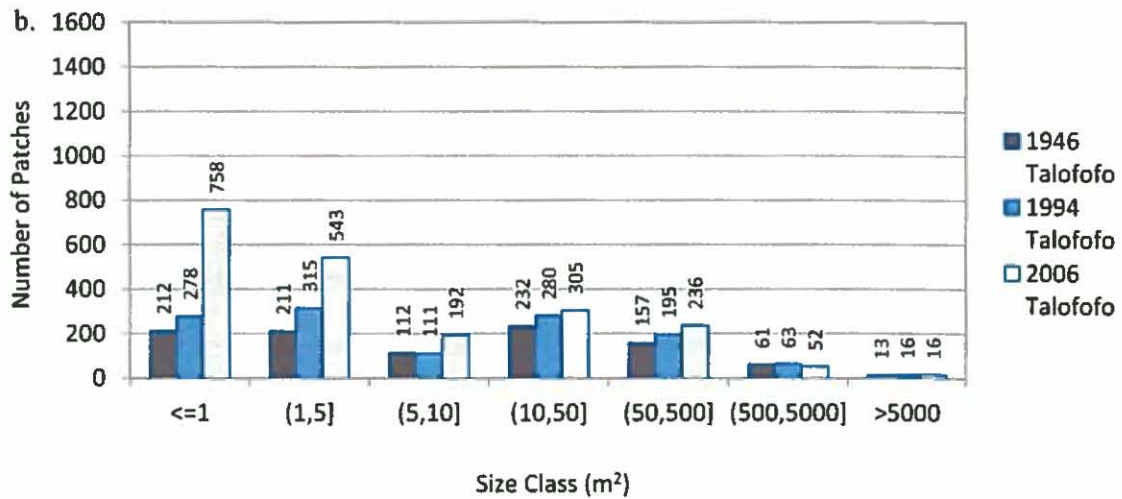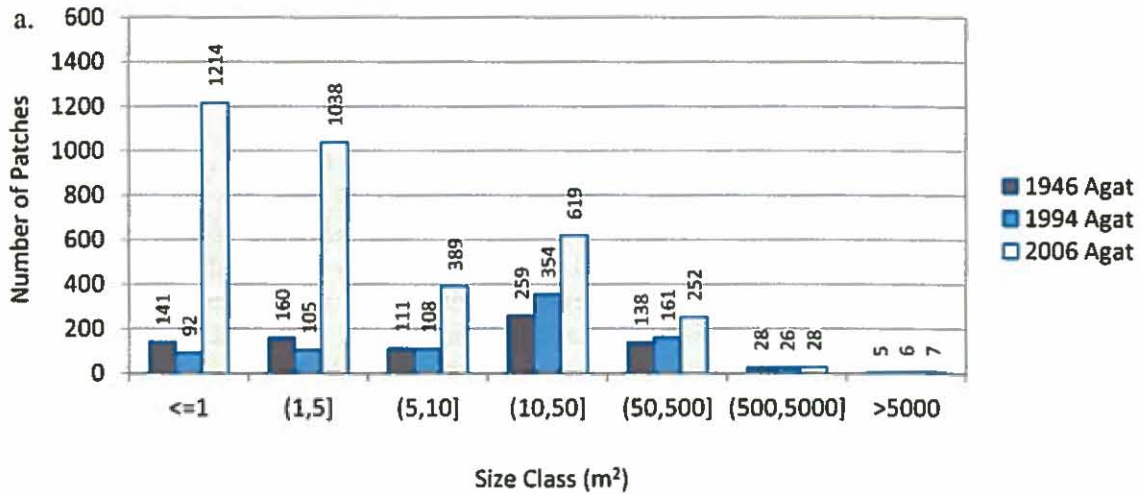
Figure 35. Histogram showing the frequency distribution of the area of badlands patches broken down into six size classes for a. Agat; b. Yona, and c. Talofofo. Each histogram shows the number of patches for 1946, 1994, and 2006.

5.4. Soil Properties

Basic chemical and physical soil properties were tested in badlands and adjacent vegetative sites (savanna) at all three study sites to compare possible differences in badland dynamics among sites. Results from the soil analysis are presented in Table 18.

As shown, the organic matter (O.M.) content is significantly higher in vegetative sites (V) than in badlands (BL) (t-test for two samples: BL=16, V=6, t=8.247, df=20, p<0.001). The O.M. content within vegetative areas ranges from 1.73 percent in the subsoil to 6.75 percent in the topsoil. In contrast, badlands tend to have no O.M. content in the top soil and occasionally very small amounts (≤0.16%) in the subsoil; however, the difference is not significant (t=-2.024, df=20, p=0.057). The O.M. content is associated with the level of microbial activity, which is generally highest in the shallow topsoil in tropical environments. However, the near absence of O.M. in badlands is an indicator of severe erosion. Low levels in the subsoil in badlands might be due to the decreased impact of water erosion or possibly due to old plant roots. O.M. is an important indicator of soil quality, hence, for plant growth. It provides most of the nutrients in the highly leached upland soils of Guam but also binds soil particles into stable aggregates and increases infiltration rates (Young, 1988). The lack of O.M. makes the badland soils more prone to erosion and makes it even harder for plants to establish, thereby creating a vicious cycle of degradation.

All tested soils were acidic with a pH between 4.62 and 5.83 with no difference between BL and V (BL=16, V=6, t=-0.344, df=20, p=0.734). The pH has implications on the availability of nutrients to the plants. For example, a pH of 5.0 is low enough to make aluminum soluble, which is toxic to some plants. For this reason, only pioneer plants like *Dicranopteris linearis* (false staghorn fern), which are aluminum-tolerant, can be found in badlands. Even though the pH is similar in vegetative sites, it does not affect plant growth because the O.M. binds the soluble aluminum and takes it out of solution.

With respect to nutrient content, P, K, and Ca values were very low (≤0.97 ppm, ≤23.75 ppm, and ≤243.53 ppm, respectively) for all samples, regardless of depth and presence or absence of vegetation. P levels did not differ between BL and V (BL=16, V=6, t=-0.2366, df=20, p=0.815). K levels were significantly higher in V than in BL at all sites (BL=16, V=6, t=3.332, df=20, p=0.0036). Ca levels in Agat and Talofofo were significantly higher in V than BL (BL=8, V=4, t=6.249, df=10, p≤0.001); in Yona, Ca levels varied widely with extremely high values in two badlands samples. These high values are likely the result of calcite, which is present in many outcrops in the Alutom Formation, although it is usually leached out (Tracey *et al.*, 1964). Mg levels were generally low, however, in one BL sample in Yona and in Talofofo levels were extremely high (≥403.05 ppm and 525.57 ppm, respectively). These samples might have been taken from areas with exposed Mg oxide. The higher levels of K and Ca in vegetative sites may be attributed to the higher O.M. content and the associated mineralization of these elements. Overall, the low nutrient levels in badland as well as vegetative savanna indicate poor soil quality, which is common throughout southern Guam.

All soil samples in badlands and vegetative areas were classified as clay except one sample in the upper layer (0–15 cm) of a badland which was classified as sandy clay according to the soil texture triangle chart (see Appendix D). Soil moisture at badland sites was generally higher in the lower soil layer compared to the upper soil layer, which dries out more easily; however, the difference was statistically not significant (one sample t=-1.298, df=15, p=0.214). Soil moisture at vegetative sites was equal or greater in the upper layer due to the higher O.M. content, associated water-holding capacity, and roots that draw water from the lower layer. Contrary to expectations, the average soil moisture was higher in badlands then vegetative sites in Agat and in Yona. Although samples were sealed right after sampling, samples were not analyzed immediately and moisture might have escaped from some bags, skewing the number

Table 18. Results of the soil analysis.

Location	Sample ID	Depth in cm	% O.M.	pH	P	K	Ca	Mg	% Sand	% Silt	% Clay	% Soil Moisture
					ppm							
Agat												
Badland	I	0-15	0.00	4.71	0.00	8.45	9.65	9.55	29.22	17.58	53.20	50.0
		15-30	0.16	4.70	0.60	7.14	12.47	8.85	23.22	15.58	61.20	57.1
	II	0-15	0.00	4.73	0.24	5.84	15.40	18.52	18.02	33.18	48.80	25.0
		15-30	0.08	4.72	0.72	6.34	10.38	17.14	17.62	31.58	50.80	44.4
Vegetation	III	0-15	4.28	5.04	0.24	12.7	67.11	47.94	21.22	21.58	57.20	25.0
		15-30	1.98	5.08	0.47	7.26	79.96	42.35	20.02	18.78	61.20	25.0
Yona												
Badland	IV	0-15	0.00	4.64	0.24	9.81	58.92	41.46	25.20	21.60	53.20	50.0
		15-30	0.08	4.51	0.60	12.16	35.25	36.16	26.81	25.59	47.60	62.5
	V	0-15	0.08	4.63	0.47	6.09	24.28	23.52	18.81	25.59	55.60	25.0
		15-30	0.08	4.70	0.47	7.06	21.14	19.32	18.81	21.59	59.60	50.0
	VI	0-15	0.00	5.70	0.60	16.17	192.92	456.3	---	---	---	50.0
		15-30	0.00	5.83	0.60	18.06	243.53	403.5	---	---	---	20.0
	VII	0-15	0.00	5.04	0.24	10.43	129.35	26.81	30.41	22.39	47.20	38.5
		15-30	0.00	4.93	0.12	8.63	104.51	23.04	21.62	29.18	49.20	52.9
Vegetation	VIII	0-15	3.21	4.78	0.35	18.07	89.87	81.37	26.81	19.59	53.60	30.0
		15-30	1.73	4.71	0.24	5.91	54.44	71.24	29.20	17.20	53.60	20.0
Talofofo												
Badland	IX	0-15	0.00	4.78	0.60	12.65	20.69	43.81	25.62	25.58	48.80	27.3
		15-30	0.08	4.84	0.60	13.02	26.80	57.49	21.62	27.58	50.80	41.2
	X	0-15	0.00	5.00	0.72	19.45	8.46	532.07	48.02	11.18	40.80	28.6
		15-30	0.00	5.10	0.97	22.01	10.24	525.57	39.22	14.38	46.40	30.0
Vegetation	XI	0-15	6.75	4.62	0.60	23.75	44.75	168.1	19.62	13.58	66.80	66.7
		15-30	4.03	4.90	0.84	14.85	41.00	146.5	19.22	13.98	66.80	57.1

61

5.5. Accuracy Assessment

An overall classification accuracy of 0.87, 0.91, and 0.93 was achieved for the 1946, 1994, and 2006 classification, respectively (Table 19). Except for the producer's accuracy for the 1946 badlands (0.69), all accuracies are within the 0.85-target Thomlinson *et al.* (1999) set for overall accuracy with no class less than 0.70. The probability of a pixel classified as badland to be truly badland is 0.85, 0.92, and 0.94 (1946, 1994, and 2006), while the probability of a pixel truly badland classified as badland is 0.69, 0.81, and 0.86, respectively. However, the true accuracy is believed to be higher than the calculated accuracy because many sampling points were located right on the border of badlands, where it was rather subjective to decide the category (badland or non-badland). In the future, such points may not be included in the error matrix.

Table 19. Error matrix including producer's and user's accuracy for the 1946, 1994, and 2006 image classification.

1946		Reference			
Classification	BL	NBL	Total	Producer's Accuracy	User's Accuracy
BL	60	11	71	BL = 0.69	BL = 0.85
NBL	27	202	229	NBL = 0.95	NBL = 0.88
Total	87	213	300	Overall Accuracy = 0.87	

1994		Reference			
Classification	BL	NBL	Total	Producer's Accuracy	User's Accuracy
BL	81	7	88	BL = 0.81	BL = 0.92
NBL	19	193	212	NBL = 0.97	NBL = 0.91
	100	200	300	Overall Accuracy = 0.91	

2006		Reference			
Classification	BL	NBL	Total	Producer's Accuracy	User's Accuracy
BL	93	6	99	BL = 0.86	BL = 0.94
NBL	15	186	201	NBL = 0.97	NBL = 0.93
	108	192	300	Overall Accuracy = 0.93	

Chapter 6   Summary & Conclusion

This study demonstrated that time-series analysis based on historic aerial photographs and satellite imagery provides a useful tool to track small-scale changes in badland cover on a sub-basin scale in southern Guam. Despite challenges in registering (overlaying) the historical images, general trends of badland dynamics could be detected.

The change detection analysis revealed a net increase in badland cover at all three study sites from 1946 to 2006. However, at the same time some badland patches decreased or disappeared entirely, hence re-vegetated. Changes in badland cover over time varied within and between study sites but also between the two time periods, 1946–1994 and 1994–2006. Variations are linked to both human and natural factors. Intensive human activity, mostly in the form of off-roading and, to a lesser extent, farming activities, has certainly contributed to accelerated badland expansion. In contrast, badland expansion in areas with no off-roading or farming activities is mostly attributed to natural mass wasting, likely triggered by tropical cyclones.

The overall number of badland patches has increased at all three study sites from 1946 to 2006. However, the number of large patches (>500 m^2) increased only slightly. Since the majority of these large patches existed before 1946, it seems that it generally takes a long time for such extensive badland areas to develop. The fact that these extensive badland patches existed before 1946 and generally did not expand drastically since suggests that they likely developed hundreds if not thousands of years ago.

The study also revealed that "newer" (more recently developed) badland areas were more likely to recover than older badland areas. This behavior is probably due to different degrees of erosion: newer badlands may still contain a subsoil layer, where certain plants can establish, whereas older badlands may be eroded down to saprolite, which is unable to support any vegetative growth. For this reason, re-vegetation efforts should rather be focused on recently developed badland areas than older ones.

The results from the terrain analysis demonstrated that natural badland occurrence is strongly controlled by topography. At all study sites, southeast-facing slopes had consistently higher badland cover than north- or northwest-facing slopes. Slope gradient was only positively correlated to badland cover where steep slopes were exposed in the form of remnant hills at higher elevations. Also, elevation was only a good indicator of badland cover on the windward study sites. Overall, the influence of terrain on badland occurrence can be explained by the differential exposure to wind, rain and sun.

Soil sampling of badlands and adjacent vegetative savanna confirmed high clay content, low pH, and low nutrient levels, which are common characteristics of poor soil quality throughout southern Guam. The most obvious difference between badlands and adjacent area was the level of organic matter (O.M.) content. The O.M. content was almost entirely absent in badlands ($\leq 0.16\%$) but vegetative areas had an average of 2.58 percent in the subsoil and 4.75 percent in the topsoil. The lack of organic matter in badlands largely explains the absence of vegetation. Increasing O.M. content will increase soil fertility and, hence, facilitate plant growth.

It is important to note that this research focused on the spatial extent of badlands, or horizontal erosion rate, and not the vertical erosion rate, which has been investigated by other researchers. The results of this study showed that off-roading, and to some extent mis-managed farming, can initiate badland development and expansion (hence, horizontal erosion). Nonetheless, the accelerated vertical erosion caused by these human activities is also important to consider. In addition, wildfires are also a big concern in respect to accelerated erosion rate and potentially initiating badland development. However, the role of wildfires in badland dynamics was not investigated in this study.

The main concern of badlands and the reason for this study is the high erosion rate they exhibit and the associated sediment movement downstream, where it adversely affects stream and ocean water quality. Since badland areas have generally expanded over the last 60 years and will likely continue to expand without intervention, sediment loads originating from eroding badlands will continue to increase, putting additional stresses on the coral reef system of southern Guam. As shown in this study, badlands expansion can occur naturally, but human activities, chiefly in the form of off-roading activities, exacerbate badland expansion causing accelerated erosion and associated sedimentation. With the anticipated military buildup and related population boom on Guam, off-roading activities are likely to increase significantly, resulting in accelerated badland expansion and increased vertical erosion. For this reason, it is essential to manage, regulate, and enforce the off-roading activities.

Chapter 7   Recommendations

The availability of high temporal and spatial resolution satellite imagery will make future monitoring of badland changes easier and more efficient. Change detection analysis, as used in this study, can identify new badlands, especially large-scale mass wasting, which should then be stabilized to avoid accelerated erosion. Arson, which may have a large impact on badland development, was not investigated in this study because of insufficient historical data. Fires are currently being mapped, and future research could incorporate these data with updated satellite imagery to analyze their impact. Since georeferencing of historical aerial images, especially over larger areas, proved to be a challenging and very time-consuming task, it is recommended to use smaller study sites, like individual badland patches or cluster of patches, when investigating fine-scale changes. By choosing smaller study sites, it is also feasible to use imagery from more years (*e.g.*, 1953, 1964, and 1975) to trace inter-decadal changes; additionally, inter-decadal variances in climate could be correlated with these changes.

It is critical to identify badlands with the highest erosion rates and focus management efforts accordingly. Specifically, it is recommended to measure and compare differences in vertical erosion rates of different land uses (especially off-roading), of older, persistent badlands and recently developed badlands, of deep-seated and shallow landslides, and of different geologic formations. The effect of aspect should also be taken into account when measuring erosion rates. Using the same study sites as in this study would eliminate the legwork of determining the age of the badlands and also terrain attributes.

Two general management strategies to decrease badland erosion and associated sedimentation are recommended: re-vegetation of badlands and management of human activities that cause or accelerate badland erosion. Badland re-vegetation is costly and time-consuming; thus, it needs to be planned wisely. Instead of trying to restore entire badland patches, it is recommended to plant vegetative barriers using vetiver grass (Golabi *et al.*, 2005b) or other effective plants (Doerge and Smith, 2008) around the down-slope perimeter of badlands. This way the vegetative barriers can catch the eroded material at the source; hence, improving water quality downstream. Priority areas are badlands with the highest erosion rates, especially the ones near streams. Since off-roading areas are believed to contribute the highest sediments loads, these areas should be addressed first. However, future research may identify other badlands, like new mass wasting as priority sites. In addition, re-vegetating ravine forests will stabilize landslide-prone river valleys but also catch sediments from uphill. These reforestation efforts should be focused on areas that recently changed from forest to savanna since it is proof of suitable forest habitat. A good point of reference would be the historical aerial imagery from 1946. Off-roading activities also need to be regulated and enforced by law to effectively decrease their impact. Regulations should include designated areas with sediment control techniques and banning the formation of new trails. Registration for off-road vehicles should include a management fee to help fund badland restoration projects. Public education and awareness programs about the adverse effects of off-roading also need to be implemented. Best management farming practices should also be promoted to avoid accelerated erosion.

REFERENCES

Athens, J.S. and Ward, J.V. 2004. Holocene Vegetation, Savanna Origins and Human Settlement of Guam. In A Pacific Odyssey: Archaeology and Anthropology in the Western Pacific. Papers in Honour of Jim Specht, ed. Val Attenbrow and Richard Fullagar, pp. 15–30. Records of the Australian Museum, Supplement 29. Sydney: Australian Museum.

Bell, F., Falanruw, M., Lawrence, B., Limtiaco, D., and Nelson D. 2002. Draft Vegetation Strategy for Southern Guam. Honolulu, HI. U.S. Department of Agriculture, Forest Service, U.S. Department of Agriculture, Natural Resources Conservation Service, Government of Guam Division of Forestry.

Bryan, R., and Yair, A. 1982. Badlands Geomorphology and Piping. GeoBooks, University Press, Cambridge.

Calzolari, C., and Ungaro, F. 1998. Geomorphic Features of a Badland (Biancana) Area (Central Italy): Characterization, Distribution and Quantitative Spatial Analysis. Catena 31: 237–256.

Cantón, Y., Del Barrio, G., Solé-Benet, A., and Lázaro, R. 2004. Topographic Controls on the Spatial Distribution of Ground Cover in the Tabernas Badlands of SE Spain. Catena 55: 341–365.

Clark, M. L. and Rendell, H.M. 2006. Process-form Relationships in Southern Italian Badlands: Erosion Rates and Implications for Landform Evolution. Earth Surface Processes and Landforms 31: 15–29.

Congalton, R. 1991. A Review of Assessing the Accuracy of Classifications of Remotely Sensed Data. Remote Sensing of Environment 37: 35–46.

Congalton, R.G., Balogh, M., Bell, C., Green, K., Milliken, J.A., and Ottman, R. 1998. Mapping and Monitoring Agricultural Crops and Other Land Cover in the Lower Colorado River Basin. Photogrammetric Engineering & Remote Sensing. Vol. 64. No.11: 1107–1113. http://www.iiasa.ac.at/Admin/PUB/Documents/IR-98-081.pdf

Coffman, J. C. 2010. Oral communication. Guam National Park Service.

Crago, L.M. 2005. Riparian Plant Restoration Phase III – Western Pacific Cooperative Agreement No. 68-3A75-4-72, Modification No. 10. Quarterly Report. Prepared for Tropical Technology Consortium, National Resources Conservation Service, U.S. Department of Agriculture.

De Pineda, A. 1792. Guam Diary of Naturalist Antonia De Pineda y Ramirez February 1792.Translated by V.F. Mallada, edited by M.G. Driver, Micronesian Area Research Center, University of Guam, 1990.

Doerge, B.C. and Smith, C. 2008. Mechanisms of Erosion of Volcanic Soils on Non-Agricultural Land in Guam. American Society of Agricultural and Biological Engineers (ASABE). Presented at the 2008 ASABE Annual International Meeting, 29 June–2 July, 2008, Rhode Island.

Donnegan, J. A., Butler, S. L., Grabowiecki, W., Hiserote, B.A., and Limtiaco, D. 2004. Guam's Forest Resources, 2002. Resources Bulletin PNW-RB–243. Portland, OR: U.S. Department of Agriculture, Forest Service, Pacific Northwest Research Station.

Endress, B.A., and Chinea, J.D. 2001. Landscape Patterns of Tropical Forest Recovery in the Republic of Palau. Biotropica 33(4): 555–565.

Environmental Systems Research Institute (ESRI) 2010. Desktop Help. ArcEditor 9.3.

Falanruw, M.C. 1976. Life on Guam – Savanna, Old Fields, Roadsides. Guam Department of Education, Agana.

Foody, G.M. 2002. Status of Land Cover Classification Accuracy Assessment. Remote Sensing of Environment 80: 185–201.

Fosberg, R. 1960. The Vegetation of Micronesia. Bulletin of the American Museum of Natural History 119: 1–75.

Gavenda, R. 2009. Oral communication. Natural Resources Conservation Service, U.S. Department of Agriculture, Guam.

Gerakis, A. and Bear, B. 2000. Program to Plot Results of Textural Analysis on Textural Triangle. http://nowlin.css.msu.edu/software/triangle_form.html

Golabi, M.H., Iyekar, C., Minton, D., Raulerson, C.L., and Chargualaf, D. 2005a. Watershed Management to Meet Water Quality Standards by Using the Vetiver System in Southern Guam. AU J.I. 9(1): 64–70.

Golabi, M.H., Iyekar, C., and Denney, M.J. 2005b. Challenges and Actions Regarding the Rehabilitation of Degraded Lands: Case Study from the Pacific Island of Guam. Sociedade & Natureza, Uberlândia, Special Issue, May, 2005. p. 87–106.

Grimm, G. 2009. Oral communication. NAVFACMAR, U.S. Navy, Guam.

Hudak, A.T. and Wessman, C.A. 1998. Textural Analysis of Historical Aerial Photography to Characterize Woody Plant Encroachment in South African Savanna. Remote Sensing Environment 66: 317–330.

Hunter-Anderson, R. 2009. Savanna Anthropogenesis in the Mariana Islands, Micronesia: Re-Interpreting the Paeleoenvironmental Data. Archaeol. Oceania 44(2009): 125–141.

Khosrowpanah, S., Wen, Y., and Kottermair, M. 2010. Spatial Distribution of Badlands in the Ugum Watershed: Characterization and Temporal Analysis. Technical Report No.126. Water and Environmental Research Institute, University of Guam.

Khosrowpanah, S., Wen, Y., Jocson, J., and Taborosi, D. 2008. Natural Resources Atlas of Southern Guam. Technical Report No.116, Water and Environmental Research Institute, University of Guam. www.hydroguam.net

Kottermair, M. and Olsen, A. unpublished. Typhoon Atlas of Micronesia 1945–2007.

Lander, M.A. 2009. Oral communication. University of Guam.

Lander, M.A. 1994. Meteorological Factors Associated with Drought on Guam. Technical Report No.75, Water and Environmental Research Institute, University of Guam.

Lander, M.A. unpublished. Andersen AFB, Guam, Temperature Time Series for the Period 1953 through 2009. Water and Environmental Research Institute, University of Guam.

Lander, M.A. and Guard, C.P. 2003. Creation of a 50-Year Rainfall Database, Annual Rainfall Climatology, and Annual Rainfall Distribution Map for Guam. Technical Report No.102, Water and Environmental Research Institute, University of Guam.

Landscape and Resource Management Research Group (LARG). 2005. V-LATE - Vector-based Landscape Analysis Tools Extension. University of Salzburg, GIS Centre for GeoInformatics. http://www.geo.sbg.ac.at/larg/vlate.htm

Levesque, L.M. 2000. Investigating Landscape Change and Ecological Restoration: An Integrated Approach Using Historical Ecology and GIS in Waterton Lakes National Park, Alberta. M. S. Thesis in Interdisciplinary Studies, School of Environmental Studies Department of Geography, University of Guelph.

Lewis. R.R. 1999. Quantifying Geomorphic Processes of Guam's Taelayag River Badlands by Determining Rates for Basin Yield, Slope Retreat and Fracture Movement. M.S. Thesis, University of Guam.

Lillesand, T.M., Kiefer, R.W., and Chipman, J.W. 2008. Remote Sensing and Image Interpretation. Sixth Edition, John Wiley & Sons, Inc., New York.

Mast, J.N., Veblen, T.T., and Hodgson, M.E. 1997. Tree Invasion within a Pine/Grassland Ecotone: an Approach with Historic Aerial Photographs and GIS Modeling. Forest Ecology and Management 93: 181–194.

McGarigal, K., Cushman, S.A., Neel, M.C., and Ene, E. 2002. FRAGSTATS: Spatial Pattern Analysis Program for Categorical Maps. Computer software program produced by the authors at the University of Massachusetts, Amherst. www.umass.edu/landeco/research/fragstats/fragstats.html

Minton, D. 2006. Fire, Erosion, and Sedimentation in the Asan-Piti Watershed and War in the Pacific NHP, Guam. Technical Report 150, Pacific Cooperative Studies Unit, University of Hawaii at Mānoa.

Moretti, S. and Rodolfi, G. 2000. A Typical "Calanchi" Landscape on the Eastern Apennine Margin (Atri, Central Italy): Geomorphological Features and Evolution. Catena 40: 217–228.

Mueller-Dombois, D. and Fosberg, F.R. 1998. Vegetation of the Tropical Pacific Islands. Springer Press, New York. Chapter V. Micronesia. p. 241–275.

Munsell Color. 1975. Munsell Soil Color Charts, 1975 edition. Baltimore, Maryland, Macbeth Division of Kollmorgen Corporation.

National Geophysical Data Center (NGDC). 2010. Global Significant Earthquake Database, 2150 B.C. to present. (The Significant Earthquake Database). NOAA Satellite and Information Service. http://www.ngdc.noaa.gov/hazard/earthqk.shtml

National Oceanic and Atmospheric Administration (NOAA). 2009. Coastal Change Analysis Program (CCAP) for Guam.

National Park Service (NPS). 2009. Off-Road Vehicle Assessment Mt. Tenjo Unit – War in the Pacific National Historic Park. U.S. Department of Interior, Guam. Prepared by PCR Environmental, Inc., Guam.

Natural Resources Conservation Service (NRCS). 2006. Preliminary GIS Erosion Estimates for Cetti and Sella Watersheds. U.S. Department of Agriculture, Natural Resources Conservation Service, Pacific Islands Area.

Natural Resource Conservation Service (NRCS). 2001. Fena Watershed Resource Assessment: Erosion and Sediment Identification for Critical Area Treatment, Territory of Guam. U.S. Department of Agriculture, Hagåtña, Guam.

Natural Resources Conservation Service (NRCS). 1996. Ugum Watershed Management Plan, Territory of Guam. U.S. Department of Agriculture, Hagåtña, Guam.

Neuendorf, K.K.E., Mehl, J.P., and Jackson, J.A. 2005. Glossary of Geology. American Geological Institute, Alexandria, Virginia, Fifth Edition.

Olsen, S.R., Cole, C.V., Watanabe, F.S., and Dean, L.A. 1954. Estimation of Available Phosphorus by Extraction with Sodium Bicarbonate. USDA Circ. 939 U.S. Government Printing Office, Washington, DC.

Park, M. 2007. Developing a GIS-based Soil Erosion Model of Ugum Watershed. M.S. Thesis, Water and Environmental Research Institute, University of Guam.

PCR Environmental, Inc. 2009. Off-road Vehicle Assessment Mt. Tenjo Unit, War in the Pacific National Historic Park. Prepared for National Park Service, War in the Pacific National Historic Park/ American Memorial Park. May 2009.

Reagan, M.K. and Meijer, A. 1984. Geology and Geochemistry of Early Arc-Volcanic Rocks from Guam. Geological Society of America Bulletin 95: 701–713.

Scheman, N. 2002. Identification of Erosion Processes and Sources of Exposed Patches in the La Sa Fua Watershed of Southern Guam. M.S. Thesis, Water and Environmental Research Institute, University of Guam.

Siegrist, H.G.Jr. and Reagan, M.K. 2008. Geologic Map and Section of Guam, Mariana Islands. Based on Tracey *et al.* (1964). Water and Environmental Research Institute, University of Guam.

Stone, B.C. 1970. The Flora of Guam – a Manual for the Identification of the Vascular Plants of the Island. Micronesica. Vol.6. University of Guam.

Summa, V., Tateo, F., Medici, L., and Giannossi, M.L. 2007. The Role of Mineralogy, Geochemistry and Grain Size in Badlands Development in Pisticci (Basilicata, Southern Italy). Earth Surface Processes and Landforms 32: 980–997.

Thomlinson, J.R., Bolstad, P.V., and Cohen, W.B. 1999. Coordinating Methodologies for Scaling Landcover Classifications from Site-Specific to Global: Steps toward Validating Global Map Products. Remote Sensing of Environment 70: 16–28.

Torri, D., Colica, A., and Rockwell, D. 1994. Preliminary Study of the Erosion Mechanisms in a Biancana Badland (Tuscany, Italy). Catena 23: 281–294.

Tracey, J.I., Schlanger, S.O., Stark, J.T., Doan, D.B., and May, H.G. 1964. General Geology of Guam, Mariana Islands. United States Government Printing Office, Washington.

Tuttle, M. and Griggs, G. 1987. Soil Erosion and Management Recommendations at Three State Vehicular Recreation Areas, California. Environmental Geology Water Science, Vol.10 No.2: 111–123.

Walkley, A. and Black, I.A. 1934. An Examination of Degtjareff Method for Determining Soil Organic Matter and a Proposed Modification of the Chromic Acid Titration Method. Soil Science 37: 29–37.

Wen, Y., Khosrowpanah, S., and Heitz, L.F. 2009. Watershed Land Cover Change in Guam. Technical Report No.124. Water and Environmental Research Institute, University of Guam.

Wilshire, H.G. and Nakata, J.K. 1976. Off-Road Vehicle Effect on California's Mojave Desert. California Geology 29: 123–133.

Wilshire, H.G., Nakata, J.K., Shipley, S., and Prestegaard, K. 1978. Impacts of Vehicles on Natural Terrain at Seven Sites in the San Francisco Bay Area. Environmental Geology, Vol.3 No.5: 295–319.

Young, F.J. 1988. Soil Survey of Territory of Guam. USDA Soil Conservation Service.

APPENDICES

APPENDIX A. Terrain Analysis – Raw Data.

APPENDIX B. Examples of Badland Changes.

APPENDIX C. Examples of Misclassification.

APPENDIX D. Soil Samples.

APPENDIX E. Examples of Badlands at the Study Sites.

APPENDIX A. Terrain Analysis – Raw Data.

Slope - Agat

Area (m²) of badland change classes per slope category.

Code	0-10°	10-20°	20-30°	30-40°	40-50°	<50°	Total
111	26441	24939	12363	4562	1169	325	69799
112	13294	12081	6912	2385	451	78	35201
121	2476	2512	1772	832	303	126	8021
122	12250	15964	11979	6115	2162	488	48958
211	1906	1768	1188	551	271	44	5728
212	8018	7136	4554	1882	465	60	22115
221	7228	8176	5855	2898	807	1036	26000
222	384812	582366	496564	314396	117043	16760	1911941
Total	456425	654942	541187	333621	122671	23477	2127763

Proportion (% of study site) of badland change classes by slope categories.

Code	0-10°	10-20°	20-30°	30-40°	40-50°	<50°	Total
111	1.243	1.172	0.581	0.214	0.055	0.015	3.280
112	0.625	0.568	0.325	0.112	0.021	0.004	1.654
121	0.116	0.118	0.083	0.039	0.014	0.006	0.377
122	0.576	0.750	0.563	0.287	0.102	0.023	2.301
211	0.090	0.083	0.056	0.026	0.013	0.002	0.269
212	0.377	0.335	0.214	0.088	0.022	0.003	1.039
221	0.340	0.384	0.275	0.136	0.038	0.049	1.222
222	18.085	27.370	23.337	14.776	5.501	0.788	89.857
Total	21.451	30.781	25.435	15.679	5.765	1.103	100.000

Proportional abundance (%) of badland change classes per slope category.

Code	0-10°	10-20°	20-30°	30-40°	40-50°	<50°	Total
111	5.8	3.8	2.3	1.4	1.0	1.4	3.3
112	2.9	1.8	1.3	0.7	0.4	0.3	1.7
121	0.5	0.4	0.3	0.2	0.2	0.5	0.4
122	2.7	2.4	2.2	1.8	1.8	2.1	2.3
211	0.4	0.3	0.2	0.2	0.2	0.2	0.3
212	1.8	1.1	0.8	0.6	0.4	0.3	1.0
221	1.6	1.2	1.1	0.9	0.7	4.4	1.2
222	84.3	88.9	91.8	94.2	95.4	71.4	89.9
Total	100.0	100.0	100.0	100.0	100.0	100.0	100.0

Slope - Yona

Area (m²) of badland change classes per slope category.

Code	0-10°	10-20°	20-30°	30-40°	40-50°	<50°	Total
111	8192	3553	1614	372	29	0	13760
112	22658	10125	4470	1471	223	28	38975
121	1820	1457	822	455	75	10	4639
122	31808	20733	10031	3994	841	208	67615
211	3474	1813	816	331	52	0	6486
212	29856	16706	9014	3978	674	36	60264
221	22219	12380	4534	1694	376	52	41255
222	1097521	1006989	492554	182383	46337	7578	2833362
Total	1217548	1073756	523855	194678	48607	7912	3066356

Proportion (% of study site) of badland change classes by slope categories.

Code	0-10°	10-20°	20-30°	30-40°	40-50°	<50°	Total
111	0.267	0.116	0.053	0.012	0.001	0.000	0.449
112	0.739	0.330	0.146	0.048	0.007	0.001	1.271
121	0.059	0.048	0.027	0.015	0.002	0.000	0.151
122	1.037	0.676	0.327	0.130	0.027	0.007	2.205
211	0.113	0.059	0.027	0.011	0.002	0.000	0.212
212	0.974	0.545	0.294	0.130	0.022	0.001	1.965
221	0.725	0.404	0.148	0.055	0.012	0.002	1.345
222	35.792	32.840	16.063	5.948	1.511	0.247	92.402
Total	39.707	35.017	17.084	6.349	1.585	0.258	100.000

Proportional abundance (%) of badland change classes per slope category.

Code	0-10°	10-20°	20-30°	30-40°	40-50°	<50°	Total
111	0.7	0.3	0.3	0.2	0.1	0.0	0.4
112	1.9	0.9	0.9	0.8	0.5	0.4	1.3
121	0.1	0.1	0.2	0.2	0.2	0.1	0.2
122	2.6	1.9	1.9	2.1	1.7	2.6	2.2
211	0.3	0.2	0.2	0.2	0.1	0.0	0.2
212	2.5	1.6	1.7	2.0	1.4	0.5	2.0
221	1.8	1.2	0.9	0.9	0.8	0.7	1.3
222	90.1	93.8	94.0	93.7	95.3	95.8	92.4
Total	100.0	100.0	100.0	100.0	100.0	100.0	100.0

Slope - Talofofo

Area (m²) of badland change classes per slope category.

Code	0-10°	10-20°	20-30°	30-40°	40-50°	<50°	Total
111	91267	51112	23268	8674	1989	593	176903
112	48220	15699	7312	2656	393	36	74316
121	9110	3389	1660	762	164	29	15114
122	31254	10965	5427	2300	557	39	50542
211	17333	3992	2000	881	240	82	24528
212	40012	13762	5745	1836	366	54	61775
221	40820	14534	6910	2271	376	62	64973
222	1938421	725428	252416	72226	9704	810	2999005
Total	2216437	838881	304738	91606	13789	1705	3467156

Proportion (% of study site) of badland change classes by slope categories.

Code	0-10°	10-20°	20-30°	30-40°	40-50°	<50°	Total
111	2.632	1.474	0.671	0.250	0.057	0.017	5.102
112	1.391	0.453	0.211	0.077	0.011	0.001	2.143
121	0.263	0.098	0.048	0.022	0.005	0.001	0.436
122	0.901	0.316	0.157	0.066	0.016	0.001	1.458
211	0.500	0.115	0.058	0.025	0.007	0.002	0.707
212	1.154	0.397	0.166	0.053	0.011	0.002	1.782
221	1.177	0.419	0.199	0.066	0.011	0.002	1.874
222	55.908	20.923	7.280	2.083	0.280	0.023	86.498
Total	63.927	24.195	8.789	2.642	0.398	0.049	100.000

Proportional abundance (%) of badland change classes per slope category.

Code	0-10°	10-20°	20-30°	30-40°	40-50°	<50°	Total
111	4.1	6.1	7.6	9.5	14.4	34.8	5.1
112	2.2	1.9	2.4	2.9	2.9	2.1	2.1
121	0.4	0.4	0.5	0.8	1.2	1.7	0.4
122	1.4	1.3	1.8	2.5	4.0	2.3	1.5
211	0.8	0.5	0.7	1.0	1.7	4.8	0.7
212	1.8	1.6	1.9	2.0	2.7	3.2	1.8
221	1.8	1.7	2.3	2.5	2.7	3.6	1.9
222	87.5	86.5	82.8	78.8	70.4	47.5	86.5
Total	100.0	100.0	100.0	100.0	100.0	100.0	100.0

Aspect - Agat

Area (m^2) of badland change classes per aspect category.

Code	N	NE	E	SE	S	SW	W	NW	Total
111	7656	4466	3205	4486	9967	15146	14115	10758	69799
112	5833	3839	1953	1930	2864	4621	7088	7073	35201
121	777	415	294	420	816	1598	2192	1509	8021
122	8619	5358	2071	1492	2521	6143	11033	11721	48958
211	414	380	283	311	838	1640	1186	676	5728
212	2627	2283	1936	1969	2450	3797	3880	3173	22115
221	2252	1093	706	961	2172	6082	7334	4432	25032
222	320579	169226	71244	52364	129477	311648	434737	423634	1912909
Total	348757	187060	81692	63933	151105	350675	481565	462976	2127763

Proportion (% of study site) of badland change classes by aspect category.

Code	N	NE	E	SE	S	SW	W	NW	Total
111	0.360	0.210	0.151	0.211	0.468	0.712	0.663	0.506	3.280
112	0.274	0.180	0.092	0.091	0.135	0.217	0.333	0.332	1.654
121	0.037	0.020	0.014	0.020	0.038	0.075	0.103	0.071	0.377
122	0.405	0.252	0.097	0.070	0.118	0.289	0.519	0.551	2.301
211	0.019	0.018	0.013	0.015	0.039	0.077	0.056	0.032	0.269
212	0.123	0.107	0.091	0.093	0.115	0.178	0.182	0.149	1.039
221	0.106	0.051	0.033	0.045	0.102	0.286	0.345	0.208	1.176
222	15.066	7.953	3.348	2.461	6.085	14.647	20.432	19.910	89.902
Total	16.391	8.791	3.839	3.005	7.102	16.481	22.632	21.759	100.000

Proportional abundance (%) of badland change classes per aspect category.

Code	N	NE	E	SE	S	SW	W	NW	Total
111	2.2	2.4	3.9	7.0	6.6	4.3	2.9	2.3	3.3
112	1.7	2.1	2.4	3.0	1.9	1.3	1.5	1.5	1.7
121	0.2	0.2	0.4	0.7	0.5	0.5	0.5	0.3	0.4
122	2.5	2.9	2.5	2.3	1.7	1.8	2.3	2.5	2.3
211	0.1	0.2	0.3	0.5	0.6	0.5	0.2	0.1	0.3
212	0.8	1.2	2.4	3.1	1.6	1.1	0.8	0.7	1.0
221	0.6	0.6	0.9	1.5	1.4	1.7	1.5	1.0	1.2
222	91.9	90.5	87.2	81.9	85.7	88.9	90.3	91.5	89.9
Total	100.0	100.0	100.0	100.0	100.0	100.0	100.0	100.0	100.0

Aspect - Yona

Area (m²) of badland change classes per aspect category.

Code	N	NE	E	SE	S	SW	W	NW	Total
111	1257	1997	2552	2738	2469	1236	685	826	13760
112	4870	7583	7274	6056	5629	2923	1749	2891	38975
121	590	669	774	961	802	262	210	371	4639
122	11659	15257	11382	9388	7703	3652	2737	5837	67615
211	584	843	1062	1389	1373	497	252	486	6486
212	6540	10462	11515	10432	9801	4999	3116	3399	60264
221	3540	4812	6810	9484	8133	4148	1915	2413	41255
222	419555	493475	421766	345203	355932	274588	243495	279348	2833362
Total	448595	535098	463135	385651	391842	292305	254159	295571	3066356

Proportion (% of study site) of badland change classes by aspect category.

Code	N	NE	E	SE	S	SW	W	NW	Total
111	0.041	0.065	0.083	0.089	0.081	0.040	0.022	0.027	0.449
112	0.159	0.247	0.237	0.197	0.184	0.095	0.057	0.094	1.271
121	0.019	0.022	0.025	0.031	0.026	0.009	0.007	0.012	0.151
122	0.380	0.498	0.371	0.306	0.251	0.119	0.089	0.190	2.205
211	0.019	0.027	0.035	0.045	0.045	0.016	0.008	0.016	0.212
212	0.213	0.341	0.376	0.340	0.320	0.163	0.102	0.111	1.965
221	0.115	0.157	0.222	0.309	0.265	0.135	0.062	0.079	1.345
222	13.683	16.093	13.755	11.258	11.608	8.955	7.941	9.110	92.402
Total	14.630	17.451	15.104	12.577	12.779	9.533	8.289	9.639	100.000

Proportional abundance (%) of badland change classes per aspect category.

Code	N	NE	E	SE	S	SW	W	NW	Total
111	0.3	0.4	0.6	0.7	0.6	0.4	0.3	0.3	0.4
112	1.1	1.4	1.6	1.6	1.4	1.0	0.7	1.0	1.3
121	0.1	0.1	0.2	0.2	0.2	0.1	0.1	0.1	0.2
122	2.6	2.9	2.5	2.4	2.0	1.2	1.1	2.0	2.2
211	0.1	0.2	0.2	0.4	0.4	0.2	0.1	0.2	0.2
212	1.5	2.0	2.5	2.7	2.5	1.7	1.2	1.1	2.0
221	0.8	0.9	1.5	2.5	2.1	1.4	0.8	0.8	1.3
222	93.5	92.2	91.1	89.5	90.8	93.9	95.8	94.5	92.4
Total	100.0	100.0	100.0	100.0	100.0	100.0	100.0	100.0	100.0

Aspect - Talofofo

Area (m^2) of badland change classes per aspect category.

Code	N	NE	E	SE	S	SW	W	NW	Total
111	20244	30102	35143	34792	20856	12109	10254	13403	176903
112	10582	10794	10019	9991	9633	7084	6999	9214	74316
121	1909	2460	2336	2225	1731	1236	1543	1674	15114
122	7562	7748	7337	6683	5928	4122	4728	6434	50542
211	2517	3540	4624	5094	3515	1915	1572	1751	24528
212	7495	10379	10641	11155	8498	4512	3829	5266	61775
221	5266	8364	11485	14160	12116	5613	4106	3863	64973
222	466371	486835	489670	428120	303685	199013	248241	377070	2999005
Total	521946	560222	571255	512220	365962	235604	281272	418675	3467156

Proportion (% of study site) of badland change classes by aspect category.

Code	N	NE	E	SE	S	SW	W	NW	Total
111	0.584	0.868	1.014	1.003	0.602	0.349	0.296	0.387	5.102
112	0.305	0.311	0.289	0.288	0.278	0.204	0.202	0.266	2.143
121	0.055	0.071	0.067	0.064	0.050	0.036	0.045	0.048	0.436
122	0.218	0.223	0.212	0.193	0.171	0.119	0.136	0.186	1.458
211	0.073	0.102	0.133	0.147	0.101	0.055	0.045	0.051	0.707
212	0.216	0.299	0.307	0.322	0.245	0.130	0.110	0.152	1.782
221	0.152	0.241	0.331	0.408	0.349	0.162	0.118	0.111	1.874
222	13.451	14.041	14.123	12.348	8.759	5.740	7.160	10.875	86.498
Total	15.054	16.158	16.476	14.773	10.555	6.795	8.112	12.075	100.000

Proportional abundance (%) of badland change classes per aspect category.

Code	N	NE	E	SE	S	SW	W	NW	Total
111	3.9	5.4	6.2	6.8	5.7	5.1	3.6	3.2	5.1
112	2.0	1.9	1.8	2.0	2.6	3.0	2.5	2.2	2.1
121	0.4	0.4	0.4	0.4	0.5	0.5	0.5	0.4	0.4
122	1.4	1.4	1.3	1.3	1.6	1.7	1.7	1.5	1.5
211	0.5	0.6	0.8	1.0	1.0	0.8	0.6	0.4	0.7
212	1.4	1.9	1.9	2.2	2.3	1.9	1.4	1.3	1.8
221	1.0	1.5	2.0	2.8	3.3	2.4	1.5	0.9	1.9
222	89.4	86.9	85.7	83.6	83.0	84.5	88.3	90.1	86.5
Total	100.0	100.0	100.0	100.0	100.0	100.0	100.0	100.0	100.0

...egory.

	150-200m	200-250m	> 250m	Total
	3564	316	14	69799
	3867	453	62	35201
	1838	629	242	8021
	8544	3155	1146	48958
	942	246	140	5728
2077	2683	963	438	22115
6291	5870	2777	1520	25032
561288	273976	155399	155364	1912909
397191	301284	163938	158926	2127763

...change classes by elevation category.

	100-150m	150-200m	200-250m	> 250m	Total
	0.393	0.167	0.015	0.001	3.280
	0.348	0.182	0.021	0.003	1.654
	0.090	0.086	0.030	0.011	0.377
0.042	0.430	0.402	0.148	0.054	2.301
0.148	0.033	0.044	0.012	0.007	0.269
0.458	0.098	0.126	0.045	0.021	1.039
0.332	0.296	0.276	0.131	0.071	1.176
31.874	16.980	12.876	7.303	7.302	89.902
37.354	18.667	14.160	7.705	7.469	100.000

(%) of badland change classes per elevation category.

	50-100m	100-150m	150-200m	200-250m	> 250m	Total
6	6.6	2.1	1.2	0.2	0.0	3.3
1.4	2.4	1.9	1.3	0.3	0.0	1.7
0.1	0.4	0.5	0.6	0.4	0.2	0.4
1.5	2.8	2.3	2.8	1.9	0.7	2.3
0.2	0.4	0.2	0.3	0.2	0.1	0.3
2.0	1.2	0.5	0.9	0.6	0.3	1.0
0.5	0.9	1.6	1.9	1.7	1.0	1.2
92.6	85.3	91.0	90.9	94.8	97.8	89.9
100.0	100.0	100.0	100.0	100.0	100.0	100.0

Elevation - Yona

Area (m^2) of badland change classes per elevation category.

Code	0-50m	50-100m	100-150m	150-200m	200-250m	> 250m	Total
111	18	1146	8846	3750	0	0	13760
112	1009	4125	25845	7996	0	0	38975
121	24	1224	2389	1002	0	0	4639
122	3510	20585	38451	5069	0	0	67615
211	54	1402	2115	2915	0	0	6486
212	4641	17077	30030	8515	0	0	60263
221	1268	9360	15806	14821	0	0	41255
222	623384	1149147	976508	84318	0	0	2833357
Total	633908	1204066	1099990	128386	0	0	3066350

Proportion (% of study site) of badland change classes by elevation category.

Code	0-50m	50-100m	100-150m	150-200m	200-250m	> 250m	Total
111	0.001	0.037	0.288	0.122	0.000	0.000	0.449
112	0.033	0.135	0.843	0.261	0.000	0.000	1.271
121	0.001	0.040	0.078	0.033	0.000	0.000	0.151
122	0.114	0.671	1.254	0.165	0.000	0.000	2.205
211	0.002	0.046	0.069	0.095	0.000	0.000	0.212
212	0.151	0.557	0.979	0.278	0.000	0.000	1.965
221	0.041	0.305	0.515	0.483	0.000	0.000	1.345
222	20.330	37.476	31.846	2.750	0.000	0.000	92.402
Total	20.673	39.267	35.873	4.187	0.000	0.000	100.000

Proportional abundance (%) of badland change classes per elevation category.

Code	0-50m	50-100m	100-150m	150-200m	200-250m	> 250m	Total
111	0.0	0.1	0.8	2.9	0.0	0.0	0.4
112	0.2	0.3	2.3	6.2	0.0	0.0	1.3
121	0.0	0.1	0.2	0.8	0.0	0.0	0.2
122	0.6	1.7	3.5	3.9	0.0	0.0	2.2
211	0.0	0.1	0.2	2.3	0.0	0.0	0.2
212	0.7	1.4	2.7	6.6	0.0	0.0	2.0
221	0.2	0.8	1.4	11.5	0.0	0.0	1.3
222	98.3	95.4	88.8	65.7	0.0	0.0	92.4
Total	100.0	100.0	100.0	100.0	0.0	0.0	100.0

Elevation - Talofofo

Area (m^2) of badland change classes per elevation category.

Code	0-50m	50-100m	100-150m	150-200m	200-250m	> 250m	Total
111	317	62882	113704	0	0	0	176903
112	305	47134	26877	0	0	0	74316
121	744	9788	4582	0	0	0	15114
122	1494	32595	16452	0	0	0	50541
211	720	15287	8521	0	0	0	24528
212	1037	39826	20912	0	0	0	61775
221	12447	42987	9539	0	0	0	64973
222	433501	2118397	447098	0	0	0	2998996
Total	450565	2368896	647685	0	0	0	3467146

Proportion (% of study site) of badland change classes by elevation category.

Code	0-50m	50-100m	100-150m	150-200m	200-250m	> 250m	Total
111	0.009	1.814	3.279	0.000	0.000	0.000	5.102
112	0.009	1.359	0.775	0.000	0.000	0.000	2.143
121	0.021	0.282	0.132	0.000	0.000	0.000	0.436
122	0.043	0.940	0.475	0.000	0.000	0.000	1.458
211	0.021	0.441	0.246	0.000	0.000	0.000	0.707
212	0.030	1.149	0.603	0.000	0.000	0.000	1.782
221	0.359	1.240	0.275	0.000	0.000	0.000	1.874
222	12.503	61.099	12.895	0.000	0.000	0.000	86.498
Total	12.995	68.324	18.681	0.000	0.000	0.000	100.000

Proportional abundance (%) of badland change classes per elevation category.

Code	0-50m	50-100m	100-150m	150-200m	200-250m	> 250m	Total
111	0.1	2.7	17.6	0.0	0.0	0.0	5.1
112	0.1	2.0	4.1	0.0	0.0	0.0	2.1
121	0.2	0.4	0.7	0.0	0.0	0.0	0.4
122	0.3	1.4	2.5	0.0	0.0	0.0	1.5
211	0.2	0.6	1.3	0.0	0.0	0.0	0.7
212	0.2	1.7	3.2	0.0	0.0	0.0	1.8
221	2.8	1.8	1.5	0.0	0.0	0.0	1.9
222	96.2	89.4	69.0	0.0	0.0	0.0	86.5
Total	100.0	100.0	100.0	0.0	0.0	0.0	100.0

Soil - Agat

Area (m^2) of badland change classes per soil map unit.

Code	Agſayan-Akina association	Agſayan-Akina-Rock outcrop a.	Akina-Agſayan association	Akina-Badland association	Akina-Badland complex	Ritidian-Rock outcrop complex	Togcha-Akina silty clays	Togcha-Ylig complex	Total
111	162	1756	0	60911	6526	0	229	215	69799
112	745	3354	0	24809	4993	0	535	768	35204
121	63	2455	0	4949	378	0	78	123	8046
122	1976	11926	1	27653	4968	746	1471	1171	49912
211	12	1036	0	4088	408	0	53	131	5728
212	233	3820	0	9279	6105	109	1686	1000	22232
221	483	10533	0	12410	1050	449	377	645	25947
222	193156	629451	37613	729946	172617	1393064	51000	95569	3302416
Total	196830	664331	37614	874045	197045	1394368	55429	99622	3519284

Proportion (% of study site) of badland change classes per soil map unit.

Code	Agſayan-Akina association	Agſayan-Akina-Rock outcrop a.	Akina-Agſayan association	Akina-Badland association	Akina-Badland complex	Ritidian-Rock outcrop complex	Togcha-Akina silty clays	Togcha-Ylig complex	Total
111	0.005	0.050	0.000	1.731	0.185	0.000	0.007	0.006	1.983
112	0.021	0.095	0.000	0.705	0.142	0.000	0.015	0.022	1.000
121	0.002	0.070	0.000	0.141	0.011	0.000	0.002	0.003	0.229
122	0.056	0.339	0.000	0.786	0.141	0.021	0.042	0.033	1.418
211	0.000	0.029	0.000	0.116	0.012	0.000	0.002	0.004	0.163
212	0.007	0.109	0.000	0.264	0.173	0.003	0.048	0.028	0.632
221	0.014	0.299	0.000	0.353	0.030	0.013	0.011	0.018	0.737
222	5.489	17.886	1.069	20.741	4.905	39.584	1.449	2.716	93.838
Total	5.593	18.877	1.069	24.836	5.599	39.621	1.575	2.831	100.000

Proportional abundance (%) of badland change classes per soil map unit.

Code	Agſayan-Akina A.	Agſayan-Akina-Rock outcrop a.	Akina-Agſayan association	Akina-Badland association	Akina-Badland complex	Ritidian-Rock outcrop complex	Togcha-Akina silty clays	Togcha-Ylig complex	Total
111	0.1	0.3	0.0	7.0	3.3	0.0	0.4	0.2	2.0
112	0.4	0.5	0.0	2.8	2.5	0.0	1.0	0.8	1.0
121	0.0	0.4	0.0	0.6	0.2	0.0	0.1	0.1	0.2
122	1.0	1.8	0.0	3.2	2.5	0.1	2.7	1.2	1.4
211	0.0	0.2	0.0	0.5	0.2	0.0	0.1	0.1	0.2
212	0.1	0.6	0.0	1.1	3.1	0.0	3.0	1.0	0.6
221	0.2	1.6	0.0	1.4	0.5	0.0	0.7	0.6	0.7
222	98.1	94.7	100.0	83.5	87.6	99.9	92.0	95.9	93.8
Total	100.0	100.0	100.0	100.0	100.0	100.0	100.0	100.0	100.0

Soils - Yona

Area (m²) of badland change classes per soil map unit.

Code	Agfayan clay	Agfayan-Akina-Rock outcr.a.	Agfayan-Rock outcrop complex	Akina silty clay	Akina-Atate silty clays	Akina-Badland complex	Pulantat clay	Sasa-laguan clay	Togcha-Akina silty clays	Ylig clay	Total
111	68	341	462	43	399	12264	0	29	154	0	13760
112	1169	1561	3016	848	784	28897	0	288	2402	10	38975
121	56	528	565	169	195	2963	0	10	153	0	4639
122	3601	4994	11309	5619	1182	33350	49	482	6844	185	67615
211	94	361	678	47	426	4781	0	59	36	4	6486
212	4490	5348	11882	4449	1491	26042	104	118	6270	70	60264
221	1784	2268	6725	2636	2677	22111	0	946	2099	9	41255
222	248263	173713	715249	435653	67427	420675	343618	30594	232130	166040	2833362
Total	259525	189114	749886	449464	74581	551083	343771	32526	250088	166318	3066356

Proportion (% of study site) of badland change classes per soil map unit..

Code	Agfayan clay	Agfayan-Akina-Rock outcr. a.	Agfayan-Rock outcrop complex	Akina silty clay	Akina-Atate silty clays	Akina-Badland complex	Pulantat clay	Sasa-laguan clay	Togcha-Akina silty clays	Ylig clay	Total
111	0.002	0.011	0.015	0.001	0.013	0.400	0.000	0.001	0.005	0.000	0.449
112	0.038	0.051	0.098	0.028	0.026	0.942	0.000	0.009	0.078	0.000	1.271
121	0.002	0.017	0.018	0.006	0.006	0.097	0.000	0.000	0.005	0.000	0.151
122	0.117	0.163	0.369	0.183	0.039	1.088	0.002	0.016	0.223	0.006	2.205
211	0.003	0.012	0.022	0.002	0.014	0.156	0.000	0.002	0.001	0.000	0.212
212	0.146	0.174	0.387	0.145	0.049	0.849	0.003	0.004	0.204	0.002	1.965
221	0.058	0.074	0.219	0.086	0.087	0.721	0.000	0.031	0.068	0.000	1.345
222	8.096	5.665	23.326	14.208	2.199	13.719	11.206	0.998	7.570	5.415	92.402
Total	8.464	6.167	24.455	14.658	2.432	17.972	11.211	1.061	8.156	5.424	100.000

Proportional abundance (%) of badland change classes per soil map unit.

Code	Agfayan clay	Agfayan-Akina-Rock outcr. a.	Agfayan-Rock outcrop complex	Akina silty clay	Akina-Atate silty clays	Akina-Badland complex	Pulantat clay	Sasalaguan clay	Togcha-Akina silty clays	Ylig clay	Total
111	0.0	0.2	0.1	0.0	0.5	2.2	0.0	0.1	0.1	0.0	0.4
112	0.5	0.8	0.4	0.2	1.1	5.2	0.0	0.9	1.0	0.0	1.3
121	0.0	0.3	0.1	0.0	0.3	0.5	0.0	0.0	0.1	0.0	0.2
122	1.4	2.6	1.5	1.3	1.6	6.1	0.0	1.5	2.7	0.1	2.2
211	0.0	0.2	0.1	0.0	0.6	0.9	0.0	0.2	0.0	0.0	0.2
212	1.7	2.8	1.6	1.0	2.0	4.7	0.0	0.4	2.5	0.0	2.0
221	0.7	1.2	0.9	0.6	3.6	4.0	0.0	2.9	0.8	0.0	1.3
222	95.7	91.9	95.4	96.9	90.4	76.3	100.0	94.1	92.8	99.8	92.4
Total	100.0	100.0	100.0	100.0	100.0	100.0	100.0	100.0	100.0	100.0	100.0

81

Soil - Talofofo

Area (m^2) of badland change classes per soil map unit..

| Code	Agfayan-Rock outcrop complex	Akina silty clay	Akina-Atate silty clays	Akina-Badland complex	Inarajan clay	Togcha-Akina silty clays	Togcha-Ylig complex	Ylig clay	Total
111	276	0	1778	168152	0	5575	0	1122	176903
112	151	154	1662	57038	0	11351	0	3960	74316
121	542	68	91	12879	0	769	1	764	15114
122	617	643	1432	31976	0	12294	73	3507	50542
211	506	18	366	22321	0	1192	0	125	24528
212	540	167	4511	40128	0	13348	0	3081	61775
221	5988	4256	2193	47380	0	3969	24	1163	64973
222	105670	45521	521157	857150	38862	839223	38561	552861	2999005
Total	114290	50827	533190	1237024	38862	887721	38659	566583	3467156

Proportion (% of study site) of badland change classes per soil map unit..

Code	Agfayan-Rock outcrop complex	Akina silty clay	Akina-Atate silty clays	Akina-Badland complex	Inarajan clay	Togcha-Akina silty clays	Togcha-Ylig complex	Ylig clay	Total
111	0.008	0.000	0.051	4.850	0.000	0.161	0.000	0.032	5.102
112	0.004	0.004	0.048	1.645	0.000	0.327	0.000	0.114	2.143
121	0.016	0.002	0.003	0.371	0.000	0.022	0.000	0.022	0.436
122	0.018	0.019	0.041	0.922	0.000	0.355	0.002	0.101	1.458
211	0.015	0.001	0.011	0.644	0.000	0.034	0.000	0.004	0.707
212	0.016	0.005	0.130	1.157	0.000	0.385	0.000	0.089	1.782
221	0.173	0.123	0.063	1.367	0.000	0.114	0.001	0.034	1.874
222	3.048	1.313	15.031	24.722	1.121	24.205	1.112	15.946	86.498
Total	3.296	1.466	15.378	35.678	1.121	25.604	1.115	16.341	100.000

Proportional abundance (%) of badland change classes per soil map unit..

| Code	Agfayan-Rock outcrop complex	Akina silty clay	Akina-Atate silty clays	Akina-Badland complex	Inarajan clay	Togcha-Akina silty clays	Togcha-Ylig complex	Ylig clay	Total
111	0.2	0.0	0.3	13.6	0.0	0.6	0.0	0.2	5.1
112	0.1	0.3	0.3	4.6	0.0	1.3	0.0	0.7	2.1
121	0.5	0.1	0.0	1.0	0.0	0.1	0.0	0.1	0.4
122	0.5	1.3	0.3	2.6	0.0	1.4	0.2	0.6	1.5
211	0.4	0.0	0.1	1.8	0.0	0.1	0.0	0.0	0.7
212	0.5	0.3	0.8	3.2	0.0	1.5	0.0	0.5	1.8
221	5.2	8.4	0.4	3.8	0.0	0.4	0.1	0.2	1.9
222	92.5	89.6	97.7	69.3	100.0	94.5	99.7	97.6	86.5
Total	100.0	100.0	100.0	100.0	100.0	100.0	100.0	100.0	100.0
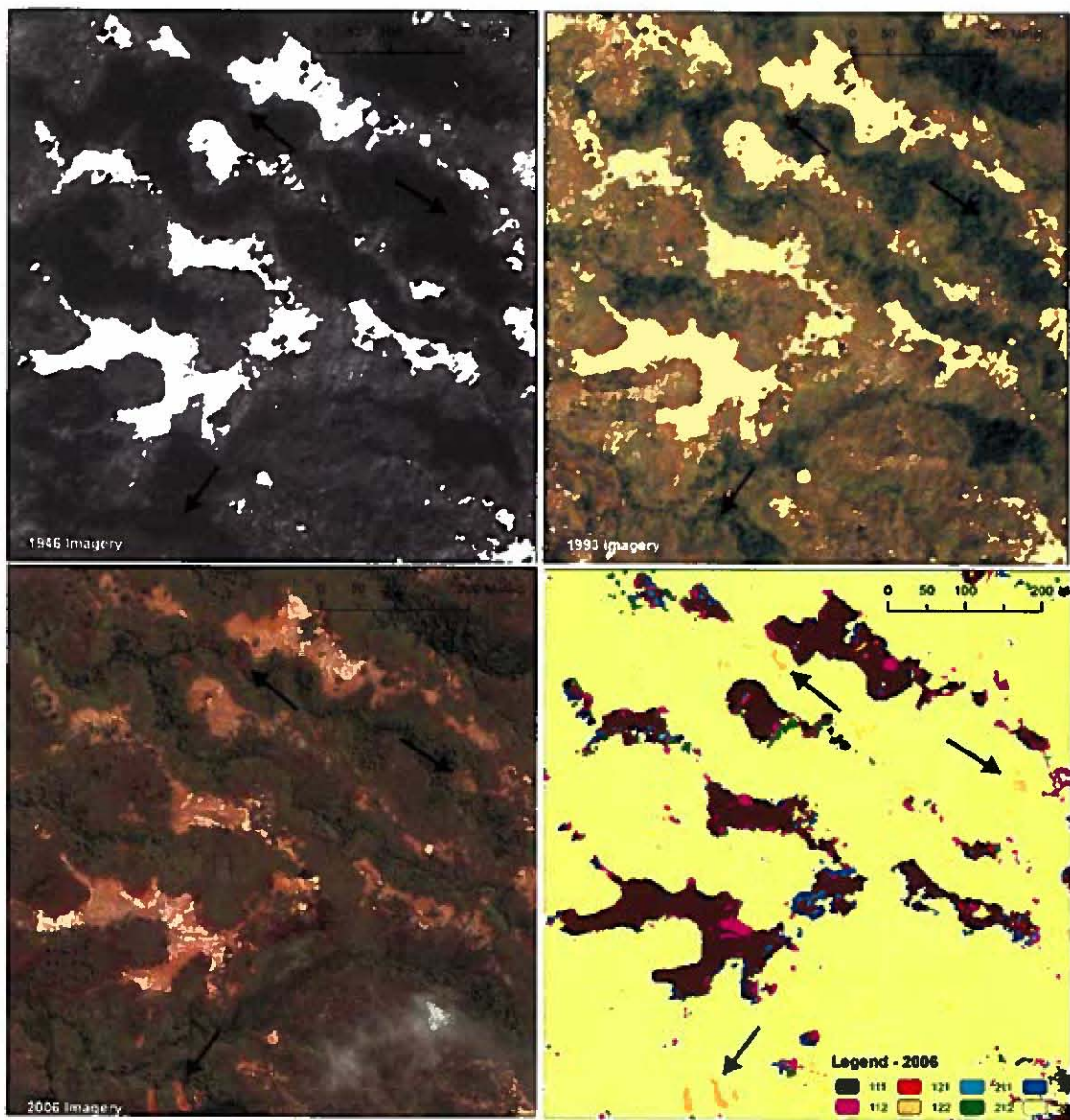
Area at the Agat site where many slumps (see arrows) were observed between 1994 and 2006, likely triggered by Typhoon Chata'an or Pongsona in 2002. Figures (clockwise from top left) show imagery from 1946, 1994, and 2006, and the change detection map.

Area at the Talofofo site where abandoned farm fields or mis-managed framing likely caused badland expansion (center). Some areas were able to re- vegetate by 2006 (right). Red outlines show the 1946 badland extent; the pink outline show the 1994 badland extent.

APPENDIX C. Examples of Misclassification.
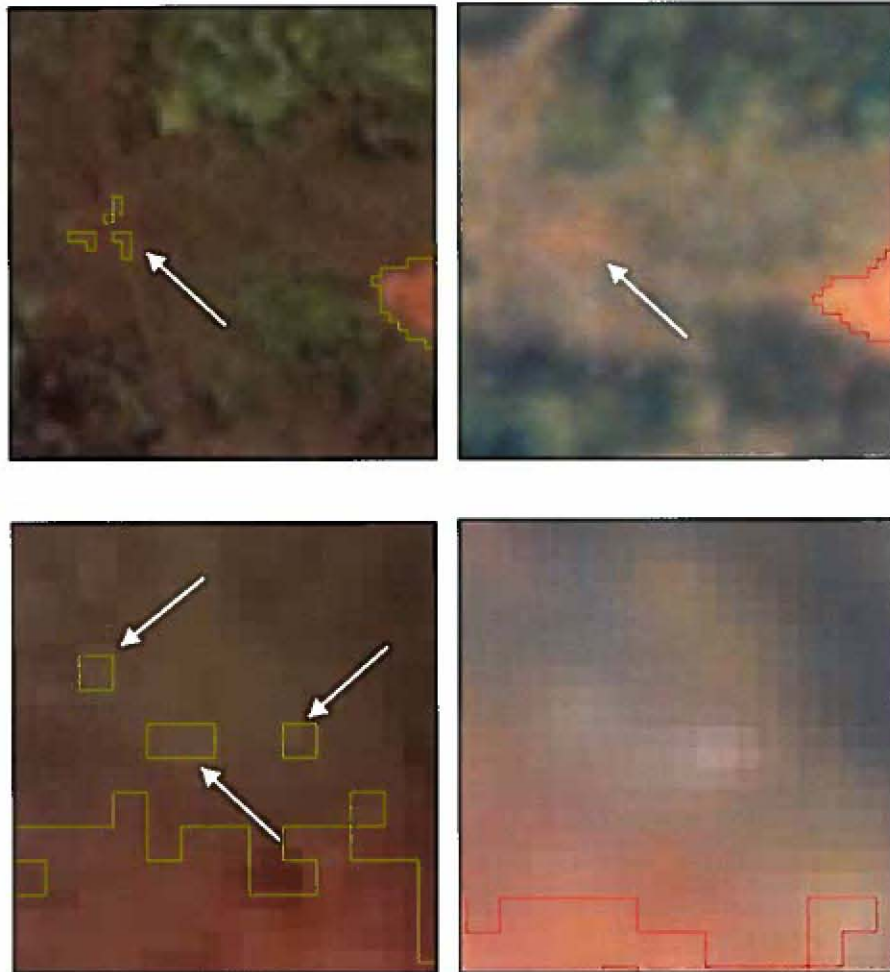
Examples of misclassified pixels in 1994 (right) and 2006 (left); a) shows a small badland area in 1994 and 2006 which was classified as badland in 2006 but erroneously not classified as badland in 1994; b) shows three small areas that were erroneously classified as badlands in 2006 but not in 1994.

APPENDIX D. Soil Samples.

List of soil samples with description of site and dominant color ([1] BL = badland, V = vegetative savanna, [2]Of dried sample (MUNSELL, 1975).

| ID	Depth	Cover[1]	Details	Study Site	Dominant Color[2]		Remarks
					Primary	Secondary	
I	0–6	BL	brecchia, pillow lava, lumps of ocher deposits, crusty	Agat	2.5R 5/6	10YR 5/8	some parts many, fine white-purple mottles
	6–12				2.5R 5/6	10YR 5/8	many, fine white-ocher, red,darkbrown mottles
II	0–6	BL	very granular, pillow lava (?)		5YR 6/3	5YR 8/1	few, medium, bright red, ocher (fewer) mottles
	6–12				5YR 5/3	5YR 8/1	common distinct, irregular very dark-brown-red fewer ocher-white-green mottles
III	0–6	V	ferns, grasses (~ 1-1.5 m high), no sword grass		2.5R 4/4		roots, uniform color
	6–12				2.5R 4/6		roots, uniform color
IV	0–6	BL	depression, ORV tracks	Yona	10R 4/6		few, coarse,white-reddish-dark-brown mottles
	6–12				10R 4/4		few, medium, white-reddish mottles
V	0–6	BL	deposited purple-white sediment mix, rel. easy to dig but looks crusted		10R 6/6		many medium-to-coarse white mottles
	6–12				10R 5/6		many medium-to-coarse white mottles
VI	0–6	BL	slight slope, heavily eroded, bedrock structure still intact (pillow lava, brecchia)		2.5R 5/4		
	6–12				2.5R 5/4		very few fine orange-to-darkbown mottles
VII	0–6	BL	purple, steep ~ 45°, tracks, fractured, very easy to dig in most places		10R 6/4		few, medium, white-darkbown mottles
	6–12				10R 5/4		few, medium, white-darkbown mottles
VIII	0–6	V	rough terrain, non-uniform slope, sword grass and fern		2.5R 4/6		many roots; few, medium white mottles
	6–2				2.5R 3/6		some roots; few coarse white mottles
IX	0–6	BL		Talofofo	2YR 4/4		breaks easily apart, superfine, white-ocher mottles
	6–12				2YR 4/4		breaks easily apart, superfine, mostly white mottles
X	0–6	BL			10YR 6/6		breaks easily apart, common fine whitish-grey mottles
	6–12				10YR 6/6		breaks easily apart, common medium white-reddish mottles
XI	0–6	V			7.5YR 3/2		many roots, very dark color, few coarse dark mottles
	6–12				7.5YR 3/2		some roots, few medium mostly whitish mottles

98

Soil Texture Triangle

Agat Study Site
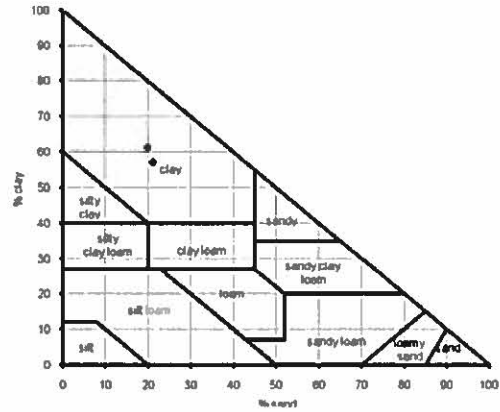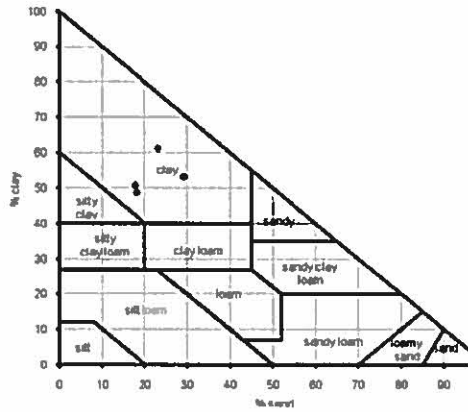
Yona Study Site
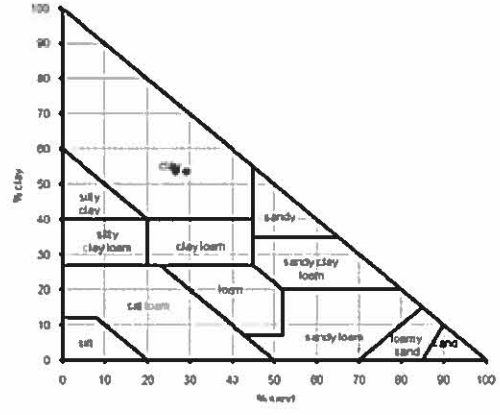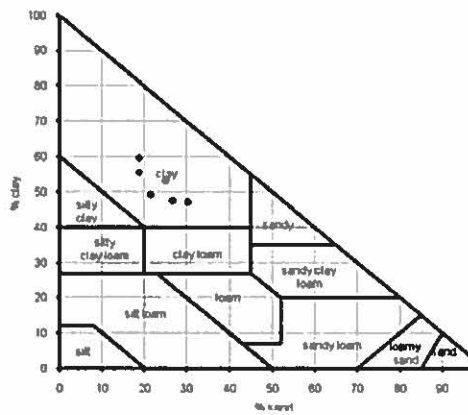
Talofofo Study Site
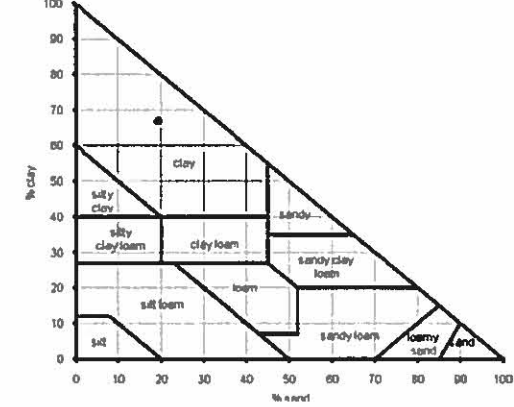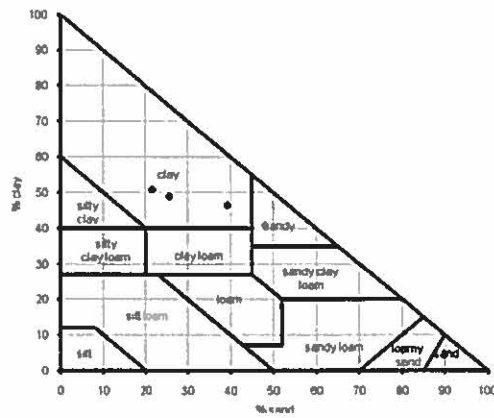
Results of texture analysis presented in texture triangle for each study site. Figures on left show badlands and figures on right show corresponding vegetative savanna.

APPENDIX E. Examples of Badlands at the Study Sites.

Agat

1.

2.

Photo 1. Weathered pillow basalt exposed in badland. **Photo 2.** Relatively flat badland area typical for this study site.

Yona

Photo 3. Popular off-roading area (note the tire marks) where sediments accumulate downhill. **Photo 4.** Natural re-vegetation of mostly Dicranopteris linearis *(false staghorn fern* in areas where sediments accumulate (bottom).

APPENDIX E. Continued.

<u>Talofofo</u>
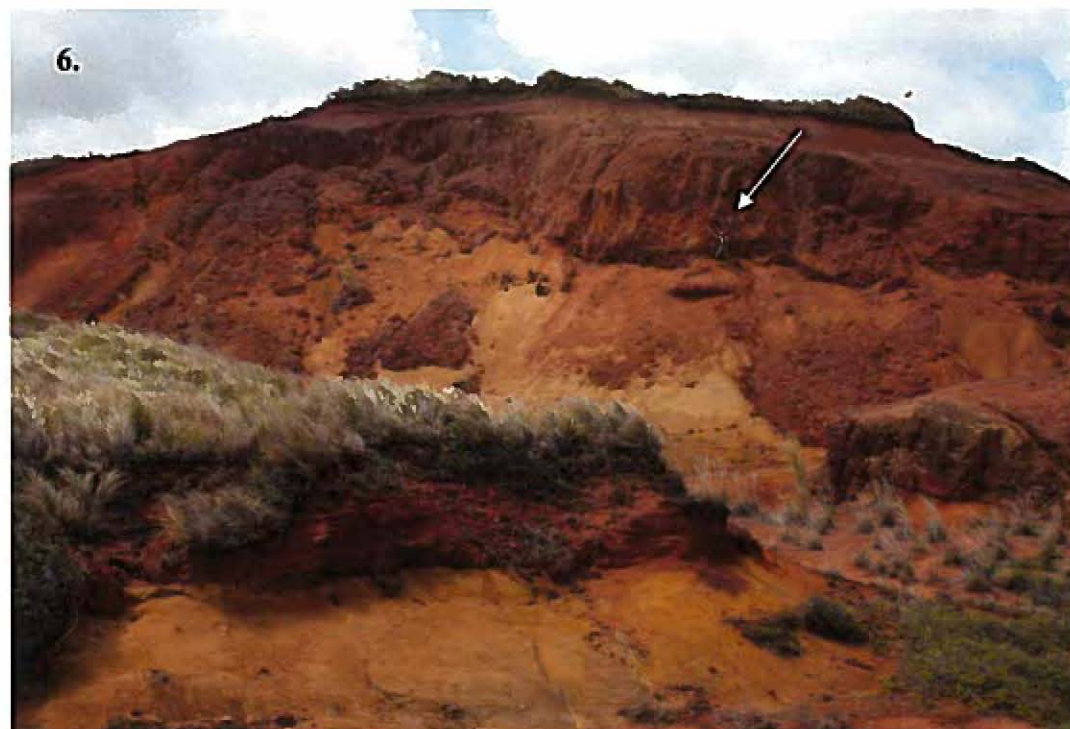
Photo 5. Badland where less resistant material eroded around pillow basalt. **Photo 6.** Large badland area with near vertical walls. Note the person standing in the middle for scale.